U.S. Department of Transportation

Federal Railroad Administration

Side Impact Test and Analysis of a DOT-112 Tank Car

Office of Research,
Development,
and Technology
Washington, DC 20590

DOT/FRA/ORD-16/38

Final Report
December 2016

REPORT DOCUMENTATION PAGE

Form Approved
OMB No. 0704-0188

1. AGENCY USE ONLY (Leave blank)	2. REPORT DATE	3. REPORT TYPE AND DATES COVERED
	December 2016	Technical Report – September 2015

4. TITLE AND SUBTITLE
Side Impact Test and Analysis of a DOT 112 Tank Car

5. FUNDING NUMBERS
DTFR53-11-D-00008
Task Order 345
TTCI-11-033

6. AUTHOR(S)
Przemyslaw Rakoczy[1] , Michael Carolan[2]

7. PERFORMING ORGANIZATION NAME(S) AND ADDRESS(ES)
[1]Transportation Technology Center, Inc.
55500 DOT Road
Pueblo, CO 81001

[2]Volpe National Transportation Systems Center
55 Broadway
Cambridge, MA 02142

8. PERFORMING ORGANIZATION REPORT NUMBER

9. SPONSORING/MONITORING AGENCY NAME(S) AND ADDRESS(ES)
U.S. Department of Transportation
Federal Railroad Administration
Office of Railroad Policy and Development
Office of Research and Development
Washington, DC 20590

10. SPONSORING/MONITORING AGENCY REPORT NUMBER
DOT/FRA/ORD-16/38

11. SUPPLEMENTARY NOTES
COR: Francisco Gonzalez, III

12a. DISTRIBUTION/AVAILABILITY STATEMENT
This document is available to the public through the FRA Web site at http://www.fra.dot.gov.

12b. DISTRIBUTION CODE

13. ABSTRACT

As part of a program to improve transportation safety for tank cars, Transportation Technology Center, Inc. (TTCI) has conducted a side impact test on a DOT-112 tank car to evaluate the performance of the DOT-112 under dynamic impact conditions and to provide data for the verification and refinement of a computational model of the tank car. The tank car was filled with water to approximately 96 percent of its volume and sealed but not pressurized. The tank car was impacted at 14.7 mph by a 297.125-pound ram car fitted with a 12- by 12-inch ram head. The ram car impacted the tank center, deforming and cracking the external jacket, but the tank's shell was not punctured.

TTCI used pre-test finite element modeling, which was performed by the Volpe National Transportation Systems Center, to estimate the overall response of the tank to the impact and the force-displacement response. To bring the model's results into better agreement with the test results, several changes were made to the model. The post-test model matched the overall force-displacement and pressure-time histories better than the pre-test model.

The models and tests demonstrate how the fluid response of an impacted tank car dominates the general force-displacement response, which underscores the importance of modeling fluid-structure interactions with appropriate techniques.

14. SUBJECT TERMS
Impact test, DOT-112 tank car, tank car performance, transportation safety, toxic by inhalation (TIH)

15. NUMBER OF PAGES
90

16. PRICE CODE

17. SECURITY CLASSIFICATION OF REPORT	18. SECURITY CLASSIFICATION OF THIS PAGE	19. SECURITY CLASSIFICATION OF ABSTRACT	20. LIMITATION OF ABSTRACT
Unclassified	Unclassified	Unclassified	

NSN 7540-01-280-5500

Standard Form 298 (Rev. 2-89)
Prescribed by ANSI Std. 239-18
298-102

METRIC/ENGLISH CONVERSION FACTORS

ENGLISH TO METRIC	METRIC TO ENGLISH
LENGTH (APPROXIMATE)	**LENGTH (APPROXIMATE)**
1 inch (in) = 2.5 centimeters (cm)	1 millimeter (mm) = 0.04 inch (in)
1 foot (ft) = 30 centimeters (cm)	1 centimeter (cm) = 0.4 inch (in)
1 yard (yd) = 0.9 meter (m)	1 meter (m) = 3.3 feet (ft)
1 mile (mi) = 1.6 kilometers (km)	1 meter (m) = 1.1 yards (yd)
	1 kilometer (km) = 0.6 mile (mi)
AREA (APPROXIMATE)	**AREA (APPROXIMATE)**
1 square inch (sq in, in^2) = 6.5 square centimeters (cm^2)	1 square centimeter (cm^2) = 0.16 square inch (sq in, in^2)
1 square foot (sq ft, ft^2) = 0.09 square meter (m^2)	1 square meter (m^2) = 1.2 square yards (sq yd, yd^2)
1 square yard (sq yd, yd^2) = 0.8 square meter (m^2)	1 square kilometer (km^2) = 0.4 square mile (sq mi, mi^2)
1 square mile (sq mi, mi^2) = 2.6 square kilometers (km^2)	10,000 square meters (m^2) = 1 hectare (ha) = 2.5 acres
1 acre = 0.4 hectare (he) = 4,000 square meters (m^2)	
MASS - WEIGHT (APPROXIMATE)	**MASS - WEIGHT (APPROXIMATE)**
1 ounce (oz) = 28 grams (gm)	1 gram (gm) = 0.036 ounce (oz)
1 pound (lb) = 0.45 kilogram (kg)	1 kilogram (kg) = 2.2 pounds (lb)
1 short ton = 2,000 pounds (lb) = 0.9 tonne (t)	1 tonne (t) = 1,000 kilograms (kg) = 1.1 short tons
VOLUME (APPROXIMATE)	**VOLUME (APPROXIMATE)**
1 teaspoon (tsp) = 5 milliliters (ml)	1 milliliter (ml) = 0.03 fluid ounce (fl oz)
1 tablespoon (tbsp) = 15 milliliters (ml)	1 liter (l) = 2.1 pints (pt)
1 fluid ounce (fl oz) = 30 milliliters (ml)	1 liter (l) = 1.06 quarts (qt)
1 cup (c) = 0.24 liter (l)	1 liter (l) = 0.26 gallon (gal)
1 pint (pt) = 0.47 liter (l)	
1 quart (qt) = 0.96 liter (l)	
1 gallon (gal) = 3.8 liters (l)	
1 cubic foot (cu ft, ft^3) = 0.03 cubic meter (m^3)	1 cubic meter (m^3) = 36 cubic feet (cu ft, ft^3)
1 cubic yard (cu yd, yd^3) = 0.76 cubic meter (m^3)	1 cubic meter (m^3) = 1.3 cubic yards (cu yd, yd^3)
TEMPERATURE (EXACT)	**TEMPERATURE (EXACT)**
[(x-32)(5/9)] °F = y °C	[(9/5) y + 32] °C = x °F

QUICK INCH - CENTIMETER LENGTH CONVERSION

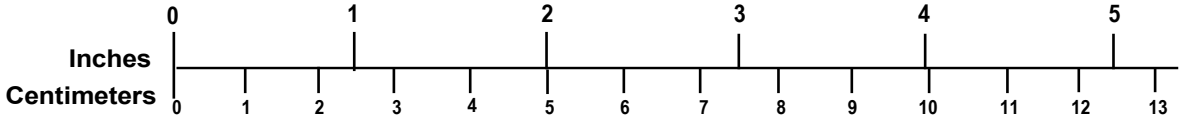

QUICK FAHRENHEIT - CELSIUS TEMPERATURE CONVERSIO

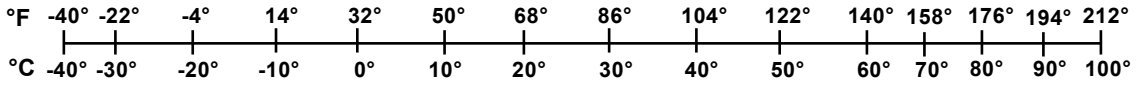

For more exact and or other conversion factors, see NIST Miscellaneous Publication 286, Units of Weights and Measures. Price $2.50 SD Catalog No. C13 10286

Updated 6/17/98

Contents

Illustrations

Tables

Acknowledgements

The tests described in this report were performed by the Transportation Technology Center, Inc. (TTCI) under Federal Railroad Administration (FRA) Contract DTFR53-11-D-00008 Task Order 345. Similarly, the analyses described in this report were performed by the Volpe National Transportation Systems Center (Volpe) under FRA sponsorship.

Authors of this report gratefully acknowledge the technical assistance of Volpe senior engineers David Jeong and Benjamin Perlman. Additionally, discussions with Karl Alexy of FRA's Office of Safety played a valuable role in developing this testing program.

The DOT-112 tank car used in this impact test was donated to FRA by CSX. Authors and FRA gratefully acknowledge CSX Director of Hazardous Materials Chris Machenberg for assisting with car donation.

Executive Summary

This report documents the combined efforts of the Transportation Technology Center, Inc. (TTCI) and Volpe National Transportation Systems Center (Volpe) to test and analyze the side impact puncture performance of a DOT-112A340W tank car (which will be abbreviated in this report to "DOT-112 tank car"). The side impact test took place on February 26, 2014, to evaluate the performance of the tank car and to provide data for the verification and refinement of a computational model of the DOT-112. All test requirements were met. Volpe performed both pretest predictions and post-test analyses of the impact response to evaluate, validate, and improve the puncture modeling capabilities.

The tank car was filled with water to approximately 96 percent of its volume, then it was sealed but not pressurized. The test was intended to strike the car at a speed that was high enough to result in significant damage to the tank without puncturing the tank's shell. The tank car was impacted at 14.7 mph by a 297.125-pound ram car fitted with 12- by 12-inch ram head. The ram car impacted the tank center, deforming and cracking the external jacket without puncturing the tank's shell.

TTCI used pretest Finite Element (FE) modeling to estimate the overall response of the tank to the impact, including the force-displacement response. Because of uncertain parameters (e.g., material properties, actual outage, actual test speed), the pre-test model was intended to provide a conservative (i.e., lower-bound estimate of puncture speed) to ensure that the test did not result in puncture of the tank. The model was overly stiff when it was compared to the test and pretest FE results.

To bring the model results into better agreement with the test results, several changes were made to the model, including reducing the coefficient of friction between the water and the inside of the tank, adjusting the outage volume, and using properties of TC128 steel corresponding to typical material (rather than minimum material properties). The post-test model was in much better agreement with the overall force-displacement and pressure-time histories than the pretest model. The post-test model overpredicted the maximum impact force, probably because the outage had been compressed to an extreme degree, which permitted the water to contact the top of the tank.

The FE modeling in this impact scenario underscored the importance of the role played by the fluid and outage in the overall response of the tank to a shell impact. In particular, the use of an unpressurized tank car with a small outage and a fairly large impactor places an increased importance on appropriately modeling the fluid and gas phase in a way that can capture the overall response of the tank. At the end of the impact event, the models tended to exhibit a greater force response than tested, possibly because the water made contact with the top of the inside of the tank.

1. Introduction

1.1 Background

In recent years, railroad tank cars have been the subject of significant research that aims to analyze and improve their impact behavior and puncture resistance. Ultimately, the results of this research will be used by government regulatory agencies in the United States and Canada (i.e., the Federal Railroad Administration [FRA] and Transport Canada, respectively) to establish performance-based testing requirements and to develop methods to evaluate the crashworthiness and structural integrity of different tank car designs when they are subjected to standardized shell impact scenarios.

FRA has an ongoing research program that provides the technical basis for developing enhanced and alternative performance standards for tank cars, and reviews new and innovative tank car designs developed by the industry and other countries. In this research program, full-scale tests provide the technical information to validate modeling efforts and to inform regulatory activities. These tests evaluate the crashworthiness of tank cars used in the transportation of hazardous materials.

These tests and associated analyses evaluate the crashworthiness of tank cars, including designs that comply with current regulations as well as innovative new designs that have improved puncture resistance. FRA is currently working closely with key industry stakeholders to use the information being generated from these programs to revise and refine the construction, design, and use of tank cars.

This report documents test results and related analyses for a side impact test that was performed on a DOT-112A340W tank car. In this report, we will refer to this tank car as a "DOT-112 tank car." The DOT-112 tank car is a pressurized car, which is equipped with head protection and thermal protection enclosed in an exterior jacket.

This report documents an impact test of a current design DOT-112 tank car and describes the model development and pretest predictions, comparisons of the test and analyses, and the subsequent post-test analyses performed to address the variations between the pretest analyses and actual test conditions.

1.2 Objectives

The side impact test's goal was to quantify the deformation mode, impact load-time history, and puncture resistance of an existing tank car in a side impact. Also, the test conditions were repeated from the impact test performed on December 18, 2013, on DOT-111 [2] tank car for a direct comparison. The DOT-112 is a pressure car, but the tank was not pressurized for this impact test, which allowed the team to compare the results from the DOT-111 and DOT-112 impact tests. Finally, the impact conditions were set so the side impact test was: (a) safe, (b) repeatable, and (c) analyzable.

The objectives of the analyses were for pretest planning and validation of tank car impact and puncture modeling capabilities.

1.3 Tank Car

The U.S. DOT-112 tank car is a pressurized tank car used in North America to carry pressurized gases. The test was performed on a DOT 112A340W tank car equipped with head protection and a thermal protection enclosed in the exterior jacket. This car was constructed in 2001, according to the certificate of construction. The 0.618-inch thick tank car shell was made of TC-128 Grade B steel. The tank employed a cylindrical shell with an outer diameter of 119.125 inches. Full height, 0.50-inch thick head shields were constructed with the same material as the shell. The tank car shell was wrapped in 0.50-inch ceramic fiber wrap for thermal protection and covered by steel jacket.

Figure 1 shows the tank car's general design.

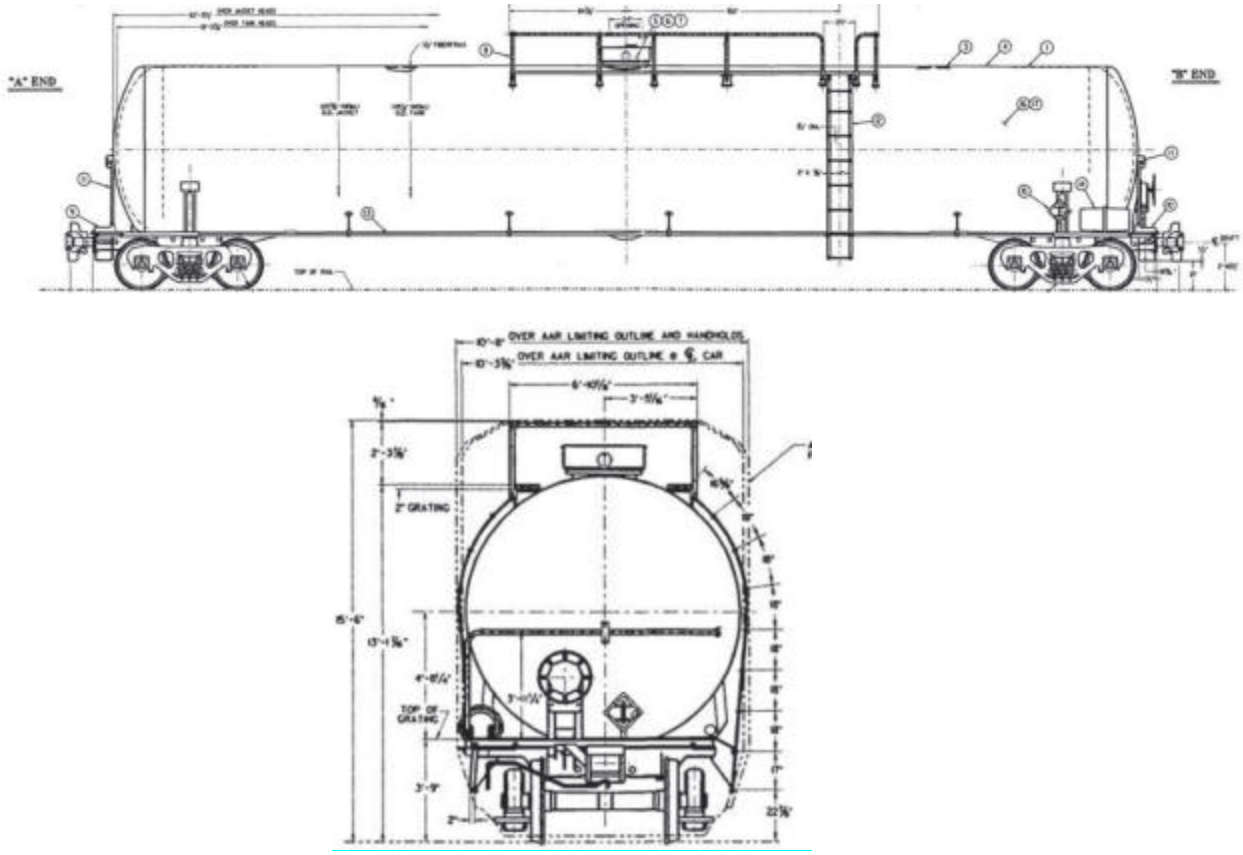

Figure 1. DOT-112 Tank Car Design Specification.

The capacity of the car had a slightly different value depending on where it was reported. The certificate of construction for the group of cars including the tested DOT-112 listed its full water capacity as 33,800 gallons. The car itself had a stenciled capacity of 33,910 gallons. During test preparations, the tank was initially filled to capacity with water before being emptied to achieve the desired outage. According to the gauge used during the filling operation, a total of 33,040

gallons filled the car to capacity. While these three values represent a small difference in tank capacity, the difference introduces uncertainty into determining the actual outage volume. In particular, when filling the car to achieve a small outage, the uncertainty in outage volume can be on the same order of magnitude as the desired outage itself. However, an accurate air-to-water ratio was achieved with the loading procedure described in Section 1.4.

The following key information from the drawings of the DOT-112 tank car was used in this test:

- Shell and head material: TC-128 Grade B
- Heads: 0.50-inch thick
- Shell: 0.618-inch thick, 119.125 inch Outside Diameter (O.D.)
- Jacket: 11-gauge ASTM A-1011, 120.375-inch O.D.

1.4 Test Setup

The side impact test was performed on February 26, 2014, at the Transportation Technology Center (TTC) in Pueblo, Colorado, when a ram car was sent into the side of a tank car that was mounted on skids and backed by a rigid impact barrier (Figure 2).

Figure 2. Target Tank Mounted on Support Skids

Before the test, the tank car structure and all interior welds were visually inspected for any damage or evidence of repair.

Figure 3 (a) shows that the two skids are oriented perpendicular to the track, with one side against the impact barrier that was underneath the tank car. Four sections of I-beams were welded to the tank car and the skids for the attachment, (see Figure 3(b)). The tank car with skids attached was placed on 1-inch steel plates. This test configuration was designed to minimize the test car rollback and allow the tank car on the skids to slide on the steel plates during the impact. The tank car jacket and shell were not modified in any way. This particular tank car's ladder was not centered on the car's side, so the ladder did not need to be removed. The tank car was filled with water until it was shell-full. Four percent of the water (by volume) to achieve a shell-full condition was then pumped out of the tangagek. The height from the top of the water to the top of the tank was measured to be approximately 8.75 inches. The manhole lid was sealed, but no additional pressure was introduced to the tank car. This condition was created to help in understanding the effects of shell thickness on puncture speed for unpressurized cars.

(a) Support skids **(b) Welded I-beam connection**

Figure 3. Tank Support Skid System

The indenter was positioned to align with the mid length and mid height of the target tank car as closely as possible. Figure 4 shows the ram car. For this test, a 12 in by 12 in indenter with 1.0-in radii on the edges and corners was used. The same indenter was used in the impact test of the DOT-111 tank car, permitting comparison of the DOT-111 and DOT-112 test results. Additionally, this large indenter was expected to result in a considerable amount of fluid motion (i.e., "sloshing") during the test, requiring careful modeling of the lading to be able to capture this motion. Figure 5 and Figure 6 show the 12 in by 12 in indenter attached to the ram car and aligned with the tank car. The ram car was weighed before the test to confirm the actual weight, and it weighed 297,125 pounds.

Figure 4. Ram Car and Head

Figure 5. Ram Arm with 12- by 12-inch Indenter

Figure 6. Ram Arm with 12- by 12-inch Indenter Aligned with Center of the Tank Car

2. Test Instrumentation

2.1 Overview

The test configuration and instrumentation were all consistent with the specifications that were defined by the test implementation plan [1]. Table 1 lists all of the instrumentation used in the test. Additional descriptions of instrumentation are provided below.

Table 1. Instrumentation Summary

Type of Instrumentation	Channel Count
Accelerometers	11
Speed Sensors	2
Pressure Transducers	11
String Potentiometers	10
Total Data Channels	**34**
Digital Video	7 cameras including 3 high speed cameras

2.2 Ram Car Accelerometers and Speed Sensors

The local acceleration coordinate systems are defined relative to the ram car. Positive x, y, and z directions are forward, left, and up relative to the lead end of the ram.

Three triaxial accelerometers were mounted on the longitudinal centerline of the ram car at the front, rear, and near the middle of the car. Two uniaxial accelerometers were mounted on the left and right sides of the car to supplement recording of longitudinal acceleration. The positions of these accelerometers are illustrated in Figure 7. A summary of the ram car accelerometer types and positions are provided in Table 2.

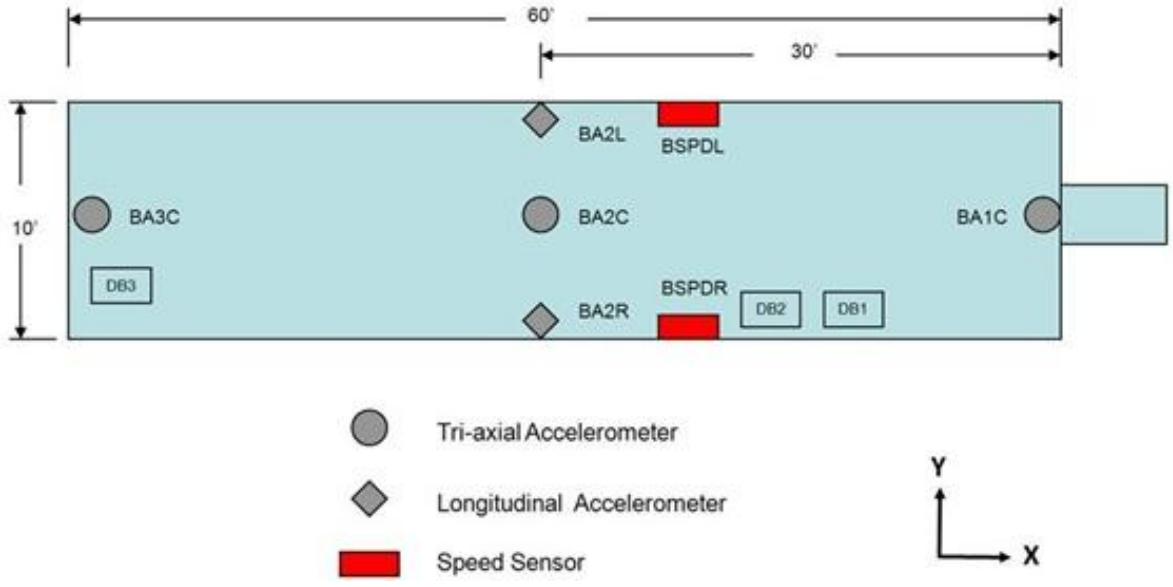

Figure 7. Ram Car Instrumentation

Table 2. Ram Car Accelerometers

Channel Name	Sensor Description	Range
BA1CX	Leading End, Centerline, X Accel	200 g
BA1CY	Leading End, Centerline, Y Accel	100 g
BA1CZ	Leading, Centerline, Z Accel	200 g
BA2LX	Middle, Left Side X Accel	100 g
BA2CX	Middle, Centerline, X Accel	50 g
BA2CY	Middle, Centerline, Y Accel	50 g
BA2CZ	Middle, Centerline, Z Accel	50 g
BA2RX	Middle, Right Side X Accel	100 g
BA3CX	Trailing End, Centerline, X Accel	200 g
BA3CY	Trailing End, Centerline, Y Accel	100 g
BA3CZ	Trailing End, Centerline, Z Accel	200 g

Speed sensors were mounted on both sides of the ram car to provide accurate measurement of the car velocity within 2 feet of the impact point. The speed sensors were reflector based light sensors, which used ground reflectors separated by a known distance in conjunction with light sensors mounted on the car that triggered as the car passed over the reflector. The last reflector was positioned to align with the sensor when the ram head was within a few inches of the impact point. The time interval between passing the reflectors was recorded, and speed was calculated from distance and time. A handheld radar gun was also used to take supplemental speed measurements.

2.3 Tank Car String Potentiometers and Pressure Transducers

The local displacement coordinate systems (except for the tank head) are defined relative to the tank car. Positive x, y, and z directions are forward, left (away from the wall), and up relative to the B-end of the tank car. Tank head displacements are positive toward the impact wall.

During the test, six string potentiometers measured the tank crush displacements around the immediate impact zone. Five of them measured the dent formation of the tank at the tank center as well as locations that were 24 inches and 48 inches to either side of the impact point. The sixth string potentiometer measured the vertical deformations of the tank at the center (aligned with the impact point). Four additional string potentiometers were used to measure the tank motions. The string potentiometers were attached to each of the tank skids and to the center of the tank heads at either end of the car. Fixed anchor positions were established so that these measurements are for the longitudinal motions of the tank head and skid movements. Table 3 provides a list of all string potentiometers inside and outside the tank car. Figure 8 and Figure 9 show how they were placed.

Table 3. Tank Car String Potentiometers

Area	Location	Axis	Channel Name	Range (inches)
Impact Area	A-end — 48-inch offset	Y	TD1Y	30
Impact Area	A-end — 24-inch offset	Y	TD2Y	50
Impact Area	Center	Y	TD3Y	50
Impact Area	Center	Z	TD3Z	30
Impact Area	B-end — 24-inch offset	Y	TD4Y	50
Impact Area	B-end — 48-inch offset	Y	TD5Y	30
Tank Head	A-end	Y	TD_A_end	50
Tank Head	B-end	Y	TD_B_end	50
Skid	A-end	Y	TD_A_skid	50
Skid	B-end	Y	TD_A_skid	50

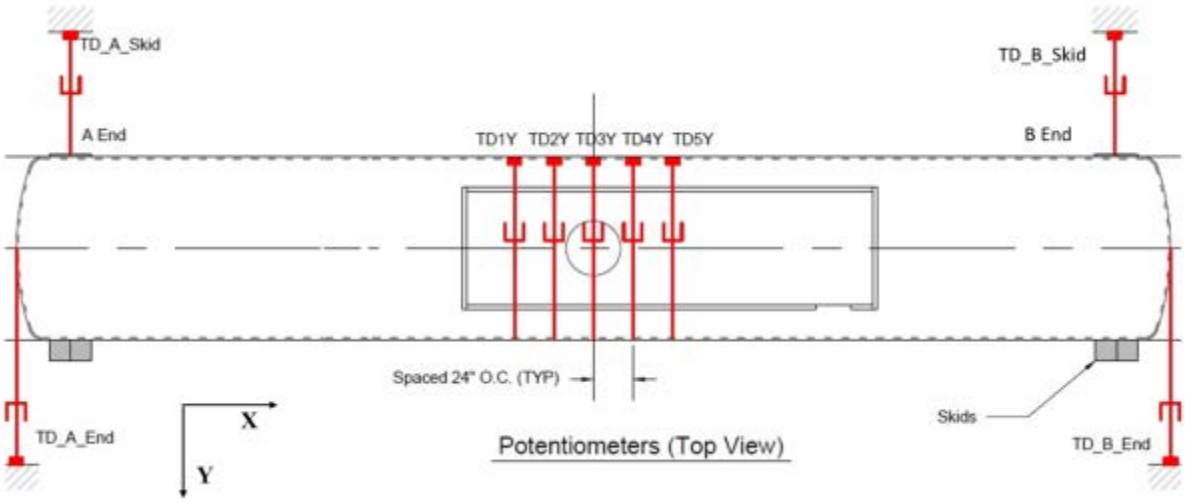

Figure 8. Tank Car String Potentiometers (Top)

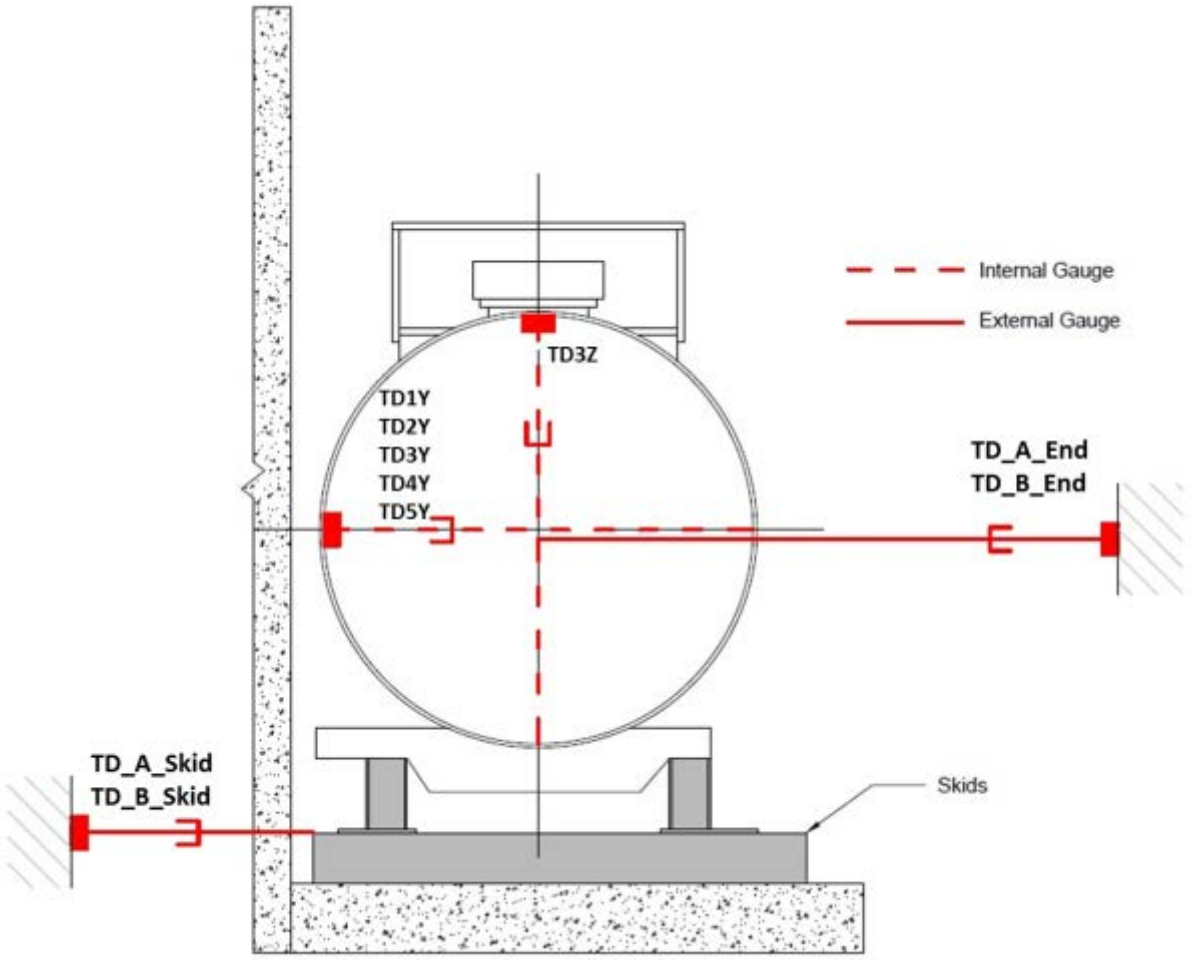

Figure 9. Tank Car String Potentiometers (Side)

An array of nine pressure transducers was set up within the tank to record what occured when the pressure pulse moved through the lading. These were mounted in three sections on the sides and bottom of the tank. Two additional pressure transducers were installed: one externally to the pressure relief valve to measure when the valve was open, and another inside the manway to measure outage pressure. Table 4 provides a list of all pressure transducers used inside the tank car. Figure 10 and Figure 11 show their placement.

Table 4. Tank Car Pressure

Location	Channel Name	Sensor Description	Range (psi)
Manhole lid	TPV	Outage Pressure	500
PR Valve	TPRV	Pressure Relief Valve (Exterior)	500
A Back wall	TP1090	A-End Back Wall Pressure	300
A Front wall	TP1270	A-End Front Wall Pressure	300
A Floor	TP1180	A-End Floor Pressure	300
M Back wall	TP2090	Mid-length Back Wall Pressure	300
M Front wall	TP2270	Mid-length Front Wall Pressure	300
M Floor	TP2180	Mid-length Floor Pressure	300
C Back wall	TP3090	Center Back Wall Pressure	300
C Floor	TP3180	Center Floor Wall Pressure	300
C Front wall	TP3270	Center Front Wall Pressure	300

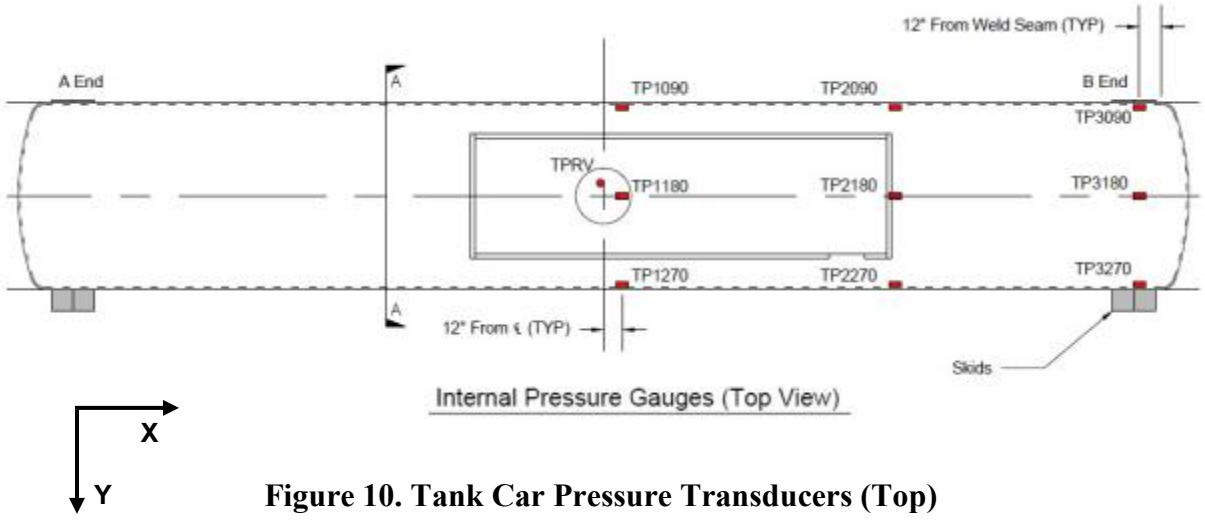

Figure 10. Tank Car Pressure Transducers (Top)

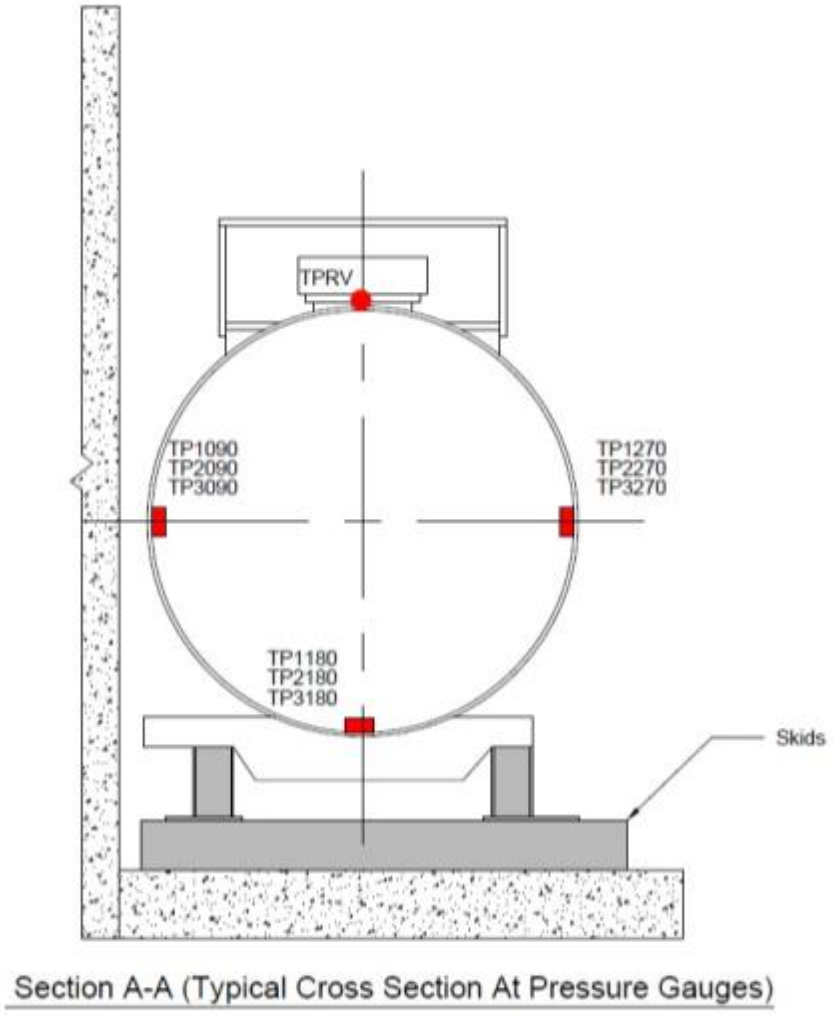

Figure 11. Tank Car Pressure Transducers (Side)

2.4 Real Time and High Speed Photography

Three high-speed and four real time high definition video cameras documented the impact event. Appendix A contains additional photographs of the impact test, and Appendix B contains a schematic of the locations of the cameras and positions of the targets.

2.5 Data Acquisition

A set of 8-channel battery-powered onboard data acquisition systems was used to record the data from instrumentation mounted on the ram car. These systems provided excitation to the instrumentation, handled analog anti-aliasing filtering of the signals, performed analog-to-digital conversion, and recorded of each data stream. A similar set of ground-based data acquisition systems was used to record data from the pressure transducers on the tank car.

The data acquisition systems were GMH Engineering Data BRICK Model III units. Data acquisition complied with the appropriate sections of SAE J211. Data from each channel was anti-alias filtered at 1,735 Hz then sampled and recorded at 12,800 Hz, and the data recorded on the data bricks was synchronized to time zero at initial impact. The time reference was derived from the moment that the tape switches were closed on the front of the test vehicle. Each data brick was ruggedized for shock loading up to at least 100 g. Onboard battery power was provided by GMH Engineering 1.7 Amp-hour 14.4 Volt NiCad Packs. Tape Switches, Inc., model 1201-131-A tape switches provided event initial contact.

Software in the data bricks was used to determine zero levels and calibration factors rather than relying on set gains and expecting no zero drift. The data bricks were set to record 1 second of data before initial impact and 4 seconds of data after initial impact.

3. Results

3.1 Test Conditions

As described in Sections 1.3 and 1.4, Test 2 was a side impact on a DOT type 112A340W tank car, performed on February 26, 2014. This test involved a 14.7 mph side impact by a structurally rigid 297,125-pound ram car with a 12-inch square impactor head into the side of the 112A340W test vehicle, backed by a rigid impact barrier. To simulate the standard commodity lading volume of a DOT-112 tank car, the test tank car was filled with water to approximately 96 percent of its capacity. The wind speed was 4 mph east and the temperature was 43°F.

3.2 Details of Test

The target speed for the test was 15 mph, and the pretest simulation predicted that there would be no puncture at this speed. The actual calculated impact speed from the speed trap was 14.7 mph. The indenter created a permanent deformation, but it did not puncture the tank car. After impact, the ram car rebounded and stopped due to the activated airbrake. Figure 12 shows the impact before rebound. The impact formed fractures along the weld seam on the external jacket. Figure 13 shows the indentation of the tank car after impact. Figure 14 shows the interior jacket and area of the removed exterior jacket section.

Figure 12. Time of Impact

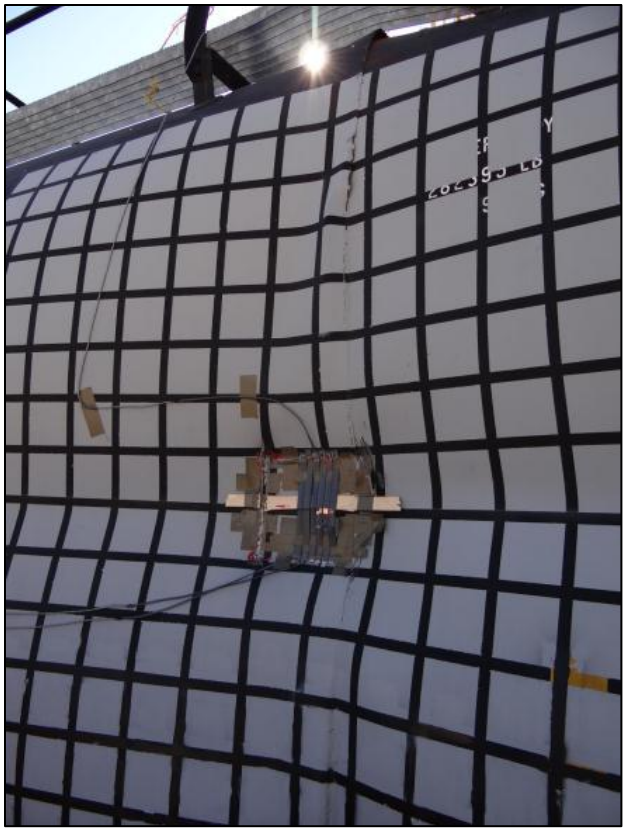

Figure 13. Tank Car Indentation – Post Impact

Figure 14. Tank Car Indentation – Removed Jacket and Insulation Section

3.3 Measured Data

The data collected in the test was processed (offset corrections, filtering, etc.) by TTCI and then it was compared to the analyses by Volpe. The offset adjustment procedure ensured that the data that was plotted and analyzed contains only impact-related accelerations and strains and excluded electronic offsets or steady biases in the data. In order to determine the necessary offset, the data was collected before impact was averaged and this offset was then subtracted from the entire data set for each channel. The post-test offset adjustment is independent of, and in addition to, the pre-test offset adjustment made by the data acquisition system.

The post-test filtering of the data was accomplished with a phaseless four-pole digital filter algorithm consistent with the requirements of SAE J211 [1]. A 60 Hz channel frequency class (CFC) filtering was applied to create the filtered acceleration data shown in this report. A brief summary of the measured data is provided in this section. Appendix B contains the plots of filtered data from all transducers.

The longitudinal acceleration of the ram car was one of the primary measurements in the test and multiple accelerometers were used on the ram car to capture this data. The ram car acceleration was used to derive the impact energy, deceleration of the ram car, and contact forces between the

ram and target tank car. The ram car's average longitudinal acceleration history from all of the ram accelerometers is shown in Figure 15.

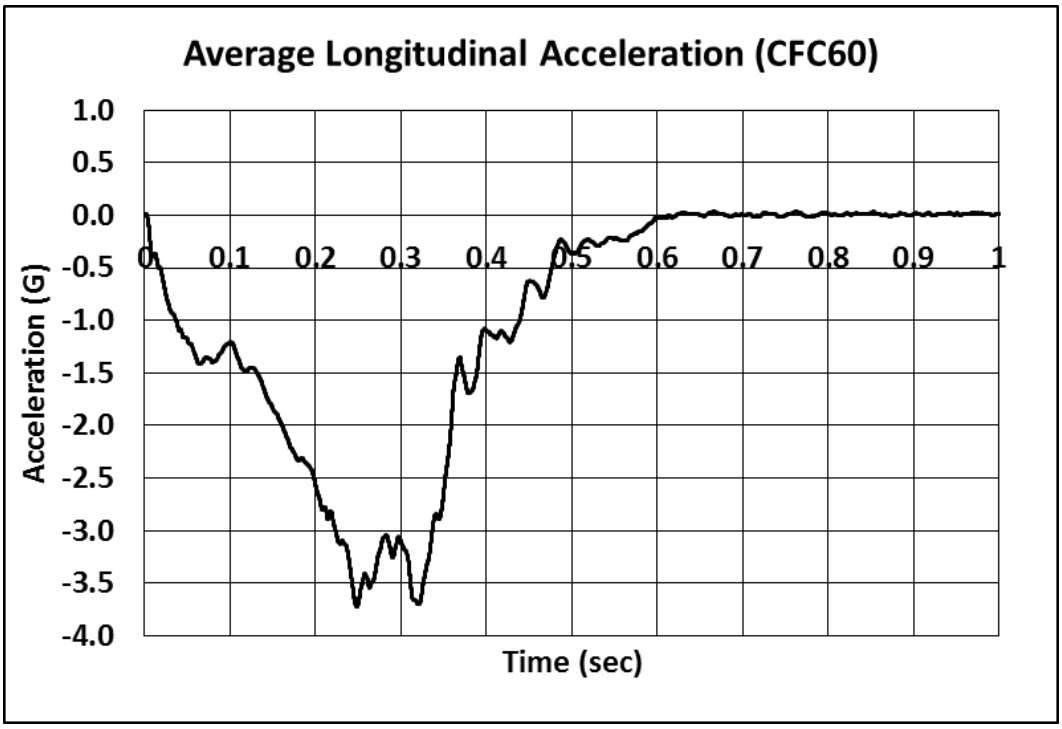

Figure 15. Longitudinal Acceleration Data (Averaged)

The ram car's velocity history in the test can be calculated by integrating the average longitudinal acceleration of the ram car and using the impact speed measurement as an initial condition. Contact forces between the ram and target tank car can be calculated as a product of the average acceleration and mass of the ram. Figure 16 shows both the force-time and velocity-time histories, where negative velocity is speed of rebounded ram car. The ram car came to a stop (0 mph) at approximately the same time as the second peak in the force data. Because the tank car did not puncture, the total impact energy of 2,146,350 ft-lb was absorbed.

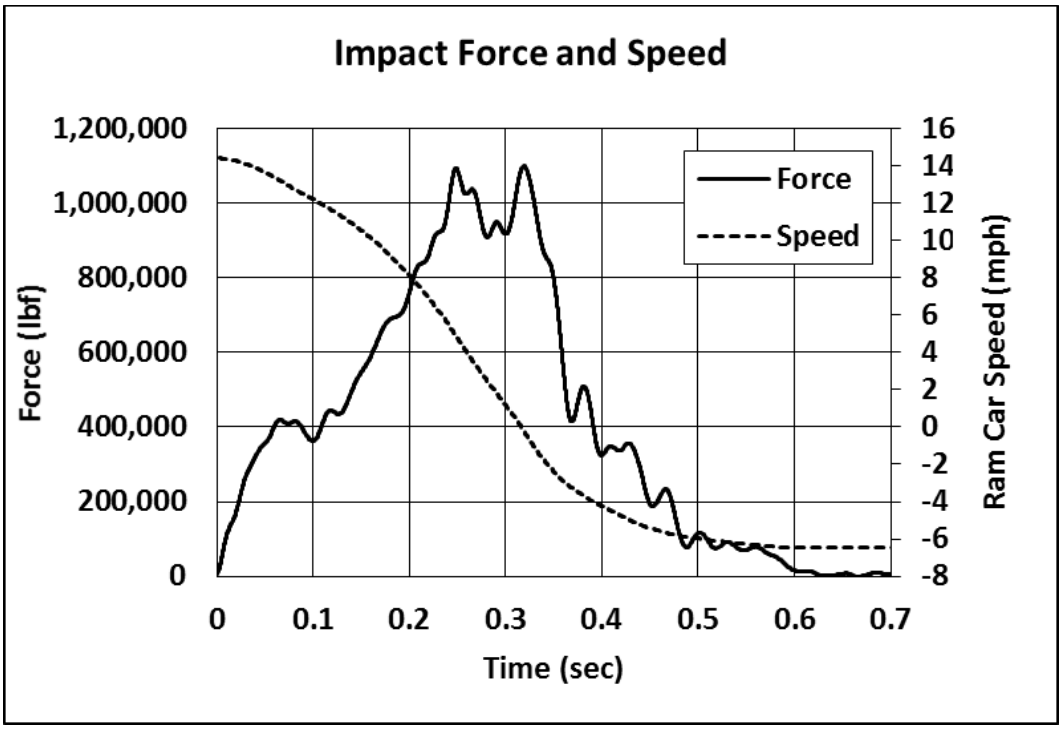

Figure 16. Impact Force and Ram Car Speed

The test also measured another significant impact response, the effects of the internal pressure as the tank indentation forms and reduces the volume of the tank. The tank is initially unpressurized relative to atmospheric pressure. However, the tank was filled to an approximately 4 percent outage volume with water, which is approximately incompressible for the impact behavior. As a result, the small gas volume in the outage, initially at one atmosphere, was compressed as the dent formation reduced the tank volume and the internal pressure rapidly increased. As described in Section 2.3, pressure transducers were mounted at several locations in the tank within the water and at the pressure release valve within the air.

Figure 17 shows pressure data from the center of the tank car (transducers TP1090, TP1180, TP1270, and TPV). When the pressure data was compared, it was evident that the pressure was dominated by the average hydrostatic pressure developed from the denting and the change in volume. However, there were additional dynamic pressures caused by the sloshing motions of the water in the tank. These pressures added local pressure variations that could be up to approximately 30 psi different from the average value. Also, it should be noted that a time delay can be seen as the pressure wave from the impacted front wall was transmitted through the structure and lading before it was fully felt along the tank bottom and back face.

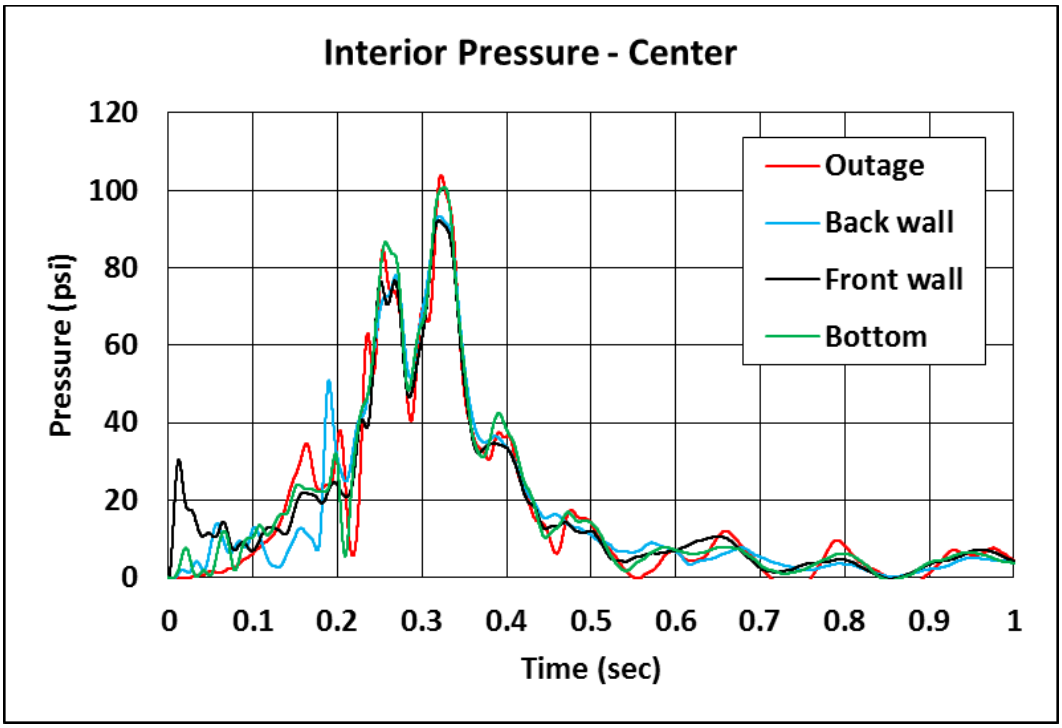

Figure 17. Pressure Data Measured at the Center of the Tank Car

The remaining quantitative measurements made of the tank impact behavior were displacement histories recorded with string potentiometers. These included both internal tank deformations and external tank movements at both ends of the tank. Layout of the string potentiometers is described in Section 2.3.

The measured displacements for the tank internal string potentiometers (TD1Y through TD5Y) are shown in Figure 18. Note that the longitudinal tank crush at the centered string potentiometer location exceeded the limit of the instrumentation, and the test traces max out at 45 inches. The string potentiometers that were offset 48 inches from the center reached a maximum value of approximately 24 inches. Overall, the data shows consistent measurements of tank deflections with the largest deflection at the impact and reduced displacements at distances further from the center of the impact indentation.

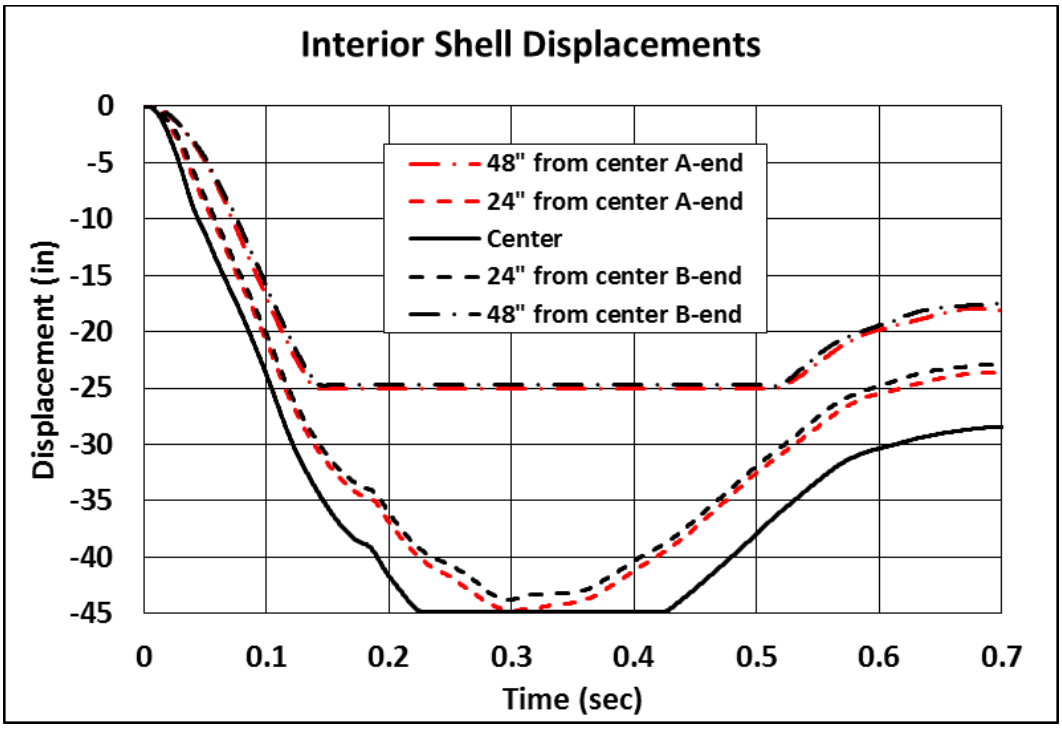

Figure 18. Internal Displacements

The measured displacements for the tank end external string potentiometers are shown in Figure 19 and Figure 20. The displacements of the car end were significantly delayed from the motions in the impact zone and little displacement is seen for the first 150 milliseconds of the response. Note that the measurements of the car end head displacements and the skid displacements are nearly identical and the response is very symmetric between the A-end and B-end of the tank until rebound occurred approximately 0.3 second after impact.

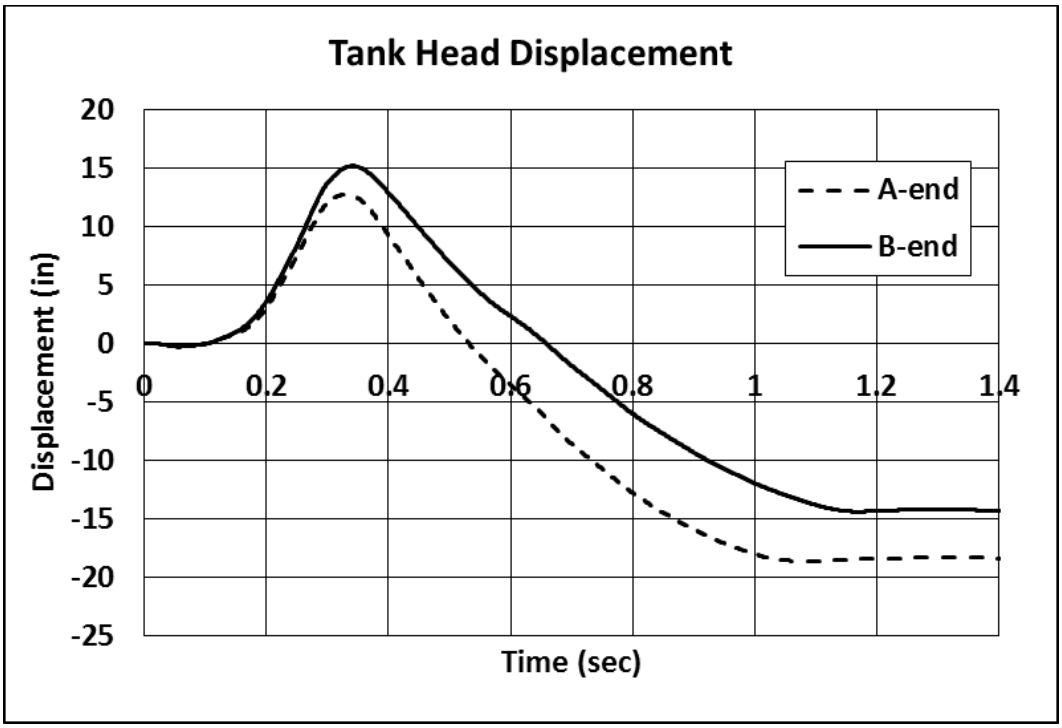

Figure 19. External Displacements – Tank Car Heads

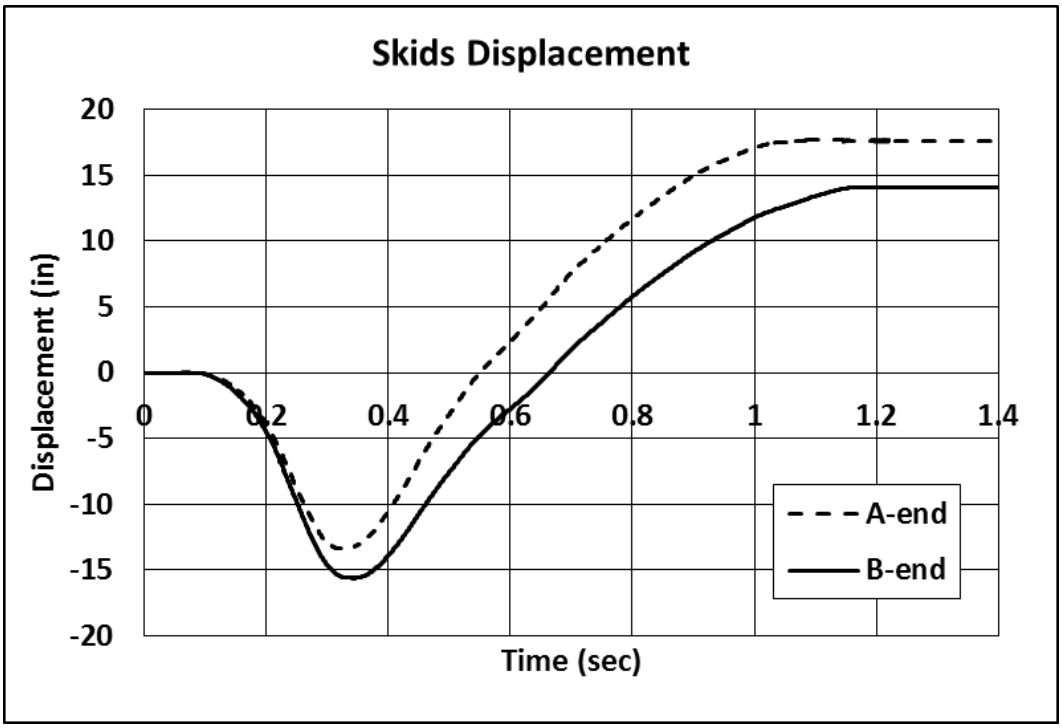

Figure 20. External Displacements - Skids

4. Finite Element Model Development

Before the test, a finite element (FE) model of the DOT-112 tank was used to plan instrumentation placement and estimate the desired impact speed. Volpe developed the FE model by incorporating and building upon several modeling techniques used during previous tank car impact tests [3, 4, 5]. These techniques included modeling an elastic-plastic material response for the tank and jacket, ductile failure implementation of the Bao-Wierzbicki (B-W) failure model, and explicit modeling of the water and air phases within the tank. Following the test, the model underwent several adjustments to obtain better agreement between the test results and the FE results.

The purpose of the pre-test model was to provide a conservative estimate of the test speed that would not puncture the tank. For example, the outage within the tested tank was measured in two ways before the test. The first method measured the volume of water necessary to achieve shell-full condition, and measured the volume of water removed from the tank to achieve a 4 percent outage. A second measurement of the height from the top of the water to the top of the tank yielded an estimated outage of 3.25 percent. Since a conservative approach was being taken in the pre-test model, the smaller outage was used.

The impact conditions for the test (and therefore the FE model) were chosen specifically to permit comparisons between this test and the 2013 test of a DOT-111 tank car [2]. As previously described, the 12-in by 12-in ram head was used in this DOT-112 impact test and the DOT-111 test. Additionally, although the DOT-112 car is typically used to transport commodities under pressure, it was not pressurized for this test, because the DOT-111 tank car is not a pressurized car. The DOT-112 was loaded as an analog to an unpressurized tank car equipped with a jacket and used to transport a liquid commodity.

The combination of an unpressurized tank car, a relatively small outage, and a large impactor was expected to present challenges in modeling the response of the water and gas phases of the lading. A larger indenter is expected to engage more of the fluid, resulting in a larger decrease in outage volume, and since the outage is already relatively small, it was expected that a significant amount of element distortion and pressure rise could occur in this model. Finally, the use of an unpressurized gas phase was expected to allow the gas phase to deform more easily than if a pressurized gas phase was used. A relatively new modeling technique, smoothed particle hydrodynamics (SPH), was employed in both the pre-test and post-test FE analyses to model the gas phase of the lading.

The impact force of the test is plotted against the relative travel of the impactor in Figure 21. This figure shows the force-displacement response of the test, the pre-test FE model, and the post-test FE model. In the test, the mass of the impactor is multiplied by the average deceleration. In both FE models, the acceleration is calculated at a single point on the ram, owing to the use of a rigid body to model the ram. Therefore, the impact forces in the FE models are simply the product of impactor mass and acceleration. A CFC60 filter has been applied to these results. The FE models were run for sufficient time to capture the impact event from first contact through the impactor rebounding from the tank.

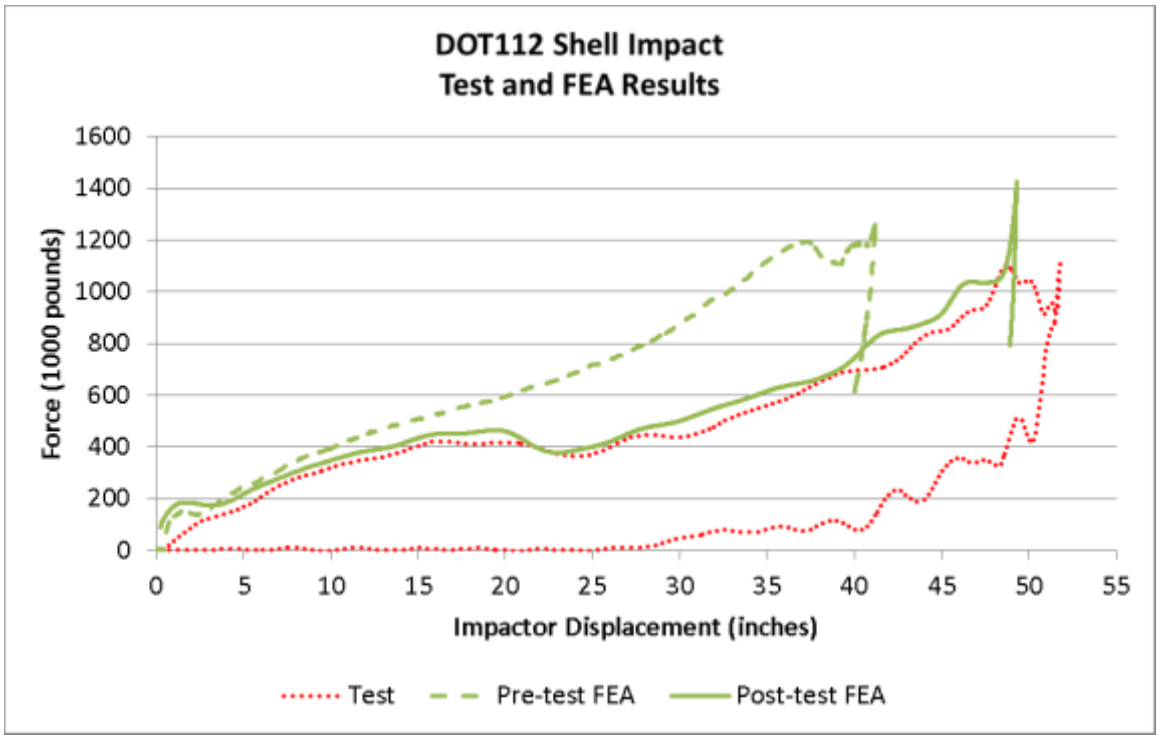

Figure 21. Comparison of Test, Pre-Test FEA, and Post-Test FEA Force-displacement Responses

Following the test, several changes were made to the model to improve its agreement with the test results. Those changes are discussed in Section 6. The post-test model was conducted to improve the ability to approximate the actual conditions of the test, and improve the agreement between the test and Finite Element Analysis (FEA) results. In the case of some pre-test conservative assumptions, less conservative assumptions that were more representative of the test conditions were applied to the post-test model. For example, the post-test model using a 4 percent outage was found to give a better force-displacement and pressure-time response than the pre-test model using a 3.25 percent outage.

The models were developed using the Abaqus/CAE preprocessor and executed in Abaqus/Explicit [6]. Abaqus/Explicit is a commercially available, general purpose nonlinear finite element solver capable of simulating dynamic impacts involving complex material behaviors such as plasticity and puncture. The Abaqus software also includes several modeling techniques to represent the water and air phases of the lading, permitting these two parts to be modeled explicitly.

4.1 Overview of Models

The pre-test and post-test FE models employ geometry that represents the different components which make up the test setup, set material parameters which describe the behavior of the materials that make up the car, and numerous constraints, boundary conditions, and loads describing the conditions of the test.

The model used a half-symmetric condition, with a vertical-longitudinal symmetry plane at the centerline of the tank car to reduce the size of the model. The tank geometry was simplified and structures such as the manway and bolster omitted. Under the test conditions, these simplifications have a relatively minor effect on the impact response of the tank. The pre-test model is shown in Figure 22. Note that the tank is not clearly visible in this figure because it is contained within the jacket. In the post-test model, the ground plane was omitted, and the symmetry wall was extended to prevent air particles from escaping from the air phase.

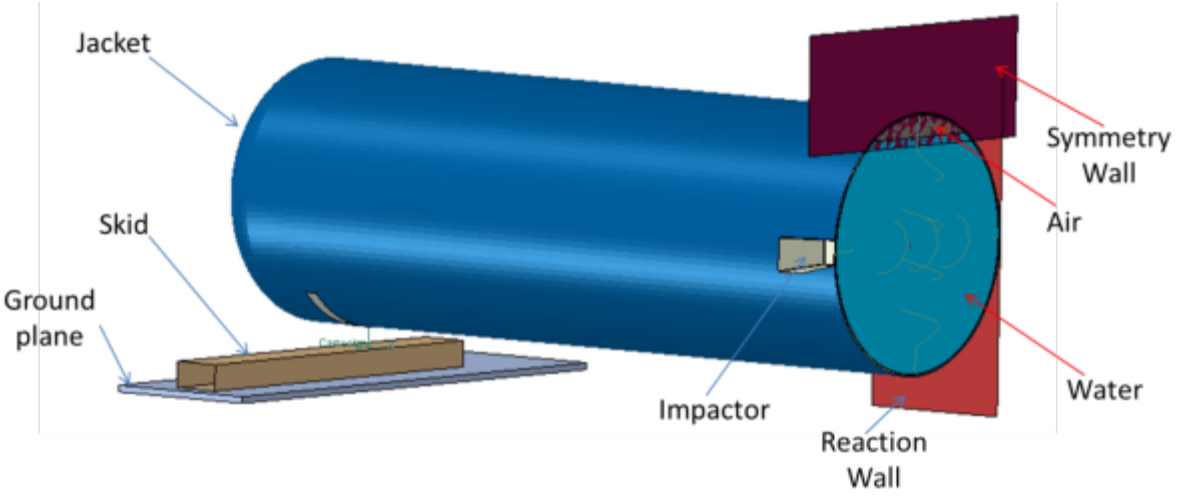

Figure 22. Annotated Pre-Test FE Model

4.2 Summary of the Assembly

The parts that make up the model can be divided into three categories: rigid bodies, deformable bodies that are made of steel, and deformable bodies that are made of other materials. Because the model was half-symmetric, the FE model's part weights generally correspond to half of the weight of the actual tested geometry except for the the skid, as the skid exists entirely to one side of the symmetry plane. Therefore, the full weight of the skid is included in the model. Table 5 contains a summary of the parts that make up the FE models. This table contains the weight of the part in the model, as well as the weight of the full part (2x model weight) for applicable parts. A full description of each part can be found in Appendix D.

Table 5. Summary of Parts in FE Models

		Number of Elements	Part Weight (in model)	Part Weight (Full)
		-	lbf	lbf
Rigid Bodies	Impactor	3,320	148,562	297,124
	Rigid Wall	15,802	N/A	N/A
	Skid	12,240	3,500	3,500
	Symmetry Wall	Pre-Test: 900 Post-Test: 3,306	N/A	N/A
Deformable, Steel	Jacket	18,681	6,615	13,230
	Tank Shell Elements	Pre-Test: 37,335 Post-Test: 36,855	25,151	50,302
	Tank Solid Elements	90,828	29	57
Deformable, Other Materials	Tank Lading Air	Pre-Test: 15,800	Pre-Test: 5.95	12
		Post-Test: 24,720	Post-Test: 7.26	15
	Tank Lading Water	Pre-Test: 130,772	Pre-Test: 137,983	275,967
		Post-Test: 433,693	Post-Test: 136,940	273,880

4.3 Material Behaviors in FE Models

Three material definitions were used in both the pre-test and post-test FE models without adjustment: steel A-1011, water, and air. A fourth material, TC128 steel, was modeled using different properties in the pre-test and post-test models. The material properties that are entered into the FE models are summarized in this section. Complete descriptions of the development of the A1011 and TC128 characterizations are given in Appendix F.

4.3.1 A1011

The outer jacket was presumed to be made of A-1011 for. To ensure a conservative FE model, the minimum properties for A-1011 were used as inputs to the model. The model included a bi-linear representation of the stress-strain response of the material. The material exhibited a linear

elastic response up to the yield strength of the material. After reaching the yield strength, the stress-strain relationship was described by a line between the yield strength and the ultimate strength. The ultimate strength was assumed to occur at a strain equal to the minimum elongation at the specified failure for the material. Table 6 gives the engineering unit values for the minimum properties for the outer jacket A-1011.

Table 6. Minimum Properties for A-1011

Property	Value
Young's Modulus (E)	$3x10^7$ psi
Yield Strength	30,000 psi
Ultimate Strength	49,000 psi
Elongation at Failure	25%

A simplified failure model was used in the pre-test and post-test FE models. In the pre-test model, if the plastic equivalent (PEEQ) strain reached 0.4 within an element, that element began to soften until it lost all load-carrying capability and was removed from the simulation. This was a conservative assumption chosen to ensure the jacket did not absorb more energy prior to puncture than would be expected of the jacket in the test. In the post-test FE model, the PEEQ strain criterion was increased to 0.5 based upon the actual results of the test.

4.3.2 Water

The liquid phase of the lading was modeled as water at approximately 40°F. Within Abaqus, the Us-Up equation of state (EOS) model describes the behavior of the liquid water. The key material properties that must be added to the model are the material's density, the speed of sound (c_0), and the dynamic viscosity of the water. The properties used in the DOT-112 tank car model are shown in Table 7. This table includes the nominal units and the specific units required for the FE model.

Table 7. Properties for Water

Property	Value (nominal units)	Value (input to Abaqus)
Density	1,000 [7] $\frac{kg}{m^3}$	$9.42x10^{-5}$ $\frac{lbf\cdot\frac{s^2}{in}}{in^3}$
Speed of Sound (c_0)	4,672 [8] $\frac{ft}{sec}$	56,064 $\frac{inch}{sec}$
Dynamic Viscosity	$3.23x10^{-5}$ [9] $\frac{lbf\cdot sec}{ft^2}$	$2.24x10^{-7}$ $\frac{lbf\cdot sec}{in^2}$

4.3.3 Air

The gas phase of the lading was modeled as air at atmospheric pressure. In Abaqus, an ideal gas relationship allows the pressure within the air to change in response to changes in outage volume as the tank deformed and the water moved through the outage. Because discrete particles were used to model the gas phase, the pressure within the air varied not only with time but also with space, as individual particles would have different pressures. The ideal gas relationship within Abaqus requires the user to define the initial density of the material, the specific gas constant (R_{spec}), and the specific heat of the material. Note that the initial pressure of the gas phase is defined as an initial condition of the model, not specifically a material property. The material properties are given in nominal units as well as the specific units required for the FE model of the DOT-112 tank car in Table 8.

Table 8. Properties for Air

Property	Value (nominal units)	Value (input to Abaqus)
Density	1.284 [10] $\frac{kg}{m^3}$	1.21×10^{-7} $\frac{lbf \cdot \frac{s^2}{in}}{in^3}$
Specific Gas Constant (R_{spec})	287 [11] $\frac{J}{kg \cdot K}$	444,580.9 $\frac{in \cdot lbf}{\left(\frac{lbf \cdot s^2}{in}\right) \cdot K}$
Specific Heat	1,003.8* [12] $\frac{J}{kg \cdot K}$	1,556,000 $\frac{in \cdot lbf}{\left(\frac{lbf \cdot s^2}{in}\right) \cdot K}$

*Due to an input error this value actually corresponds to c_p, the constant pressure specific heat for air at 1 atmosphere. Abaqus/Explicit solver requires c_v be used. This is expected to have minimal effects on the overall results of the analysis, as the temperature change in the gas phase is not a major factor in the behavior of the tank for this test.

4.3.4 TC128

This test was designed to subject the tank car to a moderately high speed impact without causing puncture of the tank. As a result, several assumptions were made to ensure that the pre-test model was conservative. In this research program, conservative refers to the model's tendency to predict a puncture speed that is below the speed at which puncture is likely to occur during the test. One assumption involved the material properties of the TC128 material which makes up the tank.

While the certificate of construction stated that the tank was manufactured from TC128 Grade B normalized steel, the stress-strain response of the steel in the test car was not known. As a conservative assumption, the pre-test model represented TC128 steel as having the minimum yield strength, ultimate strength, and ductility that complies with the specification. The ultimate strength was assumed to occur at a strain that was equal to the minimum elongation at failure specified for the material. The minimum properties in engineering units are given in Table 9.

Table 9. Minimum Properties for TC128B

Property	Value
Young's Modulus (E)	$3x10^7$ psi
Yield Strength	50,000 psi
Ultimate Strength	81,000 psi
Elongation at Failure	22%

For the post-test model, a second set of material properties were considered. In the post-test model, "typical" properties were used to be more representative of the actual material making up the tested car. Properties of numerous tank cars retired from service in the United States were documented by McKeighan [13]. A subset of the data in this reference corresponding to tank cars of a post 1990 vintage (as the tested DOT-112 was) were used to characterize typical TC-128 behavior. The resulting properties, in engineering units, are summarized in Table 10.

Table 10. Typical TC128 Properties used in Post-Test FE Model

Average Yield Strength	56,300 psi
Average Ultimate Strength	82,200 psi
Average Elongation	29.5%
Average %RA	58.2%

For both the pre-test and post-test characterizations of TC128, a bilinear stress-strain response was used. The material exhibited a linear elastic response up to the yield strength of the material. After reaching the yield strength, the stress-strain relationship was described by a line between the yield strength and the ultimate strength. While there are many plastic stress-strain responses that could pass through the points that correspond to yield and ultimate strengths, the actual plastic stress-strain response for this material was not known. A straight line representation is the shortest path between yield and ultimate strengths, ensuring that the material characterization does not have a calculated toughness (area under the stress-strain curve) higher than the actual material could have.

Figure 23 plots the pre-test minimum plastic response and the post-test typical plastic response. This figure shows the typical material exhibits a higher ductility than the material possessing the minimum properties.

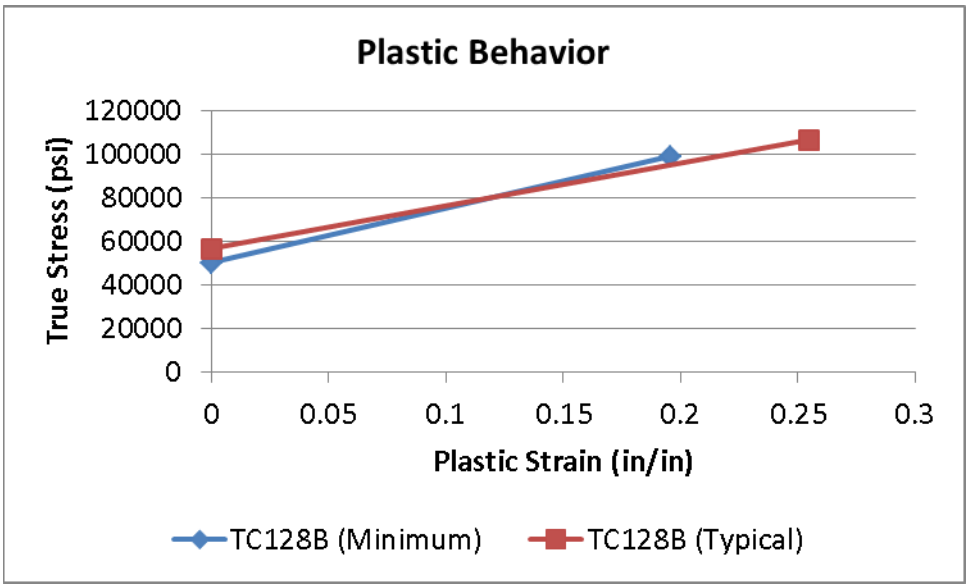

Figure 23. Pre-Test and Post-Test Characterizations of TC128 Plastic Behavior

A corresponding B-W damage initiation envelope was developed using the typical TC128 properties, using the methods described by Lee and Wierzbicki [14]. Because of the increased strength and ductility of the typical property material, the typical B-W envelope requires a higher PEEQ to initiate damage at a given triaxiality than the envelope that was developed for triaxialities greater than zero with the minimum-property TC128. Figure 24 shows the pre-test and post-test failure envelopes.

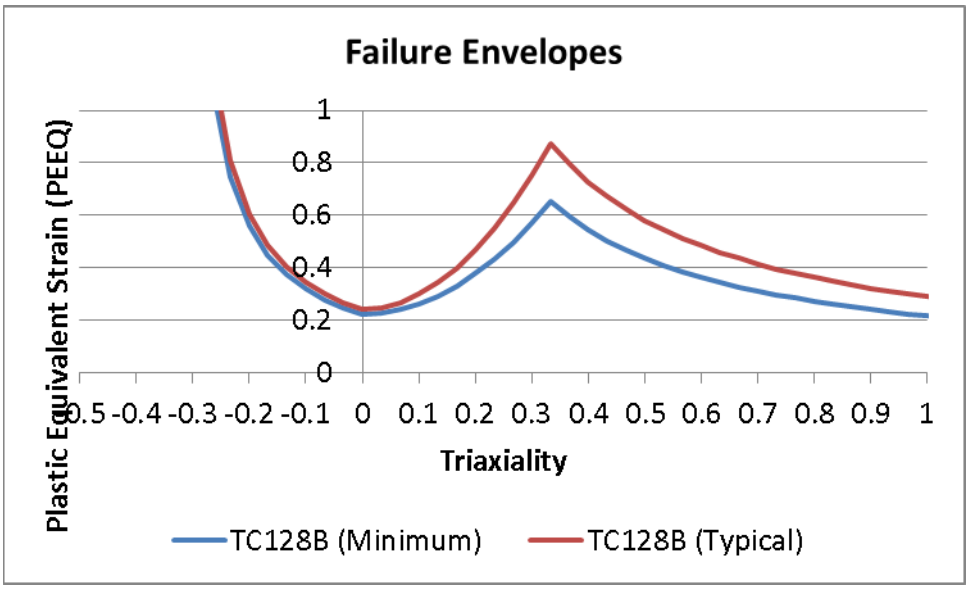

Figure 24. Pre-Test and Post-Test TC128 Failure Envelopes

4.4 Modeling Techniques Common to Pre-Test and Post-Test Models

A series of constraints, loads, initial conditions, and boundary conditions were applied to the model to approximate the loading and support conditions in the test. These techniques were generally common to both the pre-test and post-test FE models. Appendix E contains a detailed discussion of these techniques.

4.5 Modeling Techniques Adjusted between Pre-Test and Post-Test Models

Several modeling techniques were adjusted in the post-test model, on the basis of either re-examining the model or the outcome of the test. These modeling techniques and their adjustments are described in this section.

4.5.1 Friction Behavior

A significant difference to the overall stiffness of the system occurred when the coefficient of friction between the water and the tank shell was reduced. The pre-test model set the coefficient of friction between the water in the head of the tank and the interior surface of the head of the tank to 0.3. This technique prevented excessive element distortion among the water elements in the head. When the results of the pre-test model were reviewed, they revealed that the contact definition between the *entire* interior of the tank and the exterior surface of the water was using a coefficient of friction of 0.3. In the post-test model, the coefficient of friction between the shell of the tank and the water was corrected to a value of 0.02. While ideally a frictionless formulation would be used, as water has an explicitly defined viscosity within this model, frictionless contact led to model instabilities. Therefore, a value of 0.02 was chosen as a near-frictionless contact that prevented model instability from occurring.

4.5.2 Outage Behavior

The volume of the outage was the second modeling technique to have a significant effect on the global model's stiffness. Generally, a smaller outage will result in a stiffer impact response, as the water is effectively incompressible under these impact conditions. While the outage is typically defined as a percentage of the total tank volume, the practical way of defining FE model geometry requires specific dimensions to be defined, corresponding to the desired outage. In the pre-test model, the critical dimension that was used in defining the outage was the vertical height of the air between the top surface of the water and the interior of the tank at the top of the tank, as shown in Figure 25.

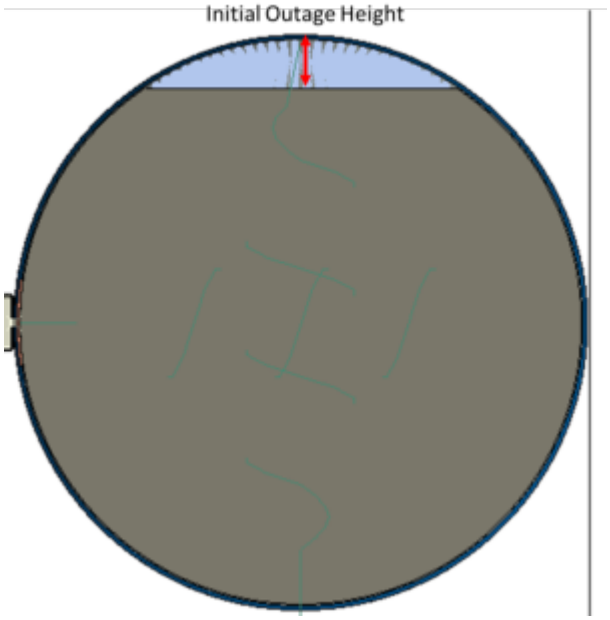

Figure 25. Initial Outage Height

To facilitate the modeling of a given outage volume, a relationship between the initial height of the outage and the corresponding outage volume was developed using a geometric model within Abaqus/CAE. The model was filled to shell-full condition with material, and the volume of this material was calculated by the Abaqus/CAE software. A portion of the material corresponding to a certain height of outage was then removed from the model, and the volume of the remaining material calculated. The outage volume corresponding to a particular outage height is therefore the ratio of the removed volume of material to the shell-full volume of material. The outage relationship for this FE model is shown in Figure 26.

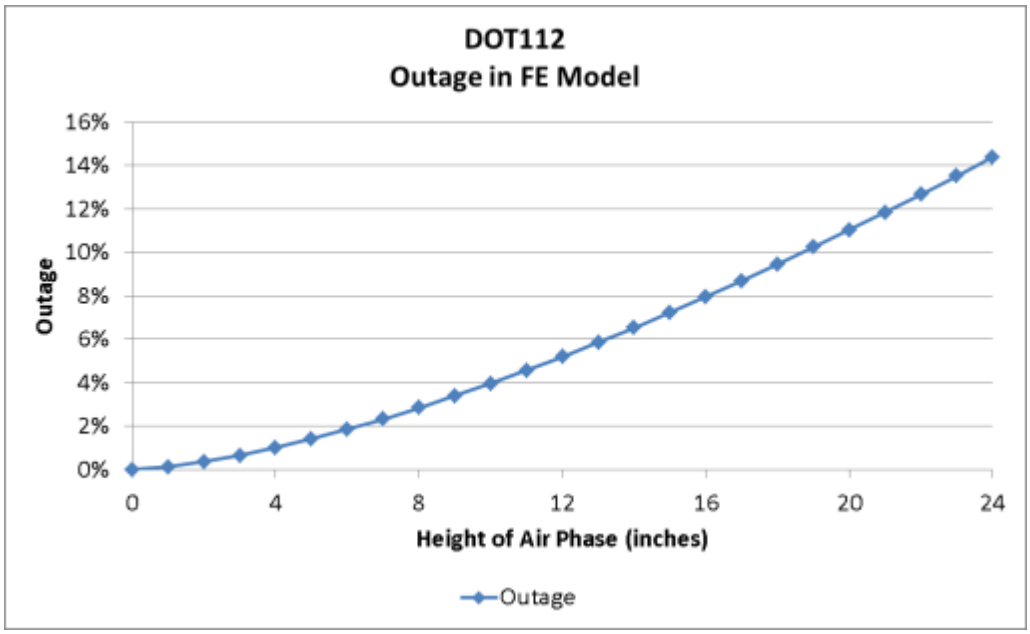

Figure 26. Outage Percentage and Outage Height Relationship

The desired outage for the test was 4 percent. From the relationship above, this corresponds to an initial outage height of approximately 10 inches in the FE model. During test preparations, the tank was filled to 100 percent of its capacity, and then 4 percent of this volume was pumped out of the tank. TTCI measured the height of the outage as approximately 8.75 inches. From the outage relationship above, an outage height of 8.75 inches corresponds to a 3.25 percent outage. This discrepancy between outage height and outage volume is probably due to imperfections in geometry of the tank and tank's shell deformation under the load. This issue was handled by conservatively modeling the smaller outage of 3.25 percent in the pre-test FE model, and modeling the 4 percent outage in the post-test FE model which resulted in better agreement between test and analysis.

4.5.3 Skid Behavior

The skid behavior plays a less important role in the model's ability to capture the overall response of the tank than the friction or the outage behavior. However, the skid behavior was adjusted after the test because of relatively poor agreement between the pre-test model and the test results. The resisting force offered by contact between the ground and the skid was approximated with a nonlinear "Cartesian" type connector in both the pre-test and post-test FE models. This approach was chosen over relying on contact between the skid and a ground plane, as contact would require modeling the effects of gravity to develop the normal forces between the skid and ground. From examination of the skid behavior in the test and the pre-test model, it was apparent that the skid motion in the FE model was greatly inhibited compared to the test results. In the post-test model, the nonlinear spring consists of an initial peak that must be overcome before a skid may begin its travel. Once this peak value is overcome, the force drops off to a near-zero level, which permits unrestricted travel of the skid. This behavior is intended to approximate static friction, which initially prevents movement of the skid and unrestricted motion once the skid begins to move. The pre-test and post-test skid behaviors are shown in Figure 27.

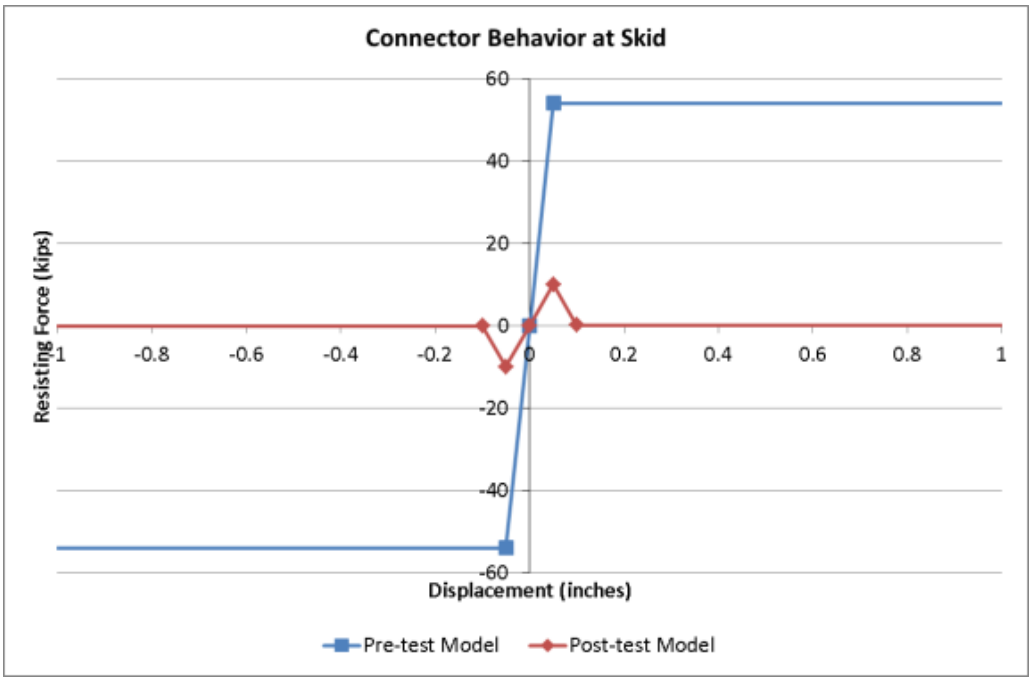

Figure 27. Connector Behavior at Skid for Pre-Test and Post-Test FE Models

To achieve better agreement between the measured test results and the response of the FE model, the behavior of the skid was adjusted to require a smaller force for initiating motion and a decrease in force once the skid has begun to move. The skid displacements are compared between the test and the pre-test and post-test models in Sections 5 and 6, respectively.

4.5.4 Tank Alignment with Wall

In the pre-test FE model, the jacket of the tank was aligned to be tangent with the rigid impact wall. Prior to the test, a ~0.5-inch gap between the back of the jacket and the rigid impact wall was observed. This initial displacement was included in the post-test FE model. This gap was expected to have a minimal effect on the overall response of the tank, but it could have potentially influenced the timing of the impact event. The initial gaps in both the test and FE model are shown in Figure 28.

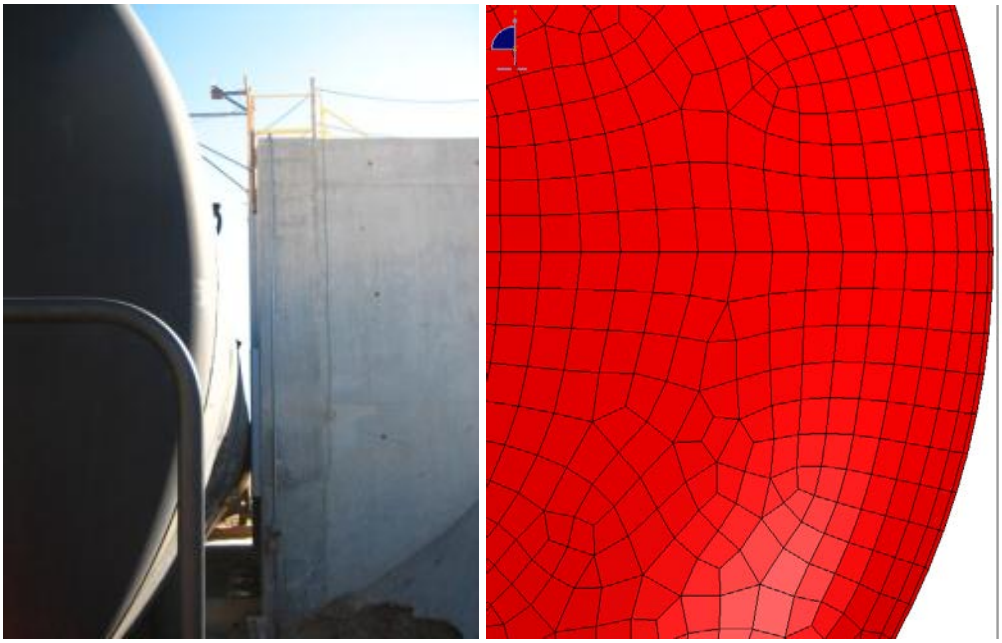

Figure 28. Initial Jacket-wall Gap in Test (left) and FE Model (right)

5. Comparison of Test Response to Pre-Test Analysis

Pre-test FE modeling was used to estimate the overall response of the tank to the impact, including the force-displacement response. Because of uncertain parameters (e.g., material properties, actual outage, actual test speed), the pre-test model was designed to provide a conservative (i.e., lower-bound estimate of puncture speed) to ensure that the test did not result in the puncture of the tank. In this context, conservative refers to the model's tendency to predict puncture at a speed below the minimum speed needed to puncture the tested tank.

The model predicted that the tank would not be punctured in a 15-mph impact. The pre-test FE model was executed with a 15 mph impact speed and an 8.75-inch high outage. Pre-test models run above 15 mph indicated that a puncture could occur at speeds between 15-16 mph. Since the actual impact speed in the test could vary from this target value by +/- 0.5 mph, the likelihood of puncture would increase if the actual test speed was at the high-end of the speed range.

The key results that were compared between the pre-test FEA and the actual test were the force-displacement responses, the pressure-time histories, the skid displacement, and the reduction in tank diameter at the impact sitepre-test. While the force-displacement response from the pre-test model generally described the behavior of the tank during the test, it was apparent that the model was behaving in an overly stiff way relative to the test measurements. The slight difference between the simulated impact speed of 15 mph and the actual test speed of 14.7 mph does not sufficiently explain the overly stiff response of the FE model. The peak force in the second peak calculated by the model was approximately 14 percent higher, compared to the peak forces obtained through the average of the test accelerometers. While the model also captured the double-peak behavior experienced by the tank at the very end of the impact event, the model did not capture the more gradual peak during the first 25 inches of impactor travel. The average force-displacement response from the test (red) and the force-displacement response from the pre-test FEA (green) are shown in Figure 29.

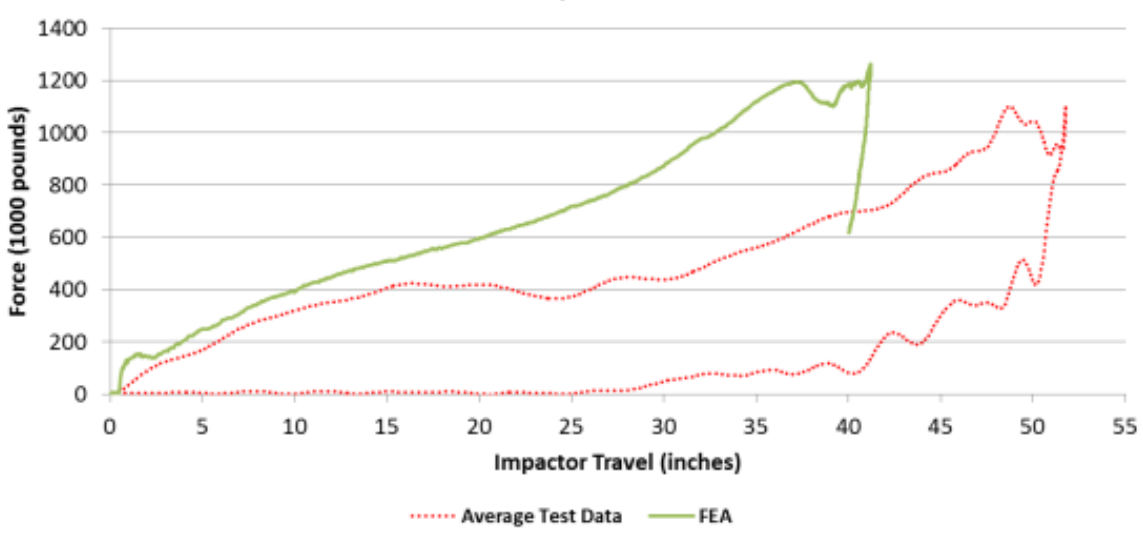

Figure 29. Pre-Test FEA and Test Force-displacement Results

Figure 30 displays a series of frames from the pre-test FE model. These images show the water sloshing within the tank and forming a wave as the impactor causes a larger displacement on the front end of the tank.

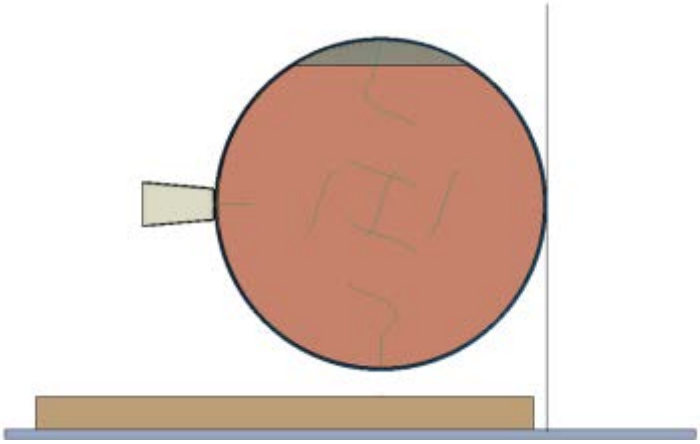

t=0.0s
Initial Position of Model

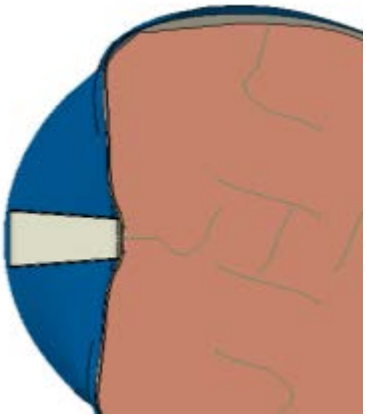

t=0.12s
Midway through Impact

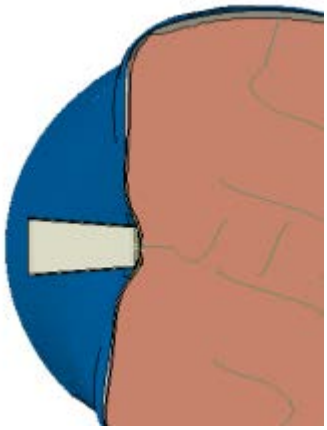

t=0.2550s
Slightly after Ram Begins to Rebound

Figure 30. Impact Progression, Pre-Test FE Model

In the test, the pressure was measured at nine locations within the lading (water). Pressure-time history was requested for elements at locations that correspond to the initial pressure transducer locations. There is a slight difference in the two methods used to measure pressure. In the test, pressure transducers were physically attached to the wall of the inside of the tank. As the tank deformed, the pressure transducers moved with the local area of the tank through the water. In the FE model, the pressure-time history was collected from specific elements that were initially at the locations corresponding to the pressure transducers within the tank. As the water deforms, these particular elements may move relative to the wall of the tank. While the pressure-time history measured in a given element describes the behavior of that particular element, it will differ from the test measurements obtained for sufficiently large motions of the water. The average pressure-time history was obtained from the nine pressure transducers in the test and corresponding water elements in the FE model. The results from the pre-test FE model and the test are plotted against one another in Figure 31. While the FE model captures the general quality of the pressure-time history, the model experiences a climb in pressure that occurs much earlier than it does in the test. The model also experienced a peak pressure greater than that measured during the test. These discrepancies were reduced after correction of coefficient of friction as described in Section 4.5.1.

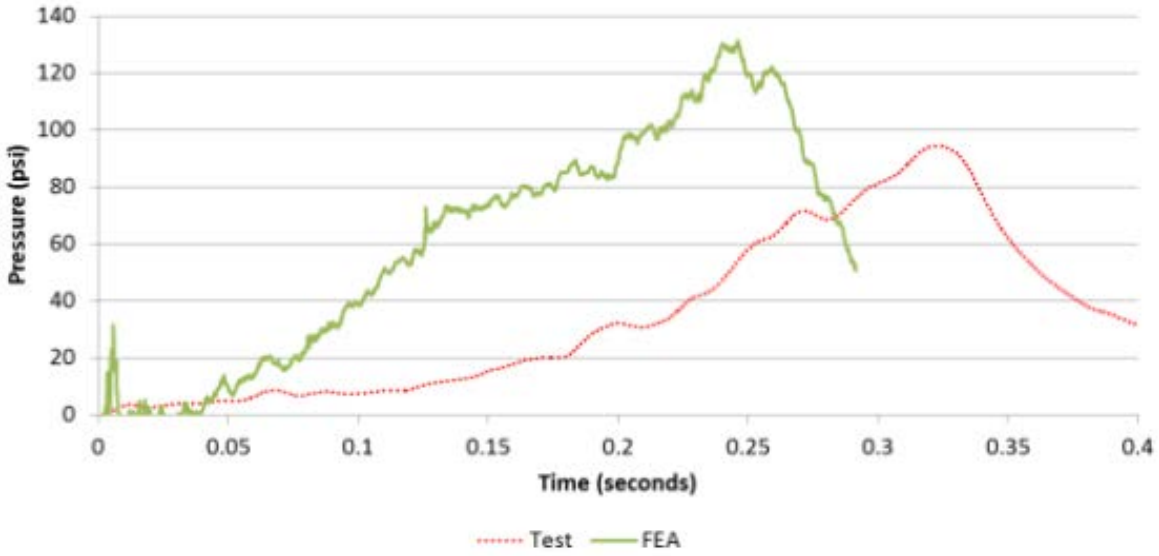

Figure 31. Average Water Pressure in Pre-Test FEA and Test

In Figure 32, displacement at the skid in the FE model is compared with the A- and B-end skid displacements that were measured during the test. This figure shows the pre-test FE model experiences significantly less skid motion than either of the skids from the test. The points on the test measurements indicate the point of maximum travel measured during the test.

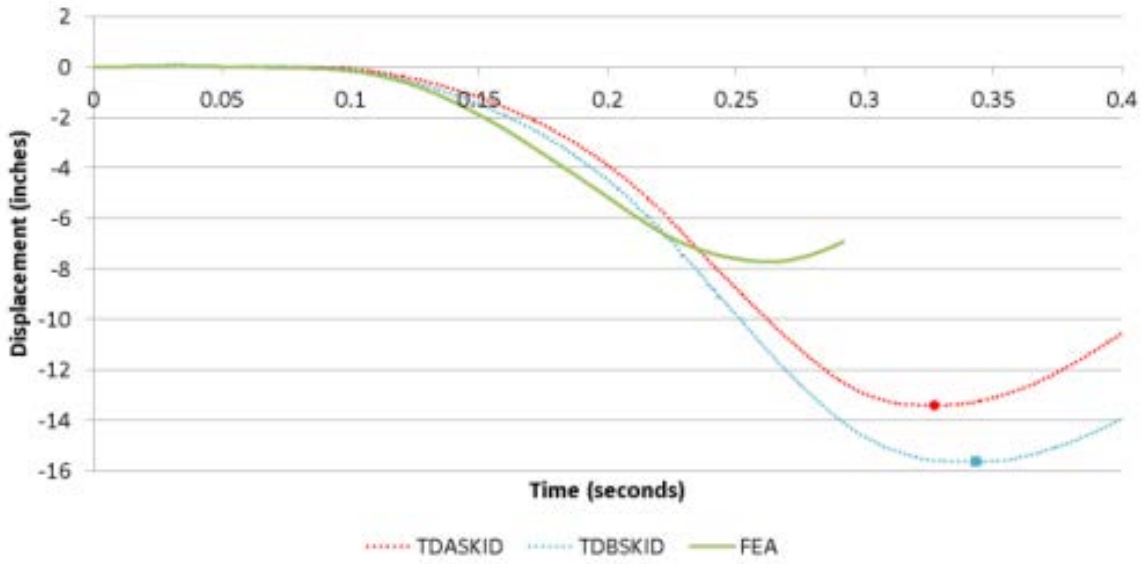

Figure 32. Skid Displacement in Pre-Test FEA and Test

The indentation at the center of the tank was measured in the test by string potentiometers and calculated in the FE model using soft springs. The two results for the center of the car are plotted in Figure 33. From this result, it is apparent that the model's response is overly stiff, as the indentation is smaller than that measured in the test.

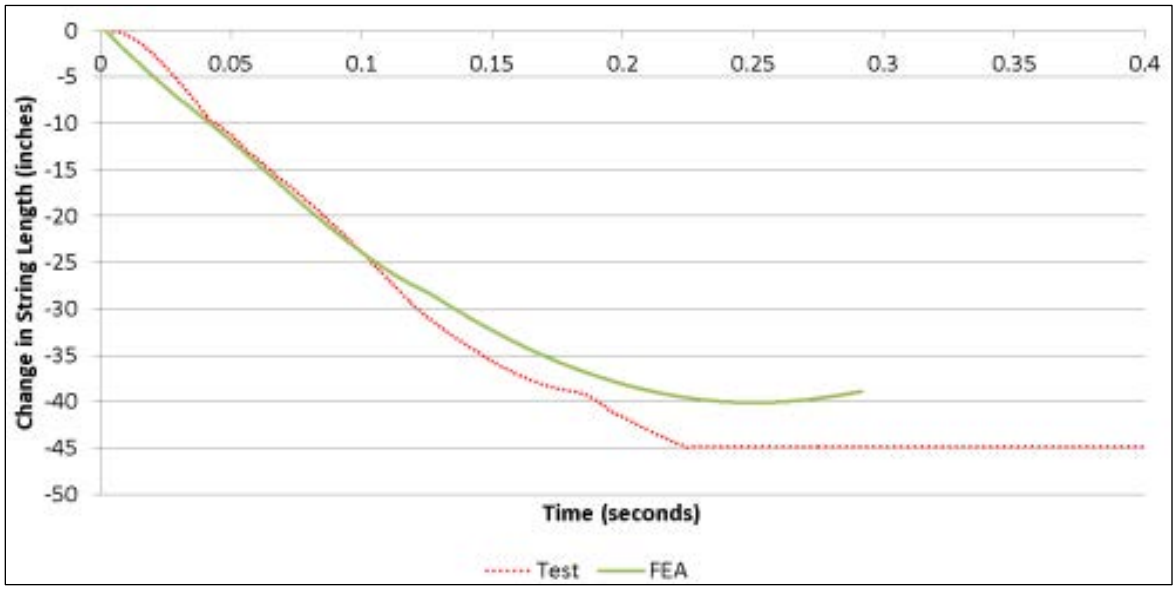

Figure 33. Internal String Potentiometer Measurement at Center of Tank in Pre-Test FEA and Test

Based on the comparisons between the pre-test model and the test results, several changes were made to the pre-test model to achieve better agreement between the model results and the test results. These model changes are described in Section 4.5. The post-test FE model is compared with the test results in the next section.

6. Comparison of Test Response to Post-Test Analysis

Several changes were made to the pre-test FE model following completion of the test to attempt to bring the model into closer agreement with the measured test results. While the overall intent of the pre-test modeling was to make conservative assumptions in order to ensure a high likelihood of a non-puncture test, some of these assumptions were reconsidered in the post-test modeling.

Mainly, the friction coefficient applied to the water was adjusted, the outage level was adjusted to what was thought to be more representative of the outage in the test, and the TC128 material behavior was adjusted. Additional minor changes included adjusting the connector behavior at the skid and including a gap between the tank and the wall (as observed in the test setup). The post-test model was run at the actual test speed of 14.7 mph. The force-displacement results from the post-test model (green) compared to the test results (red) are shown in Figure 34. There is generally good agreement both with the overall shape of the response and the force levels in both the test and the model. In particular, the post-test FE model better captures the early response of the tank over the first 25 inches. The post-test model does experience an over prediction of the second peak at the end of the impact event. This over-prediction is probably due to the air phase of the model being compressed to an extreme degree, which permits the water to make contact with the top of the tank. The maximum displacement in the post-test model was 49.3 inches, which is in good agreement with the test measurement of 51.8 inches.

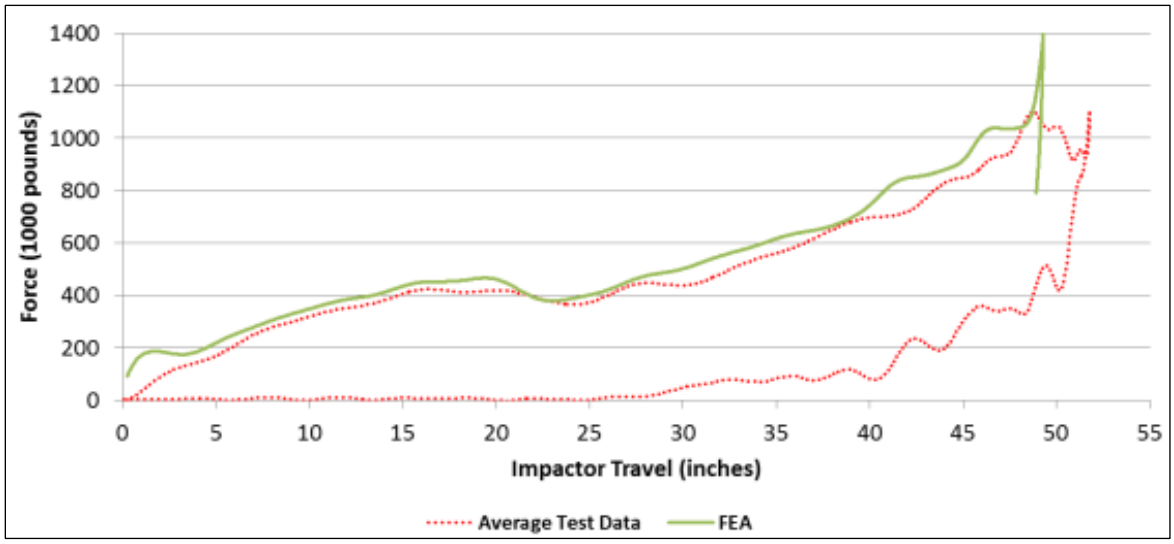

Figure 34. Post-Test FEA and Test Force-displacement Results

Figure 35 displays a series of frames from the post-test FE model. These images show the water sloshes within the tank and forms a wave as the impactor causes a larger displacement on the front end of the tank. By the end of the impact event, the outage has been compressed down to a much smaller volume than its initial value.

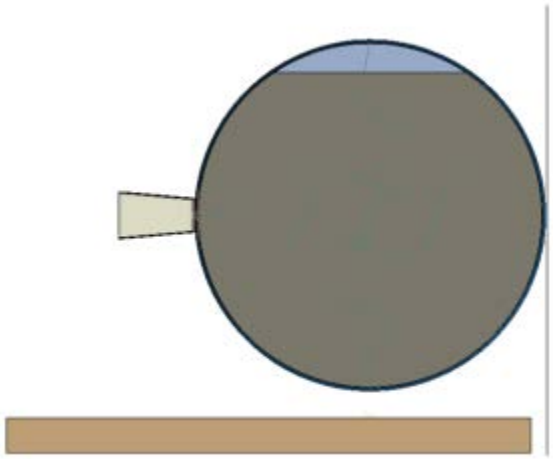

t=0.0s
Initial Position of Model

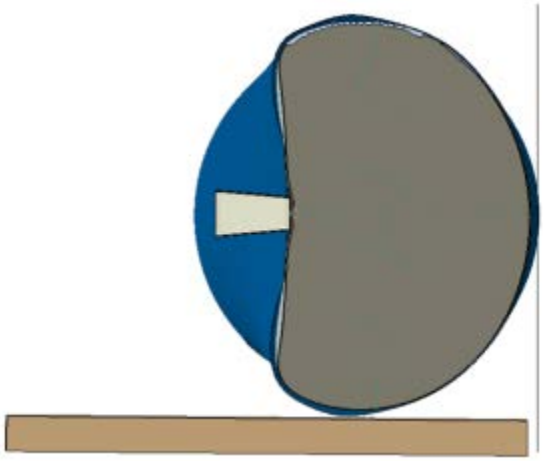

t=0.16s
Midway through Impact

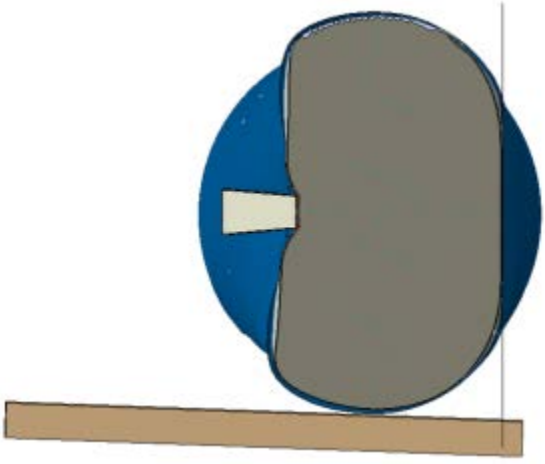

t=0.3s
Slightly after Ram Begins to Rebound

Figure 35. Impact Progression, Post-Test FE Model

Overall, the FE model does a good job of capturing fluid response during the test. The model exhibits somewhat higher pressures compared to the test, particularly as the fluid displacement increases toward the end of the impact event. Figure 36 shows side and front section views of the tank at two times. The top row corresponds to t=0, the initial position of the model. The bottom row corresponds to t=0.32 seconds, after the impactor has begun to rebound off of the tank. The bottom row of this figure shows the air volume has been greatly reduced by the end of the simulation, which probably caused the spike in force at the end of the simulation.

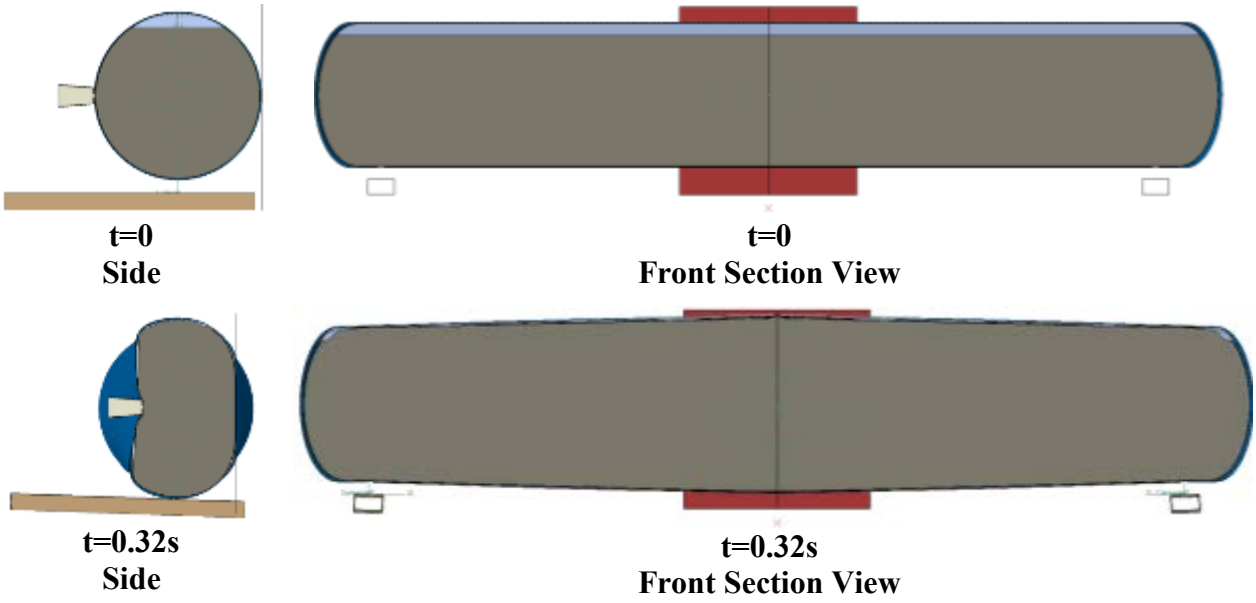

Figure 36. Front and Section Views of Lading at Start and End of Post-Test Simulations

As an overall comparison, the average pressure-time history from the nine transducers within the water in the test (red) and the nine corresponding elemental calculations in the FE model (green) are plotted in Figure 37. The general response exhibits good correlation between the test and the post-test model, but the model does exhibit higher pressures than those that were measured in the test for much of the response.

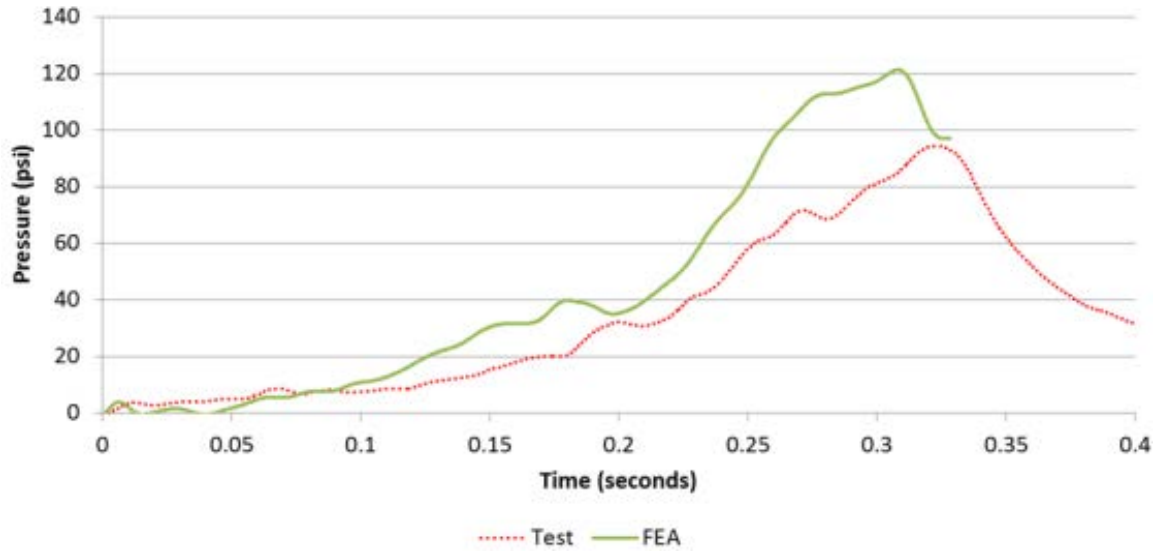

Figure 37. Average Water Pressure in Post-Test FEA and Test

Figure 38 contains a plot of the A-end (red) and B-end (blue) skid displacements measured during the test and the skid displacement calculated in the post-test FE model (green). While the skid displacement in the FE model is less than that measured during the test, there is much better agreement between test and post-test FEA than in the pre-test FE model.

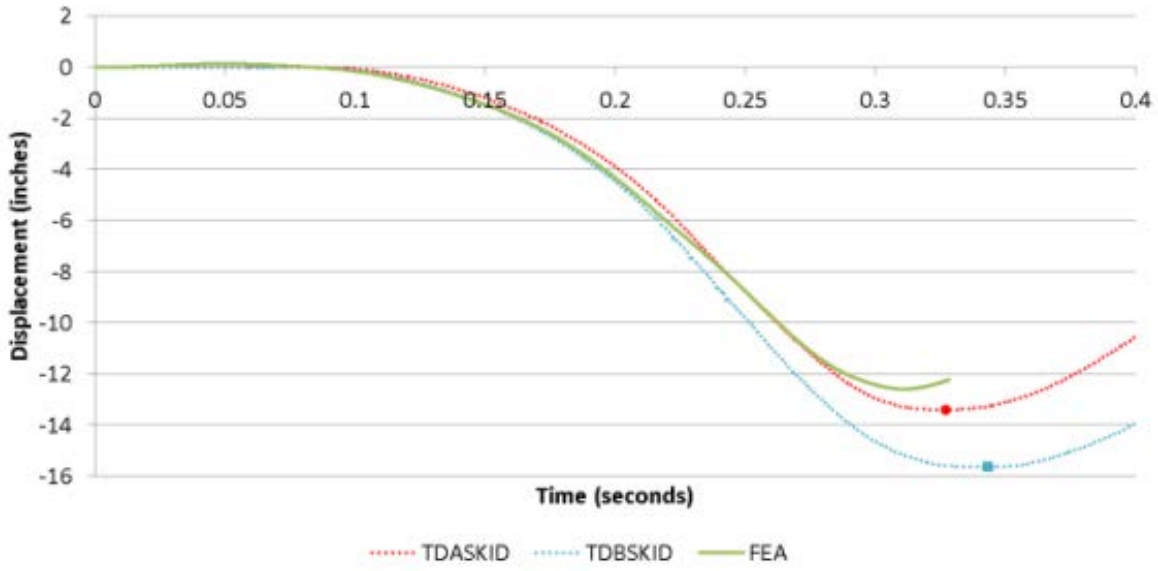

Figure 38. Skid Displacement in Post-Test FEA and Test

The indentation of the tank at the center of the tank was measured in the test by string potentiometers and calculated in the FE model using soft springs. The two results for the center of the car are plotted in Figure 39. This result shows better agreement between post-test FEA (green) and test (red) results than was seen in the pre-test FE model. Note that the test measurement reached the limit of the string's travel, while the FE model had no such limitation.

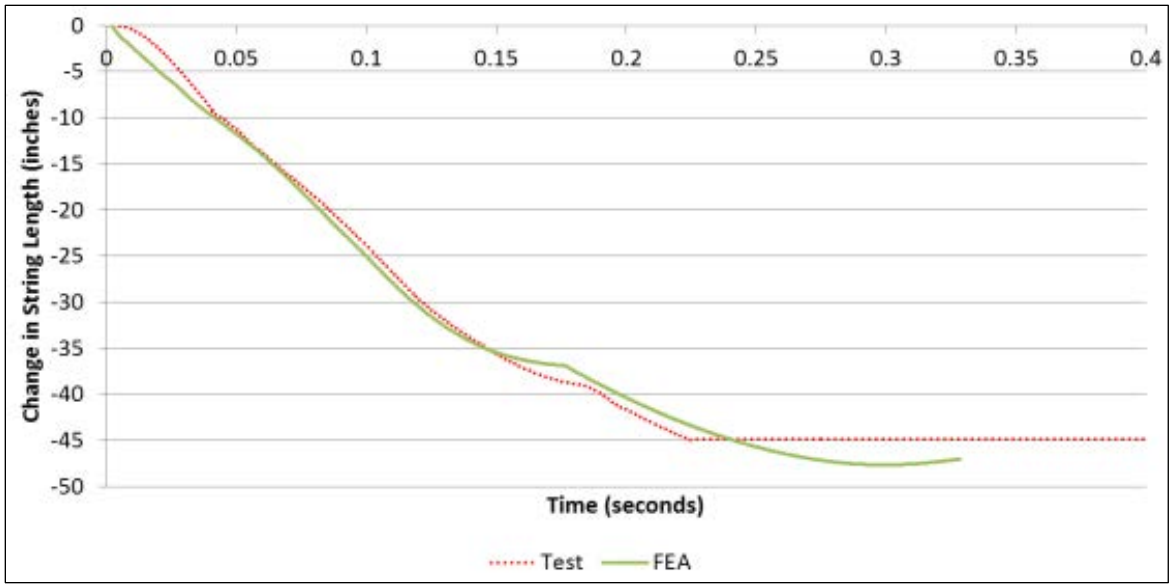

Figure 39. Internal String Potentiometer Measurement at Center of Tank in Post-Test FEA and Test

The complete set of test and post-test FEA results are compared in Appendix C.

7. Conclusion

This report documents the combined efforts of TTCI and Volpe to test and analyze the side impact puncture performance of a DOT- 112 tank car. This research supports FRA's tank car research program to provide enhanced and alternative performance standards for tank cars.

The tank car was filled with water to approximately 96 percent of its volume, then sealed but not pressurized. The test was intended to strike the car at a speed high enough to result in significant damage to the tank without puncturing the tank's shell. The tank car was impacted at 14.7 mph by a 297.125-pound ram car fitted with 12- by 12-inch ram head. The ram car impacted the tank center, deforming and cracking the external jacket without puncturing the tank's shell.

Pre-test FE modeling was used to estimate the overall response of the tank to the impact, including the force-displacement response. Because of uncertain parameters (e.g., material properties, actual outage, actual test speed), the pre-test model was intended to be conservative (i.e., at the lower-bound estimate of puncture speed) to ensure that the test did not puncture the tank. The model predicted that the tank would not puncture in a 15-mph impact. This model overpredicted the impact force by approximately 14 percent, but underpredicted the maximum indentation to the car by approximately 20 percent. Based on comparison of the test and pre-test FE results, the model was overly stiff.

Several changes were made to the model after the test to attempt to bring the model results into better agreement with the test results. These changes included reducing the coefficient of friction between the water and the inside of the tank, increasing the outage from 3.25 percent to 4 percent, and using TC128 properties corresponding to typical material, rather than minimum material properties. The post-test model gave much better agreement with the overall force-displacement and pressure-time histories than the pre-test model. The post-test model still overpredicted the maximum impact force, probably because the outage was compressed to an extreme degree, permitting the water to contact the top of the tank. With the exception of the second peak force, the post-test FE model gives very good agreement with the test results in terms of the overall response and the maximum indentation.

The test results, pre-test FE results, and post-test FE results for the peak forces and maximum displacements are summarized in Table 11. The percent difference between a given FE result and the corresponding test measurement is shown below the respective FE results.

Table 11. Summary of Test and FE Force and Displacement Results

	First Peak	Second Peak	Maximum Displacement
	million lbf	million lbf	inches
Test	*1.10*	*1.11*	*51.8*
Pre-Test FEA	1.19	1.26	41.2
	9%	14%	-20%
Post-Test FEA	1.03	1.43	49.3
	-6%	29%	-5%

The project's FE modeling underscored the importance of the role played by fluid and outage in the overall response of the tank to a shell impact in this scenario. In particular, the use of an unpressurized tank car with a small outage and a fairly large impactor places an increased importance on appropriately modeling the fluid and gas phase with a method that can capture the overall response of the tank. From the force-time or force-displacement histories measured during the test, the fluid effects are apparent in the overall response of the impactor. It is expected that the degree of fluid involvement in the impact response is proportional to the size of the impactor. A very small impactor would likely result in puncture of the tank before engaging the fluid outside of the local area of the impact, while a much larger impactor would result in an even greater displacement of the water and corresponding compression of the gas phase. Because the gas phase was initially at atmospheric pressure, it offered less resistance to the water's motion than if the gas phase was initially at a higher pressure. Finally, because of the small initial outage, a relatively small reduction in the volume of the tank could result in a significant increase in pressure of the gas phase.

The combination of a large impactor, small outage, and unpressurized gas phase presented modeling challenges that were partially overcome by explicitly modeling the fluid and gas phases. The FE modeling of this test used a Lagrangian (solid) mesh approach to model the water phase of the lading, and an SPH technique to model the air phase of the lading. This combination of techniques provided a generally good approximation of the fluid response within the tested tank, except at the end of the impact event. This approach was chosen specifically to address the large mesh distortions that can occur when an all-Lagrangian mesh is used to represent both the liquid and gas phases in a test that is likely to result in large fluid motions. While the post-test model gave generally good agreement, the model tended to exhibit a greater force response than when the response was tested at the end of the impact event, probably due to the water making contact with the top of the inside of the tank.

8. References

1. SAE J211/1 Standard. 1995 (2007). "Instrumentation for Impact Test – Part 1: Electronic Instrumentation." SAE International, Warrendale, PA, www.sae.org
2. Kirkpatrick, S.W., Rakoczy, P., MacNeill, R.A. "Side Impact Test and Analyses of a DOT 111 Tank Car." Technical Report # DOT/FRA/ORD-15/30. https://www.fra.dot.gov/eLib/Details/L17092
3. Yu, H., Jeong, D.Y., Gordon, J.E., Tang, Y.H., "Analysis of Impact Energy to Fracture Un-Notched Charpy Specimens Made from Railroad Tank Car Steel," Proceedings of the 2007 ASME Rail Transportation Division Fall Technical Conference, RTDF2007-46038, September 2007. http://ntl.bts.gov/lib/47000/47500/47518/asme_rtdf2007-46038.pdf
4. Tang, Y.H., Yu, H., Gordon, J.E., Jeong, D.Y., Perlman, A.B., "Analysis of Railroad Tank Car Shell Impacts Using Finite Element Method," Proceedings of the 2008 IEEE/ASME Joint Rail Conference, JRC2008-63014, April 2008. http://ntlsearch.bts.gov/tris/record/ntl/47391.html
5. Yu, H., Tang, Y.H., Gordon, J.E., Jeong, D.Y., "Modeling the Effect of Fluid-Structure Interaction on the Impact Dynamics of Pressurized Tank Cars," Proceedings of the 2009 ASME International Mechanical Engineering Congress and Exposition, IMECE2009-11926, Lake Buena Vista, Florida, November 2009. http://ntlsearch.bts.gov/tris/record/ntl/43028.html
6. Abaqus 6.13-1. Dassault Systemes Simulia Corp, Providence, RI, 2013.
7. "Water – Density and Specific Weight." http://www.engineeringtoolbox.com/water-density-specific-weight-d_595.html.
8. "Water – Speed of Sound." http://www.engineeringtoolbox.com/sound-speed-water-d_598.html.
9. "Water – Dynamic and Kinematic Viscosity." http://www.engineeringtoolbox.com/water-dynamic-kinematic-viscosity-d_596.html.
10. "Dry Air Properties." http://www.engineeringtoolbox.com/dry-air-properties-d_973.html.
11. "The Individual and Universal Gas Constant." http://www.engineeringtoolbox.com/individual-universal-gas-constant-d_588.html.
12. AK Steel. "Hot Rolled Steels – Product Data Bulletin." http://www.aksteel.com/pdf/markets_products/carbon/AK%20Hot%20Rolled%20Steel%20062212.pdf
13. McKeighan, P., 2007: "Mechanical Properties of Tank Car Steels Retired from the Fleet," Southwest Research Institute Report to the Volpe Center. http://ntl.bts.gov/lib/47000/47500/47510/Mechanical_properties.pdf

14. Lee, Y.W., Wierzbicki, T. “Quick Fracture Calibration for Industrial Use,” Impact & Crashworthiness Laboratory Report No. 115, August 2004.

Appendix A.
Camera and Target Positions

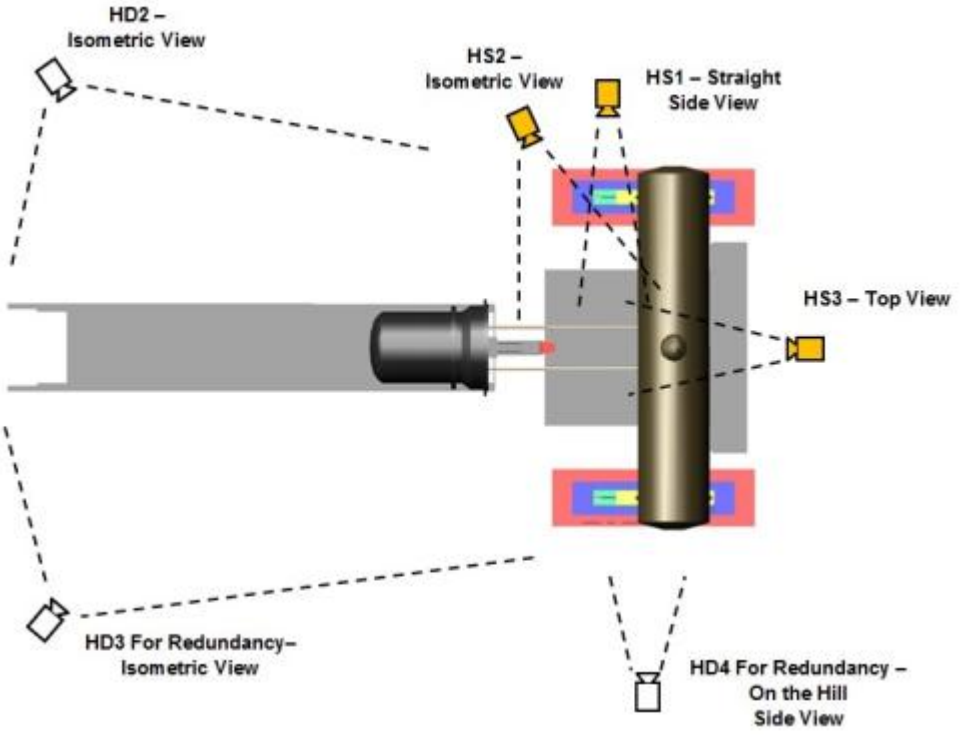

Figure A1. Camera Positions (Top) — High Speed (HS), High Definition (HD)

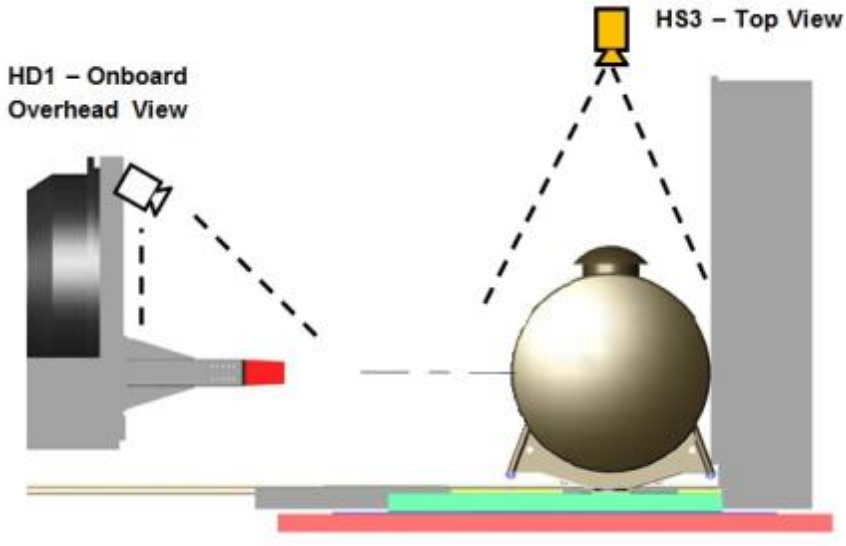

Figure A2. Camera Positions (Side) — High Speed (HS), High Definition (HD)

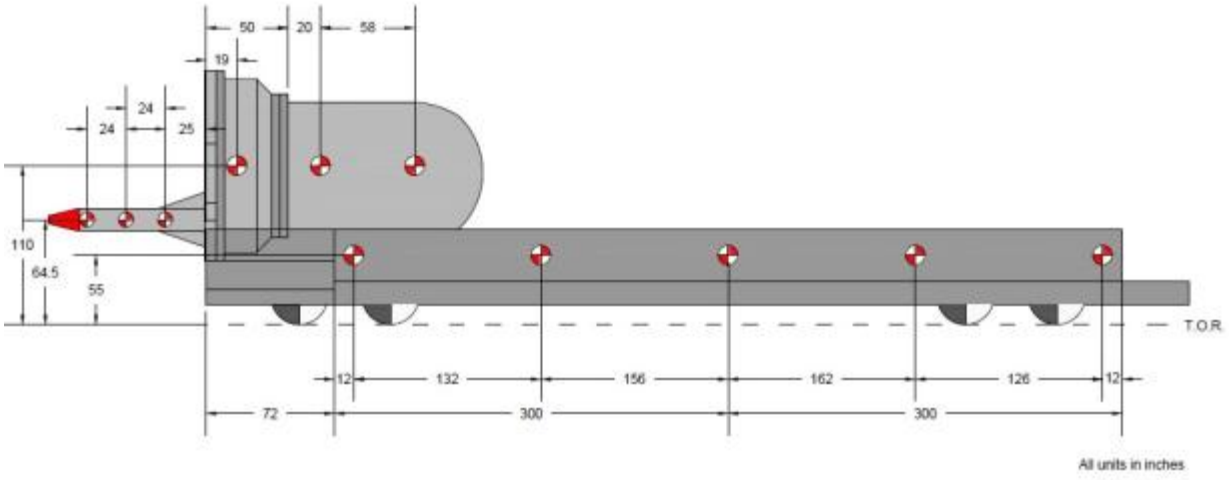

Figure A3. Ram Car Target Positions

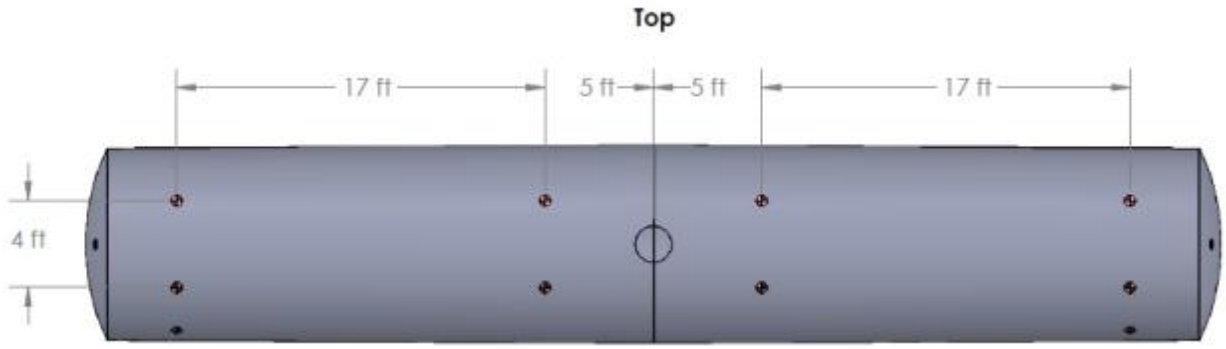

Figure A4. Tank Car Target Positions (Top)

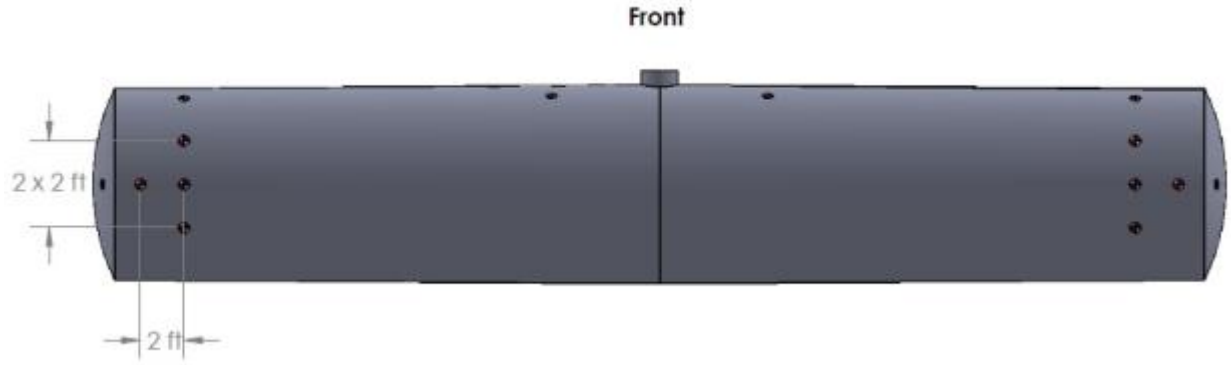

Figure A5. Tank Car Target Positions (Front)

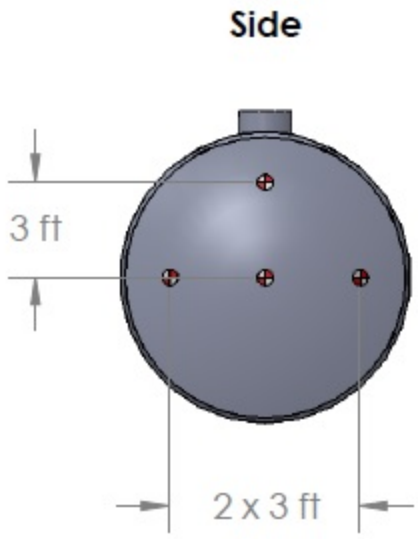

Figure A6. Tank Car Target Positions (Side)

Appendix B.
Test Data

This appendix contains raw and filtered test data. The raw accelerations and internal pressures measured on different locations on the impact cart were processed as follows. The test data from -1 seconds to -0.1 seconds on each channel were averaged, and this value was subtracted from the test measurements in order to remove any initial offsets in the data. Each channel was then filtered to channel frequency class (CFC) 60, using the procedures given in SAE J211 [1]. Displacement data did not required any filtration.

Accelerations:

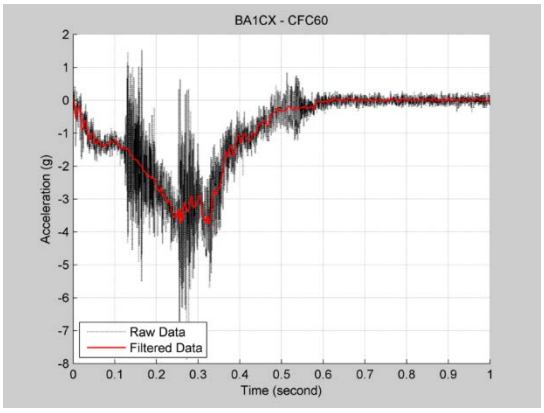

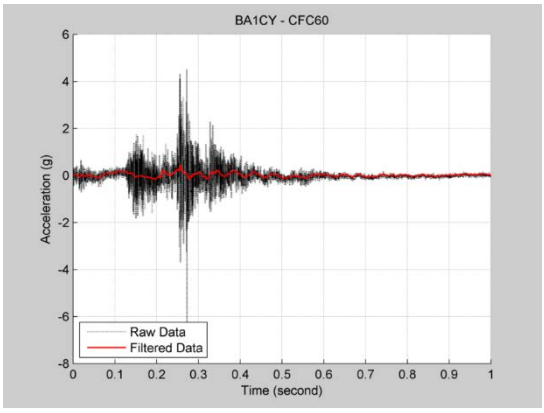

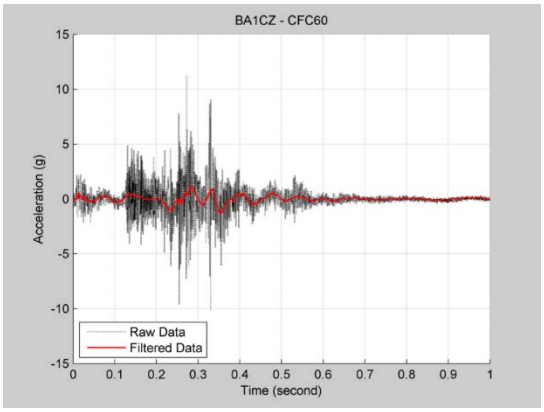

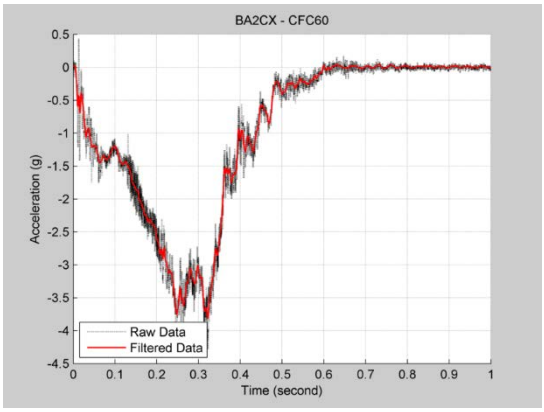

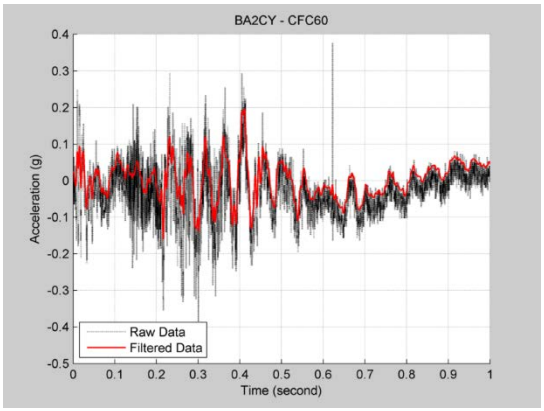

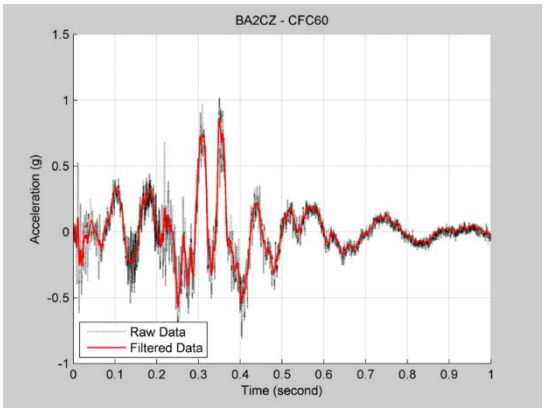

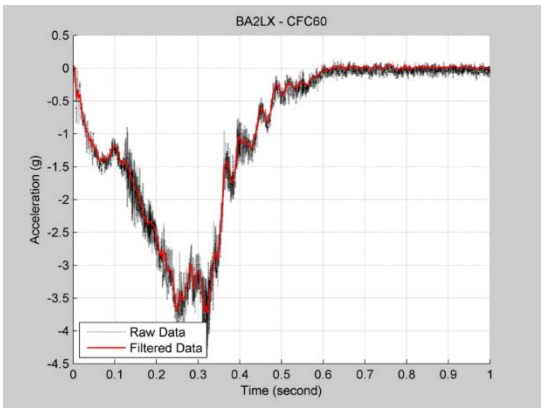
BA2LX - CFC60
Acceleration (g)
Time (second)
Raw Data
Filtered Data

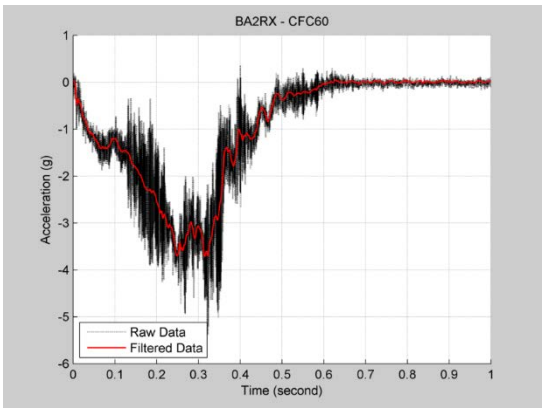
BA2RX - CFC60
Acceleration (g)
Time (second)
Raw Data
Filtered Data

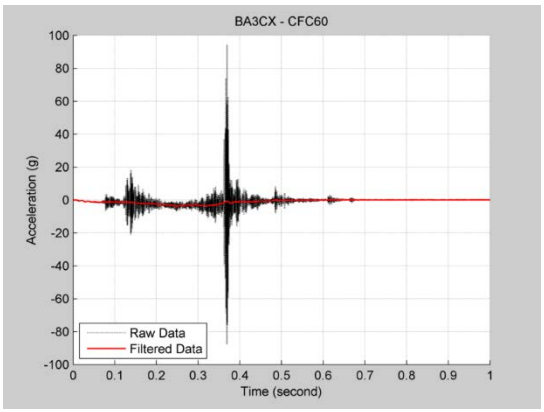
BA3CX - CFC60
Acceleration (g)
Time (second)
Raw Data
Filtered Data

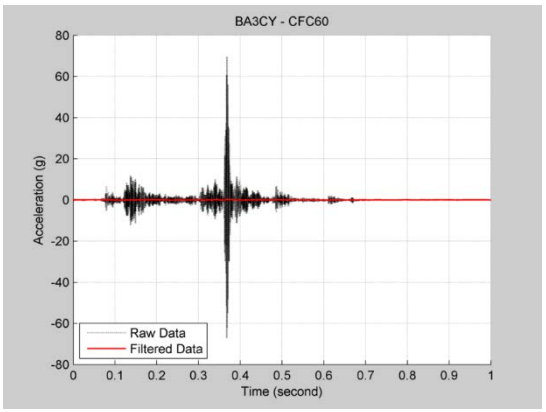
BA3CY - CFC60
Acceleration (g)
Time (second)
Raw Data
Filtered Data

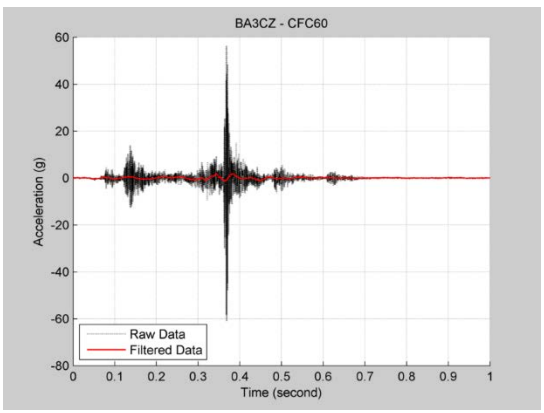
BA3CZ - CFC60
Acceleration (g)
Time (second)
Raw Data
Filtered Data

Pressures

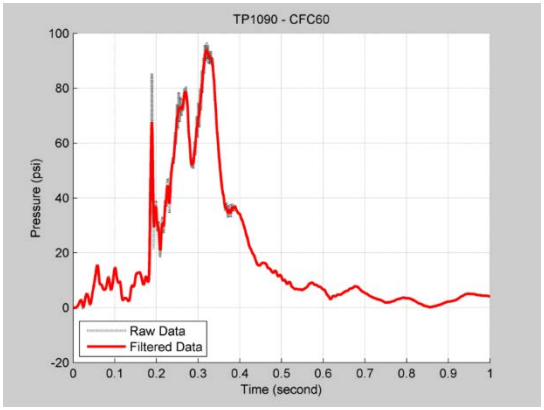
TP1090 - CFC60
Pressure (psi)
Time (second)
Raw Data
Filtered Data

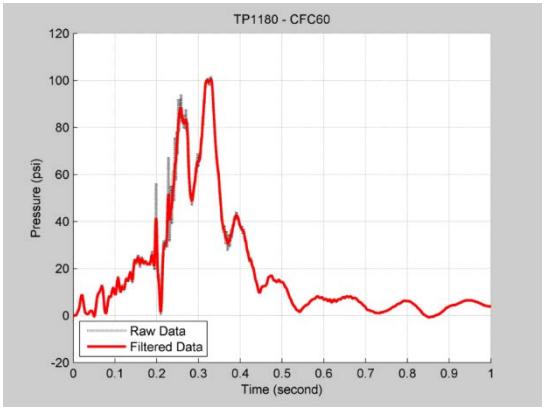
TP1180 - CFC60
Pressure (psi)
Time (second)
Raw Data
Filtered Data

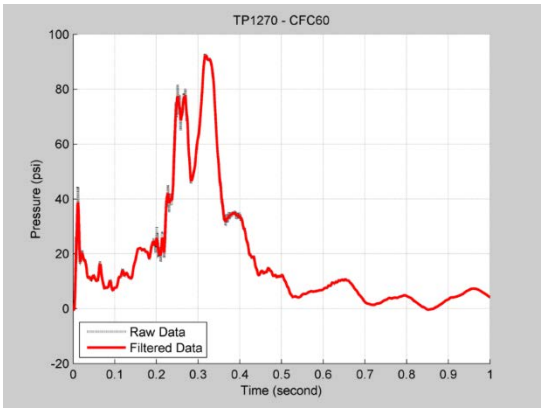
TP1270 - CFC60
Pressure (psi)
Time (second)
Raw Data
Filtered Data

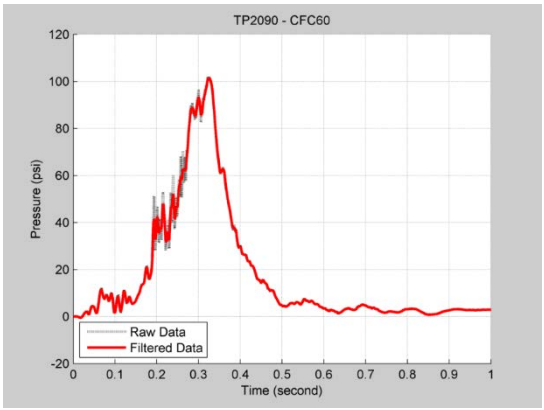
TP2090 - CFC60
Pressure (psi)
Time (second)
Raw Data
Filtered Data

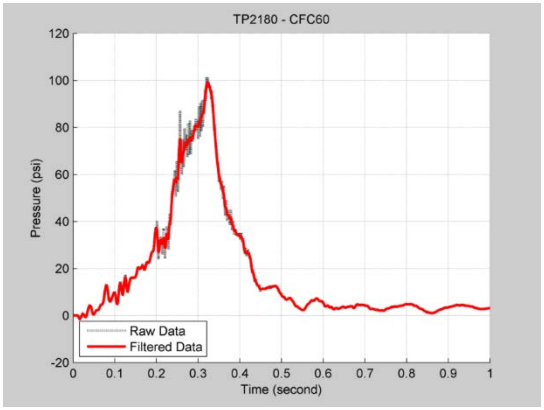
TP2180 - CFC60
Pressure (psi)
Time (second)
Raw Data
Filtered Data

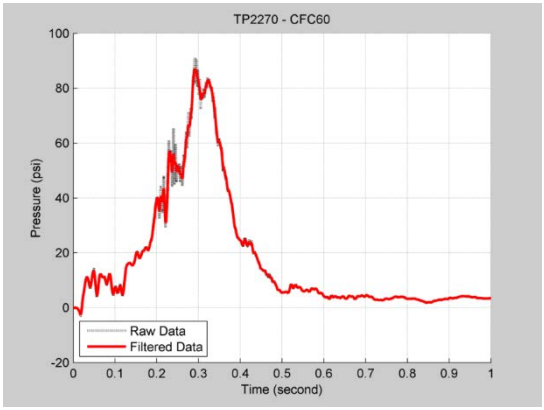
TP2270 - CFC60
Pressure (psi)
Time (second)
Raw Data
Filtered Data

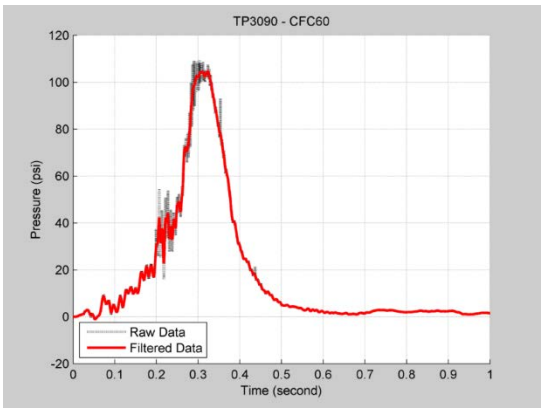
TP3090 - CFC60
Pressure (psi)
Time (second)
Raw Data
Filtered Data

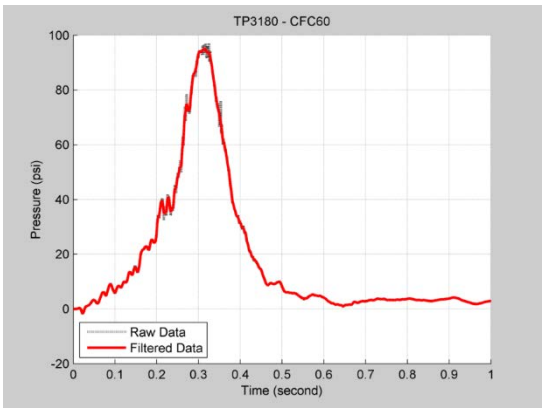
TP3180 - CFC60
Pressure (psi)
Time (second)
Raw Data
Filtered Data

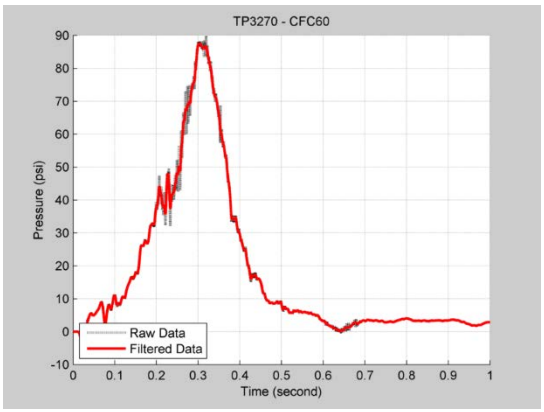
TP3270 - CFC60
Pressure (psi)
Time (second)
Raw Data
Filtered Data

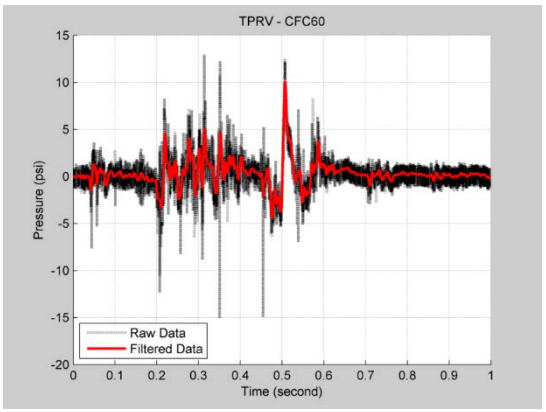
TPRV - CFC60
Pressure (psi)
Time (second)
Raw Data
Filtered Data

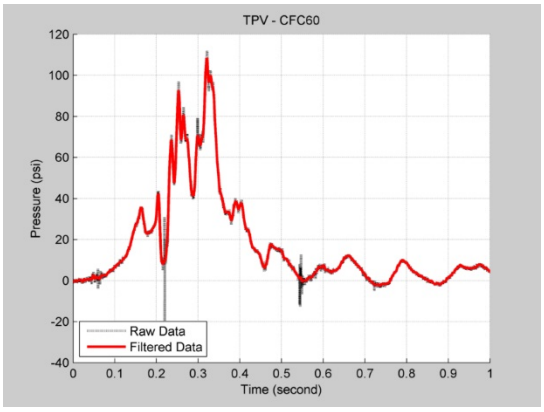
TPV - CFC60
Pressure (psi)
Time (second)
Raw Data
Filtered Data

Displacements:

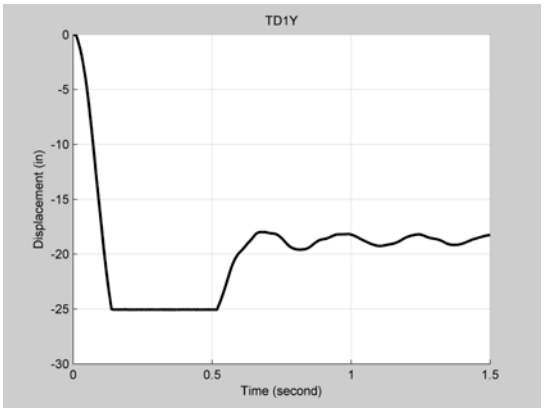

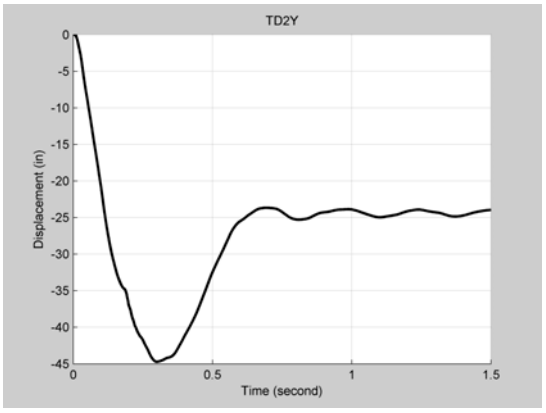

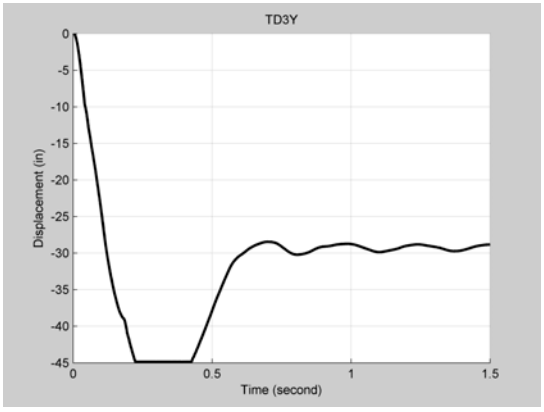

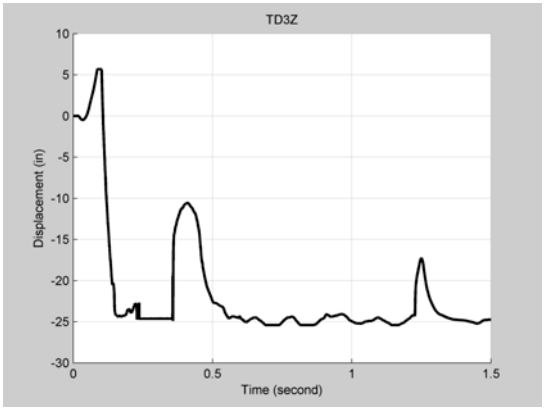

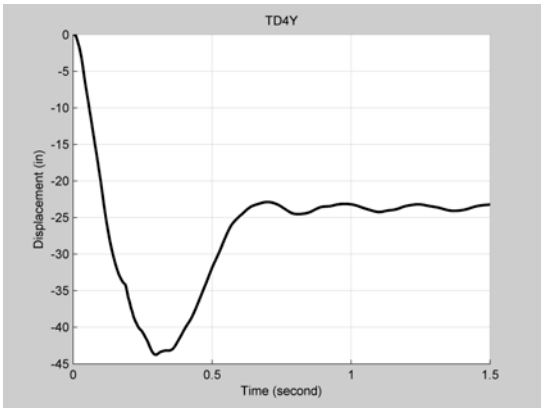

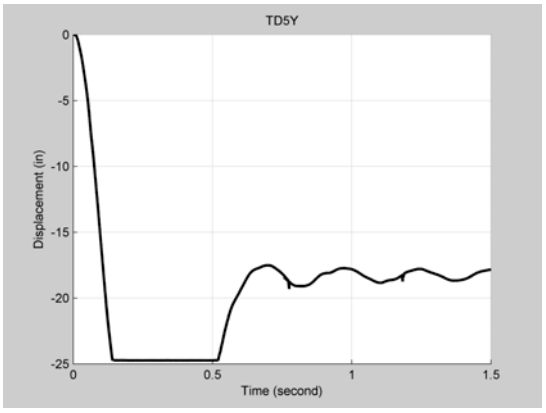

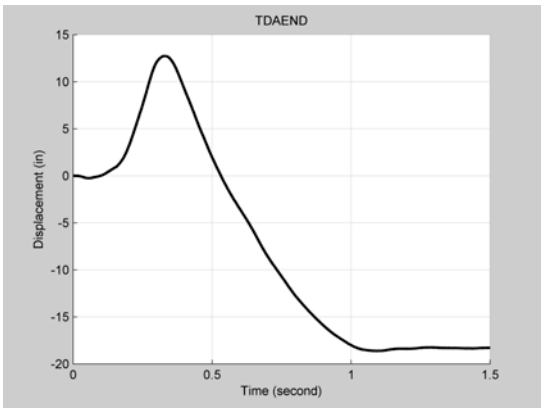
TDAEND
Displacement (in)
Time (second)
15
10
5
0
-5
-10
-15
-20
0
0.5
1
1.5

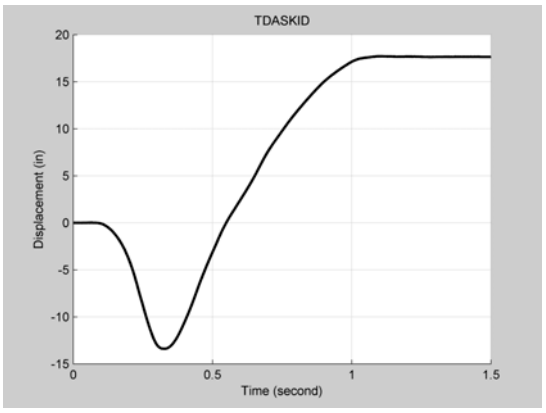
TDASKID
Displacement (in)
Time (second)
20
15
10
5
0
-5
-10
-15
0
0.5
1
1.5

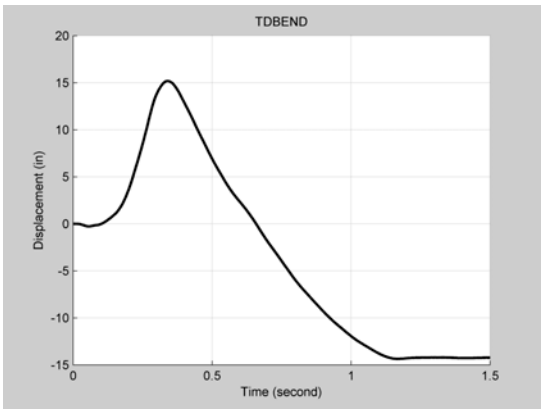
TDBEND
Displacement (in)
Time (second)
20
15
10
5
0
-5
-10
-15
0
0.5
1
1.5

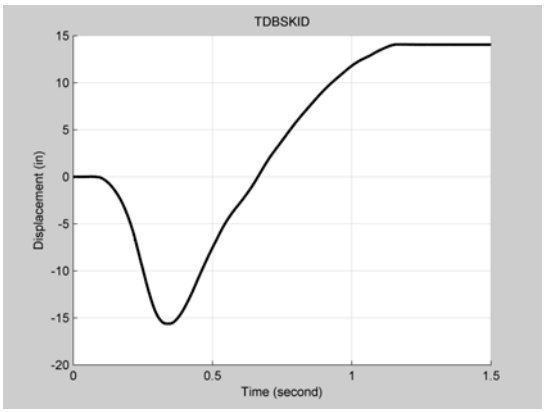
TDBSKID
Displacement (in)
Time (second)
15
10
5
0
-5
-10
-15
-20
0
0.5
1
1.5

Appendix C.
Post-Test Finite Element Analysis and Test Results

The post-test FEA results are compared to the test measurements in this appendix. Results derived from accelerometers or pressure transducers have been filtered with a CFC60 filter.

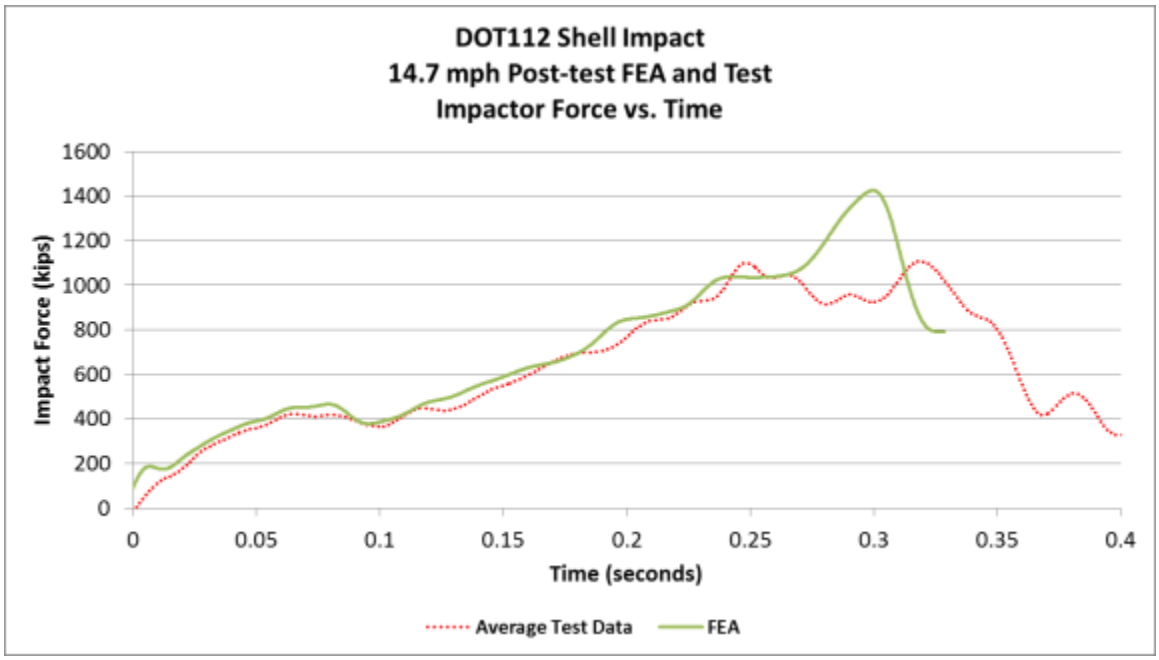

Figure C 1. Average Impactor Force, Test and Post-Test FEA

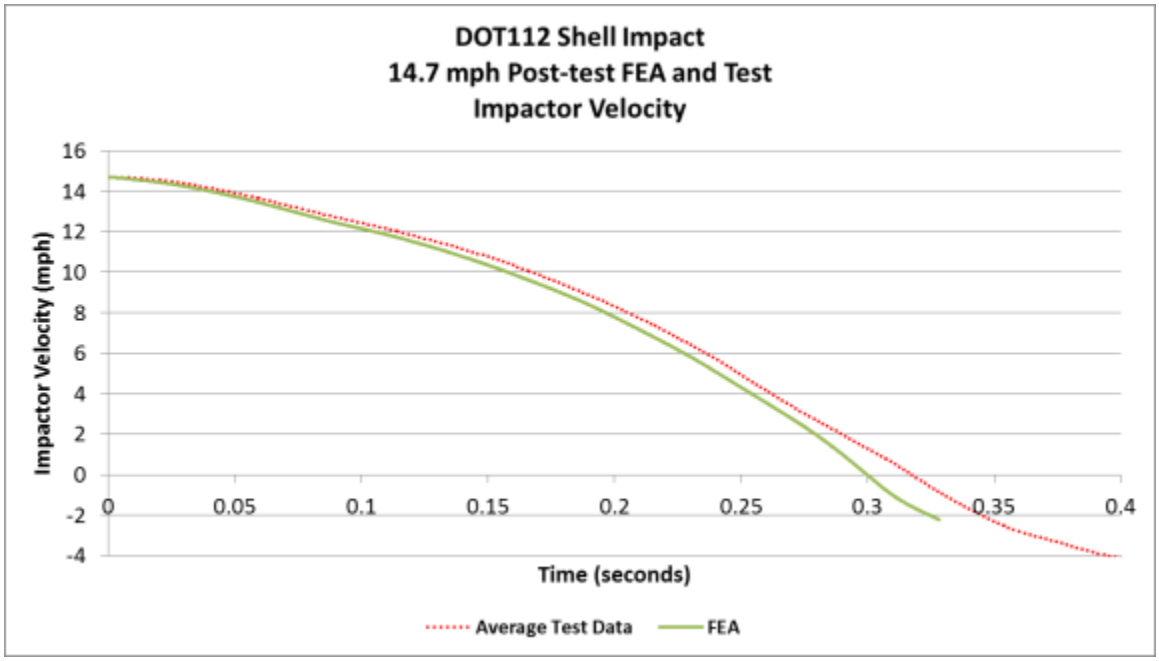

Figure C 2. Average Impactor Velocity, Test and Post-Test FEA

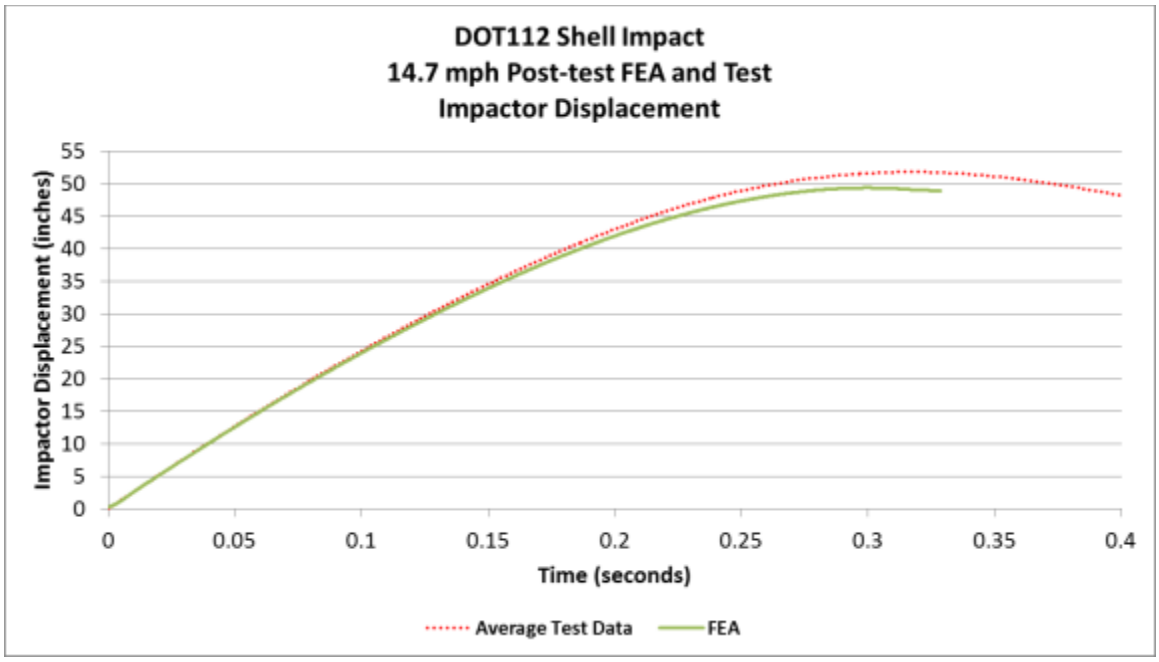

Figure C 3. Average Impactor Displacement, Test and Post-Test FEA

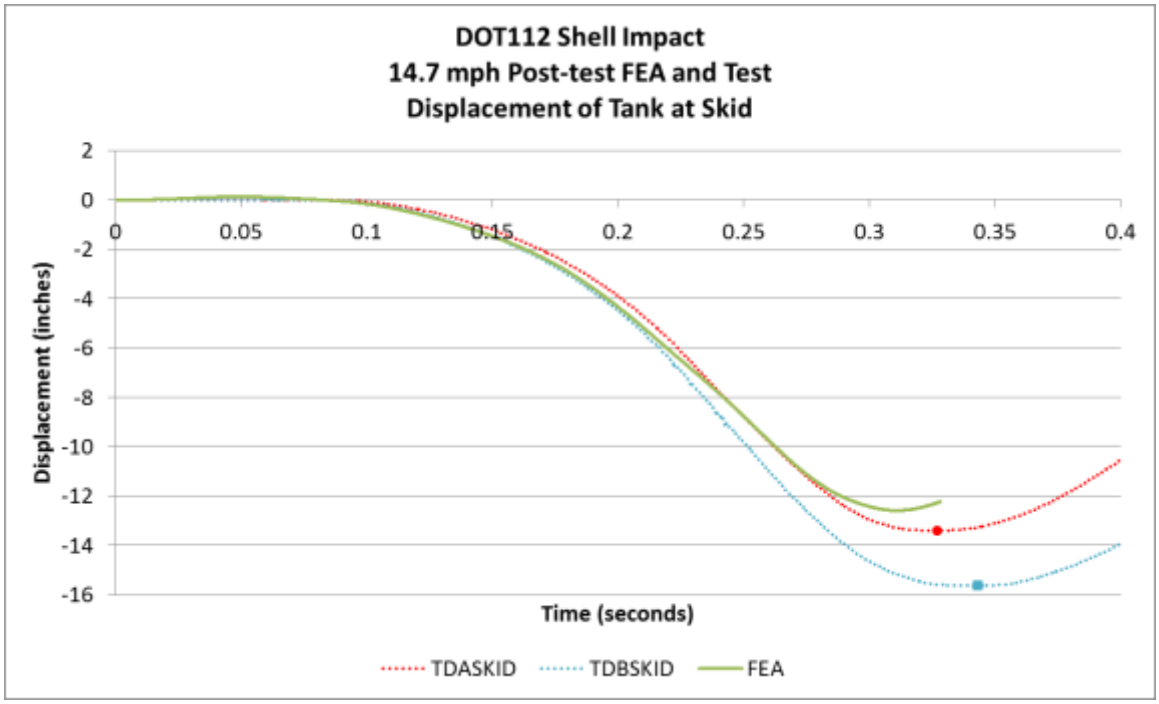

Figure C 4. A- and B-end Skid Displacements, Test and Post-Test FEA

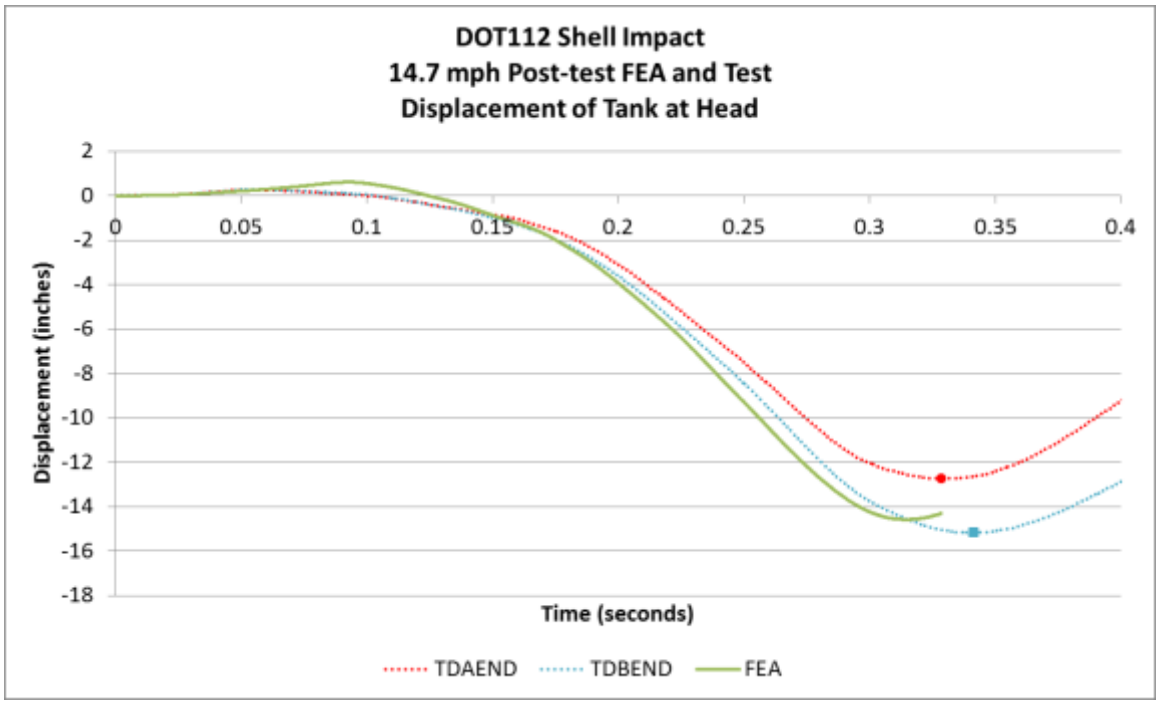

Figure C 5. A- and B-end Head Displacements, Test and Post-Test FEA

Table C 1. Pressure Transducers in Water, Test and Post-Test FEA

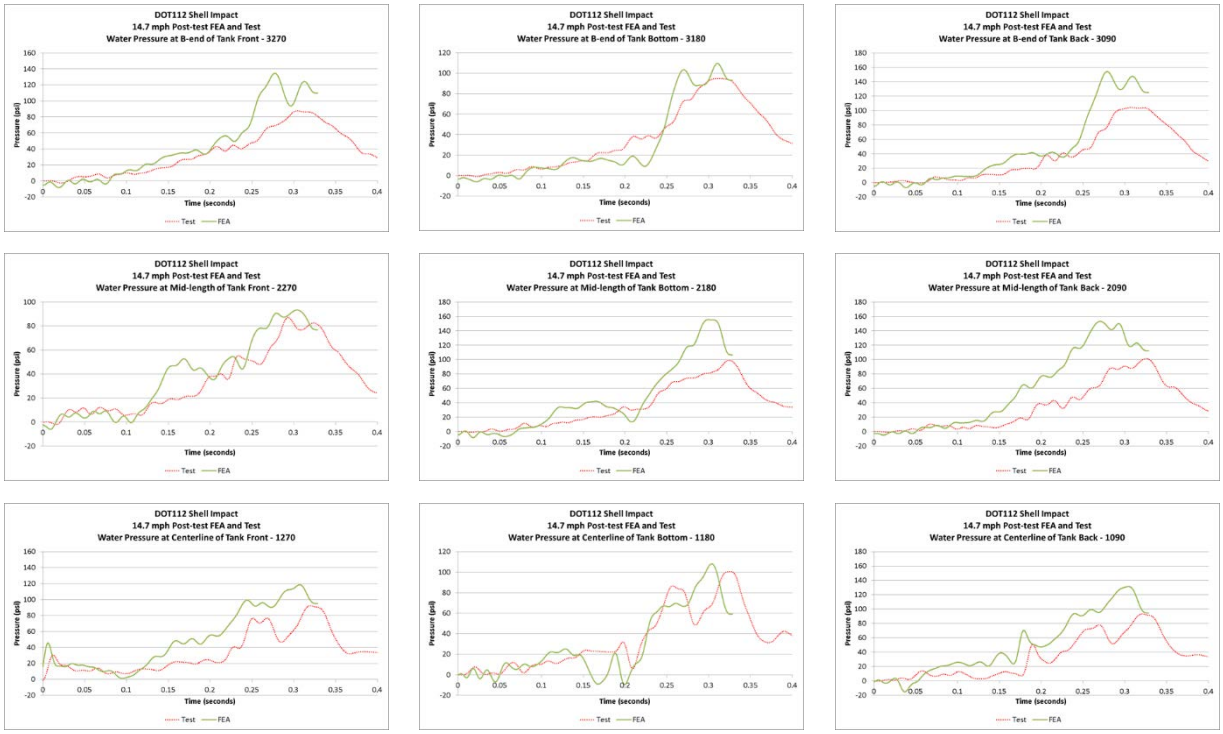

The nine pressure transducer results in the test were averaged to provide an overall average pressure within the water. The pressures from the corresponding elements within the water in the FE model were also averaged and compared to the FE results.

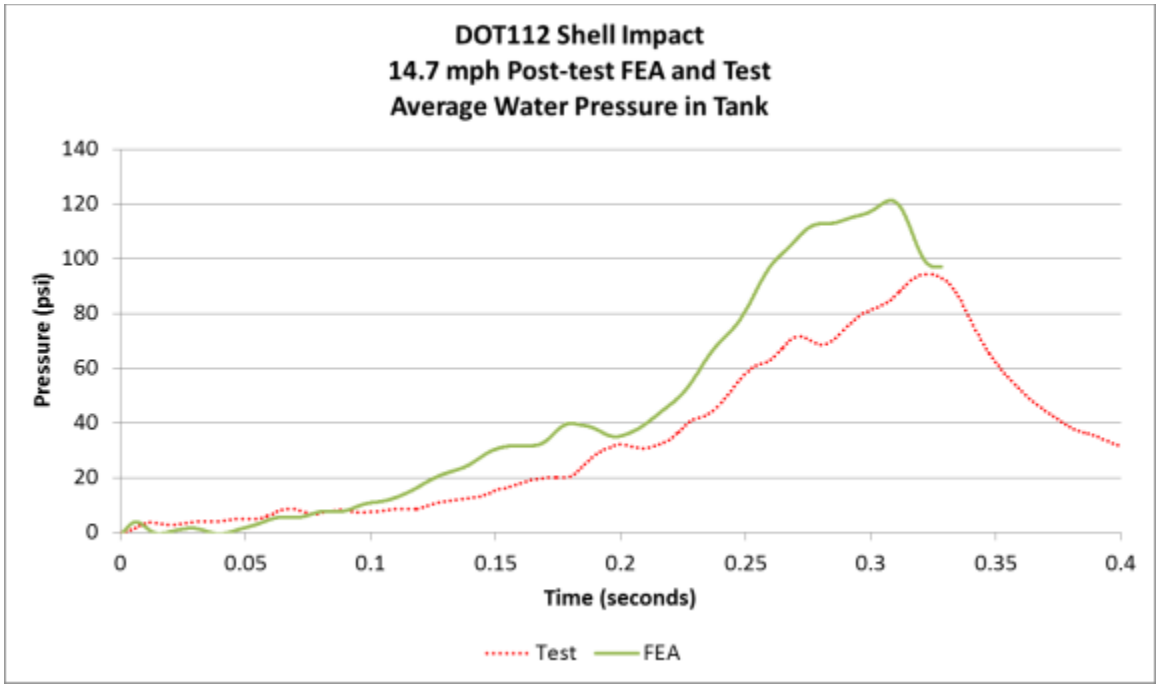

Figure C 6. Average Water Pressure, Test and Post-Test FEA

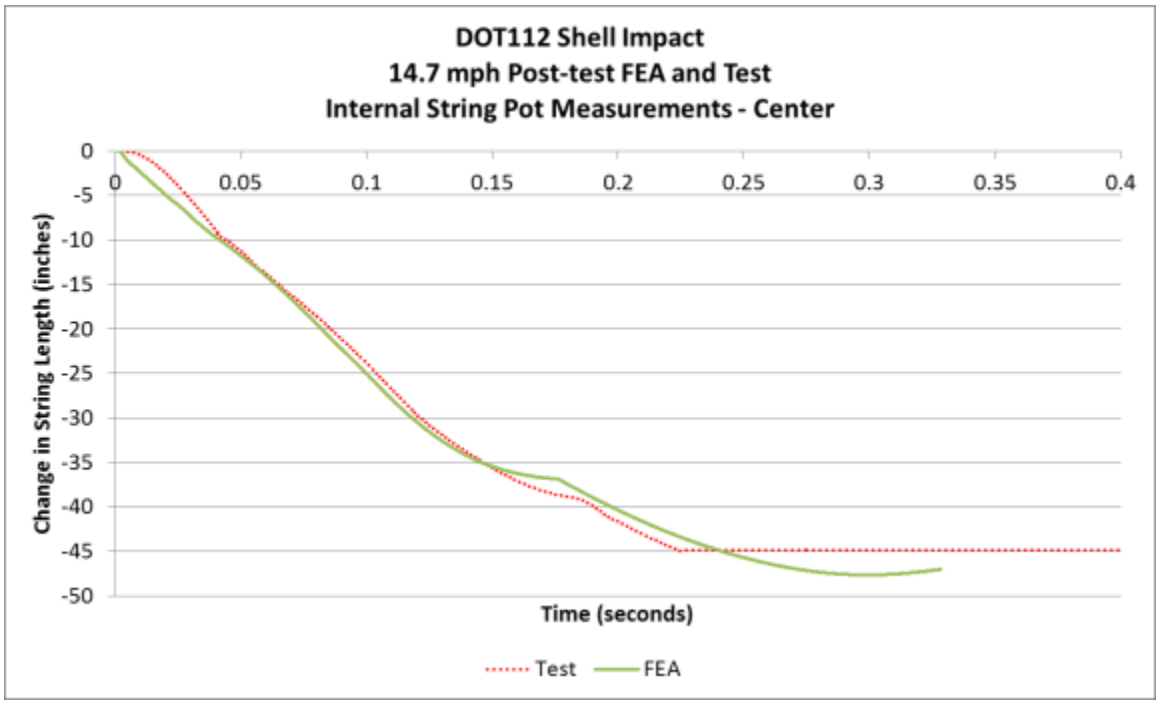

Note: String potentiometer in test reached maximum travel of ~45 inches.

Figure C 7. Internal String Potentiometer Measurements, Center (Test and Post-Test FEA)

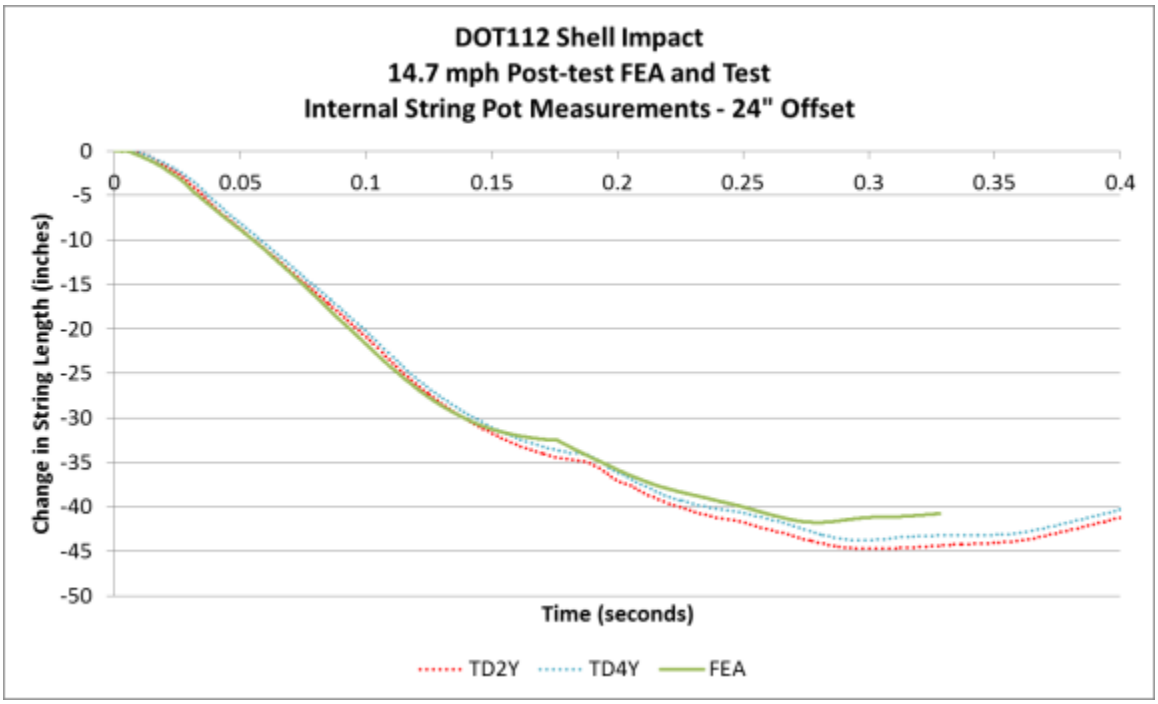

Figure C 8. Internal String Potentiometer Measurements, 24-inch Offset (Test and Post-Test FEA)

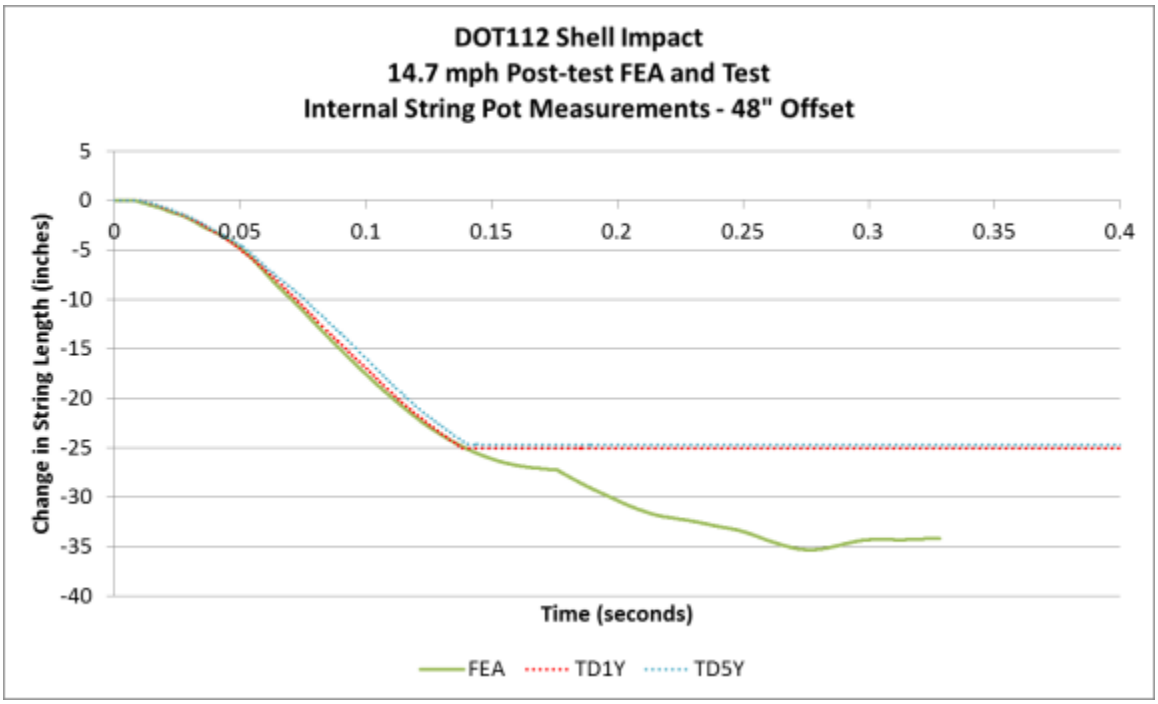

Note: String potentiometers in test reached maximum travel of ~25 inches

Figure C 9. Internal String Potentiometer Measurements, 48-inch Offset (Test and Post-Test FEA)

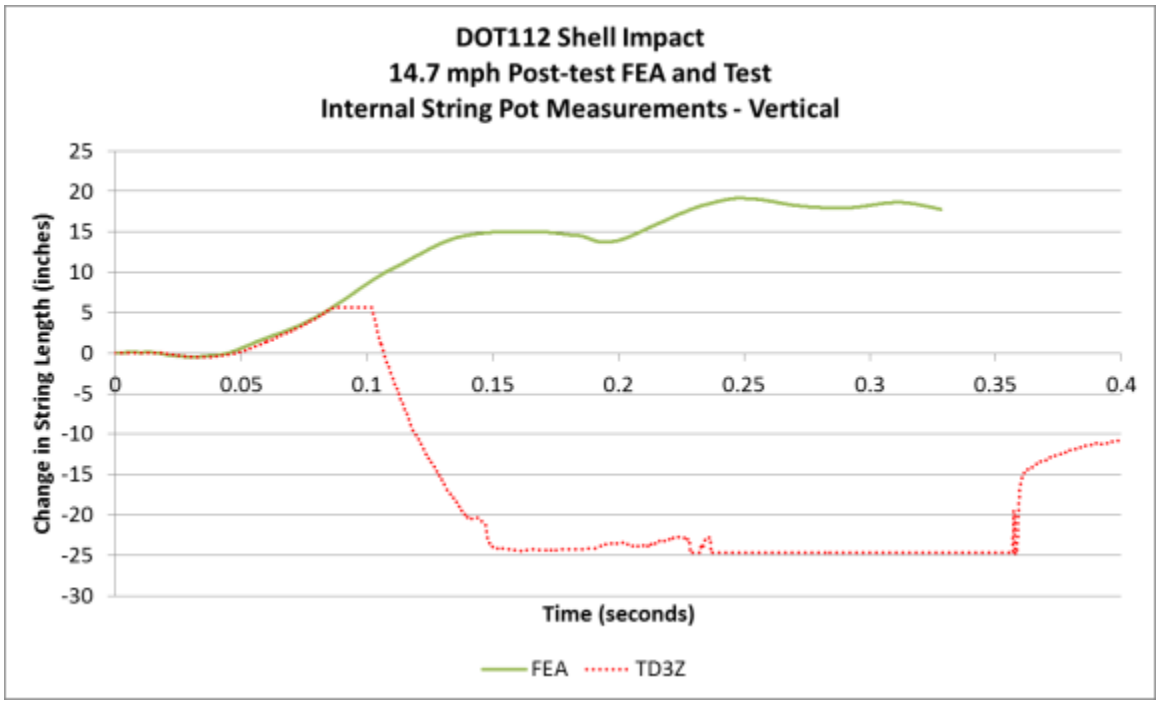

Note: String potentiometer in test reached maximum travel of ~5 inches and snapped.

Figure C 10. Internal String Potentiometer Measurements, Vertical (Test and Post-Test FEA)

Appendix D.
Geometry in Pre-Test and Post-Test Finite Element Models

A discussion of each of the parts making up the model is contained in the following paragraphs. Note that for parts that are bisected by the symmetry plane, the values reported in the following tables for mass and number of elements correspond to what was included in the FE model (i.e., half the mass of the physical body during the test).

D.1 Rigid Parts

Rigid parts were used when it was important to include a part for its inertia or for its interaction through contact, but where the deformation of the part could be neglected in the calculations. Four parts were modeled as rigid bodies.

D.1.1 Impactor

The impactor was modeled as a rigid body in the DOT-112 FE models. The simulations used a 12- by 12-inch square impactor with 1-inch radii edges around the impact face. The geometry included the impact face and the tapered cone back to the portion of the impactor where the impactor attached to the ram car. Because only the impactor itself was modeled and this model used one-half symmetry, half of the mass of the entire ram car was assigned to the reference node on the impactor. The impactor, both with and without mesh, is shown in Figure D 1.

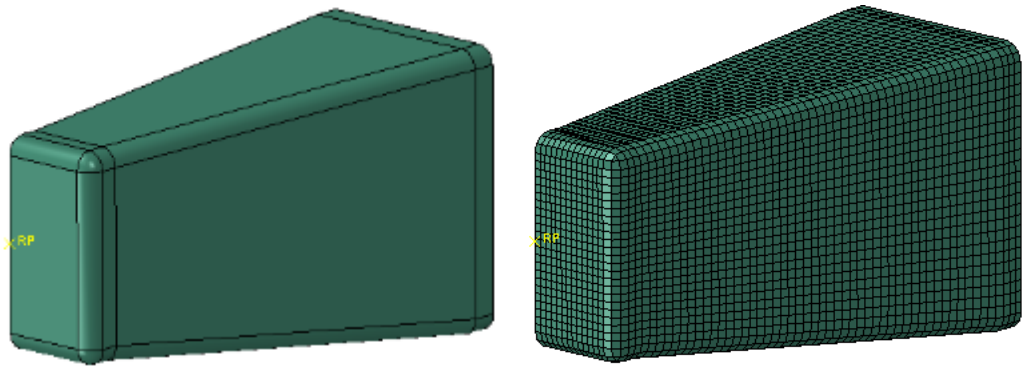

Figure D 1. Impactor Geometry (left) and Mesh (right)

Table D 1. Properties of Impactor in FE Model

Type of Part	Rigid
Number of Elements	R3D4: 3,318 R3D3: 2
Part Weight	148,562 lbf

D.1.2 Rigid Wall

The rigid wall was modeled as a rigid body in the DOT-112 FE model. Because the wall was constrained against motion in any direction, no mass needed to be defined for this part. The wall's geometry and mesh are shown in Figure D 2.

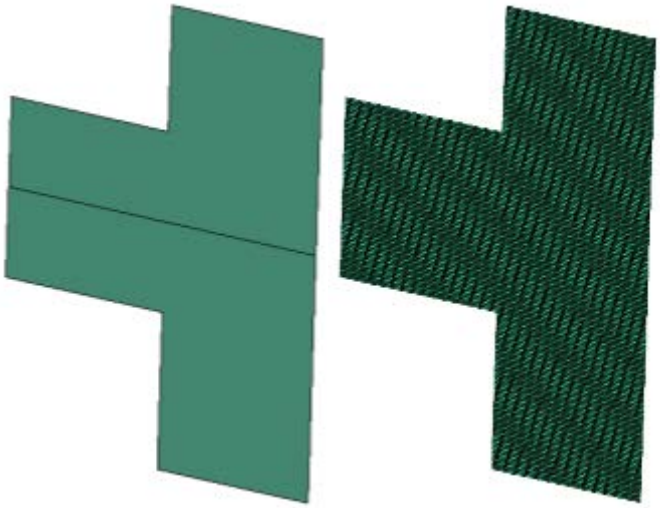

Figure D 2. Rigid Wall Geometry (left) and Mesh (right)

Table D 2. Properties of Rigid Wall in FE Model

Type of Part	Rigid
Number of Elements	R3D4: 15,802

D.1.3 Skid

The trucks of the tank car were removed prior to the test. The bolster of the car rested directly upon a set of skids, which themselves rested upon steel plates (see Figure 3). The skids were designed to inhibit rigid-body roll of the tank car following rebound from the rigid wall during a test. The skid geometry and mesh are shown in Figure D 3. Note that since this part exists entirely to one side of the symmetry plane, the mass and geometric properties correspond to the actual mass and geometry of one full skid.

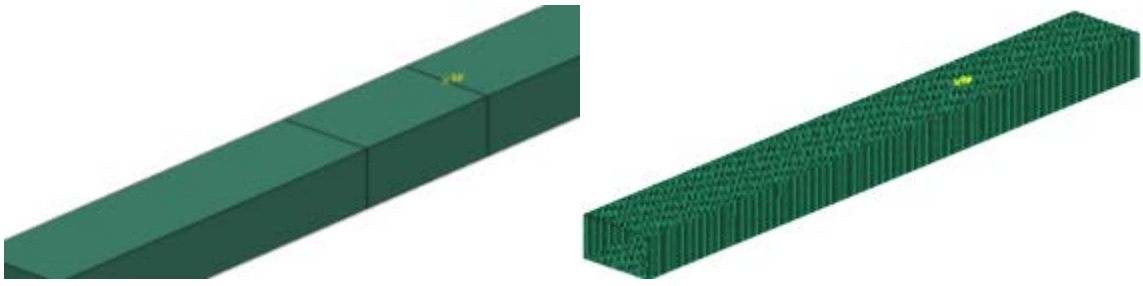

Figure D 3. Skid Geometry (left) and Mesh (right)

Table D 3. Properties of Skid in FE Model

Type of Part	Rigid
Number of Elements	R3D4: 12,240
Part Weight	3,500 lbf

D.1.4 Symmetry Wall

The symmetry wall part was necessary to apply a symmetry boundary condition to the air within the tank. While a symmetry boundary condition could be used for the jacket, tank, and water within the tank, the SPH representation of the air could not have a boundary condition applied directly to it. Therefore, this wall was placed at the symmetry plane of the model and was only permitted to contact the air. Because the wall was constrained against motion in any direction, no mass needed to be defined for this part. The geometry and mesh of the symmetry wall are shown in Figure D 4. In the post-test model, the size of this wall was increased in order to contain the air particles, as the post-test tank exhibited larger deformations.

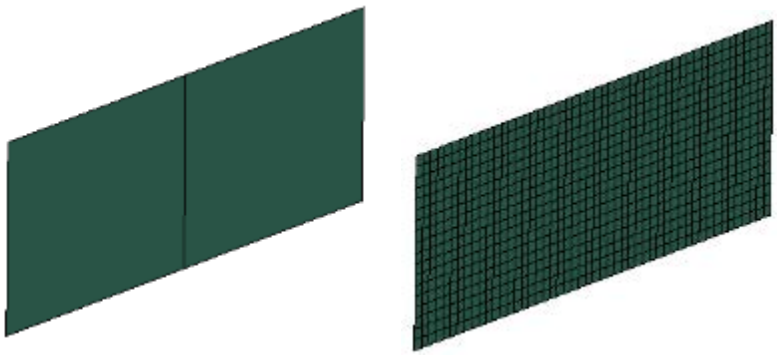

Figure D 4. Symmetry Wall Geometry (Left) and Mesh (Right)

Table D 4. Properties of Symmetry Wall in FE Model

	Pre-Test Model	**Post-Test Model**
Type of Part	Rigid	
Number of Elements	R3D4: 900	R3D4: 3,306

D.2 Deformable Parts, Steel

D.2.1 Jacket

The jacket was modeled entirely with deformable shell elements. The diameter of the jacket part was 120.25 inches, representing the mid-plane of the actual jacket. The majority of the jacket was meshed with quadrilateral, reduced integration (S4R) elements with a 3-inch mesh seed. A small number of triangular, reduced elements (S3R) were used to mesh the head. In the area of the jacket that would be contacted by the impactor, the mesh was made up of quadrilateral, full integration (S4) elements with a 0.25-inch mesh seed. A transition zone between the fine mesh and the coarse mesh also used full integration elements. Because only ½ the jacket is included in

the FE model due to symmetry, the mass of the jacket in the FE model corresponds to ½ the mass of the physical jacket.

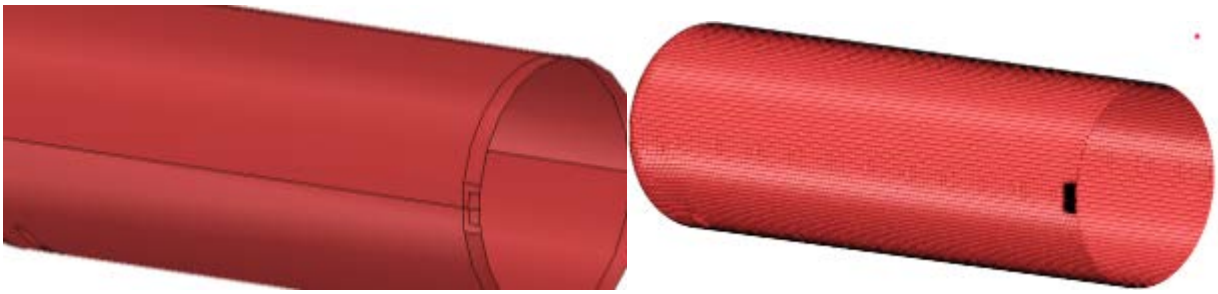

Figure D 5. Jacket Geometry (left) and Mesh (right)

The transition between 3 inches S4R mesh and 0.25 inch S4 mesh is shown in Figure D 6.

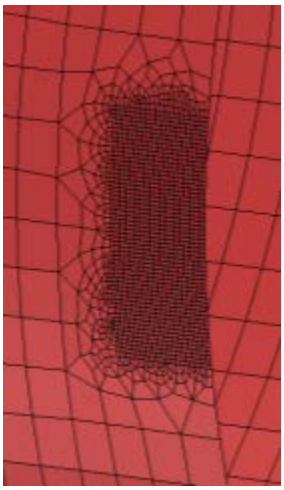

Figure D 6. Jacket Mesh in Impact Zone

Table D 5. Properties of Jacket in FE Model

Type of Part	Deformable, Shell
Number of Elements	S4R: 16,715 S4: 1,916 S3R: 50
Shell Thickness	0.1196" (11 gauge)
Head Thickness	0.5"
Material(s)	A1011
Part Weight	6,615.2 lbf

D.2.2 Tank – Shell Elements

The commodity tank was modeled using two different techniques. In the impact zone, the tank was modeled using solid "brick" elements. This part is discussed in Section D.2.3. Away from the impact zone, the tank was modeled using shell elements. The shell portion of the tank is

described in this section. Because only half the tank is included in the FE model due to symmetry, the mass of the tank in the FE model corresponds to half the mass of the physical tank.

Figure D 7 shows the shell portion of the tank. This part was globally meshed using quadrilateral reduced integration (S4R) elements with a 3-inch mesh seed. At the edges of the impact zone, the mesh was seeded such that each shell element edge would span exactly three solid elements on the impacted patch. The mesh in the region of attachment to the solid plate was meshed using quadrilateral fully integrated (S4) elements. A technique referred to as shell-to-solid coupling (SSC) was used to attach the solid patch to the edges of the shell mesh on the tank. The shell part of the tank represents the midplane surface of the tank. The shell part has a midplane diameter of 118.493 inches in the model. The pre-test model included a small number of S3R elements in the head; the tank was re-meshed in the post-test model to remove these elements.

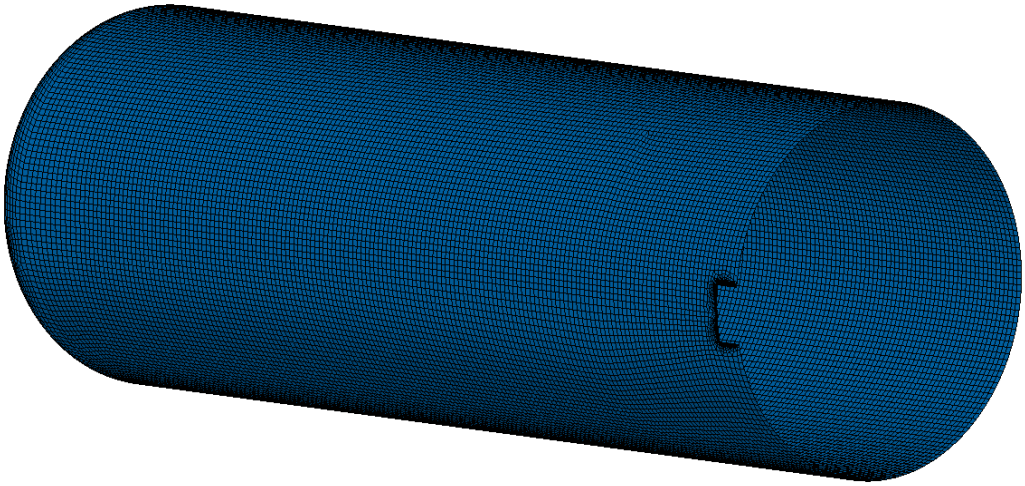

Figure D 7. Tank Mesh – Shell Elements

Table D 6. Properties of Tank (shell mesh)

	Pre-Test Model	**Post-Test Model**
Type of Part	Deformable, Shell	
Shell Thickness	0.618”	
Head Thickness	0.618”	
Number of Elements	S4R: 36,573 S4: 587 S3R: 175	S4R: 36,167 S4: 688
Material(s)	TC128-Minimum	TC128-Typical
Part Weight	25,150.8 lbf	

D.2.3 Tank – Solid Elements

The commodity tank was modeled using two different techniques. Away from the impact zone, the tank was modeled using shell elements. This part is discussed in Section D.2.2. In the impact zone, the tank was modeled using solid brick elements. The solid portion of the tank is described in this section. Because only half the tank is included in the FE model due to symmetry, the mass of the solid portion of the tank in the FE model corresponds to half the mass of the corresponding portion of the physical tank.

Figure D 8 shows the solid portion of the tank. This part measures approximately 18 inches high by 9 inches wide. The part was meshed with six elements through the thickness of the tank shell. This resulted in a mesh seeding of approximately 0.103 inch. The solid portion of the tank was meshed using C3D8I brick elements. These elements, referred to in Abaqus/Explicit as "incompatible modes," are intended to more accurately capture bending stresses compared to regular C3D8 brick elements. The solid mesh is shown in Figure D 8. The edges of the solid portion of the mesh were attached to the shell mesh of the tank using SSC.

Figure D 8. Tank - Solid Mesh

Table D 7. Properties of Tank (solid mesh)

	Pre-Test Model	**Post-Test Model**
Type of Part	Deformable, Solid	
Number of Elements	C3D8I: 90,828	
Shell Thickness	0.618"	
Material(s)	TC128-Minimum	TC128-Typical

Part Weight	8.6 lbf

D.3 Deformable Parts – Other Materials

The FE model of the DOT-112 tank car included two deformable parts made of a material other than steel: air and water. Together, these two parts made up the lading within the tank.

D.3.1 Tank Lading – Air

The gas phase of the lading was explicitly modeled within the tank. The material properties used to describe the behavior of the air are described in Section 4.3.3. In the model, the outage volume was filled with air. The air within the model was given an initial hydrostatic pressure of 14.7 psi (corresponding to 1 atmosphere). This pressure was allowed to change according to the ideal gas law as the volume of the tank changed during the impact simulation. Because only half the outage is included in the FE model due to symmetry, the mass of the outage in the FE model corresponds to half the mass of the physical air occupying the outage.

This simulation used a relatively new (as of Abaqus 6.13-1) modeling capability known as smoothed particle hydrodynamics (SPH) to model the air. This approach to modeling does not use conventional nodes and elements to represent the geometry of a part. Rather, discrete particles are assigned the material properties and initial conditions of the desired part. Because the particles are discrete, large deformations may be captured by the model without suffering from poor performance associated with distorted elements. Because the DOT-112 car was not pressurized during the test, it was thought that fluid sloshing would be a prevalent feature of the impact response. In order to ensure the best likelihood of the model capturing this behavior with some accuracy it was decided to use SPH techniques to model the air in the DOT-112.

In Abaqus/CAE, particles may be generated from an existing mesh of reduced-integration brick elements. This existing mesh is referred to as a parent mesh. The air part was initially meshed with C3D8R reduced integration brick elements. The parent mesh can then be converted to particles either at the beginning of the analysis (time=0) or after a critical time, stress, or strain is exceeded. The parent mesh is deactivated, leaving the particles to represent the underlying geometry. The parent mesh and initial particle distribution from this parent mesh are shown in Figure D 9. In the pre-test model, the parent mesh initially occupied 3.25 percent of the volume of the tank. In the post-test model, the parent mesh initially occupied 4 percent of the volume of the tank.

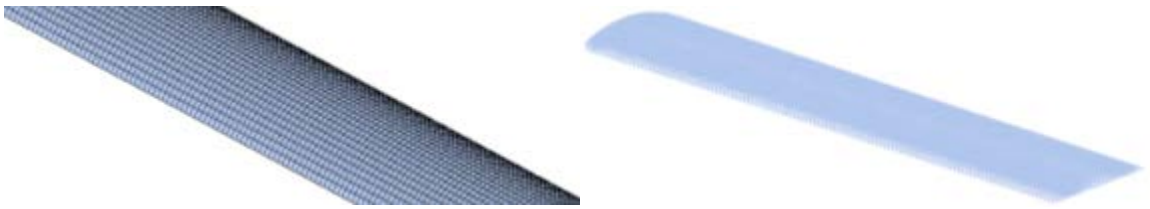

Figure D 9. Air - Parent Mesh (left) and Particles (right)

The properties of the air part are summarized in Table D 8 for the pre-test and post-test models. In the post-test model, the outage was increased. The mesh density of the air was also increased in this model, resulting in more particles.

Table D 8. Properties of Air Mesh

	Pre-Test Model	Post-Test Model
Type of Part	Deformable, Solid-to-particle	
Material(s)	AIR-1-ATM	
Number of Elements	C3D8R: 15,800 PC3D: 15,800	C3D8R: 24,720 PC3D: 24,720
Air Volume	127,246 in^3 (551 gallons)	155,263 in^3 (672 gallons)
Part Weight	5.95 lbf	7.26 lbf

D.3.2 Tank Lading – Water

The volume of the lading made up of water was also explicitly included within the model for the DOT-112 tank car. The tank car was filled to approximately 96 percent of its capacity with water during the test. The material properties used to describe the behavior of the water are given in Section 4.3.2. The water within the model was given an initial pressure of 1 atmosphere (14.7 psi). This pressure was allowed to change during the simulation as the water was forced to move through the tank as a result of the impactor's travel. Because only half the tank is included in the FE model due to symmetry, the mass of the water in the FE model corresponds to half the mass of the water in the physical tank. The water volume was meshed using C3D8 fully integrated brick elements. These elements include eight integration points per element. The water part mesh is shown in Figure D-10. In the post-test model, the outage was increased and the mesh density was also increased. Additionally, the water was given a slight (0.1 inch) "dip" at its center to help prevent air particles from slipping between the edge of the tank and the edge of the water.

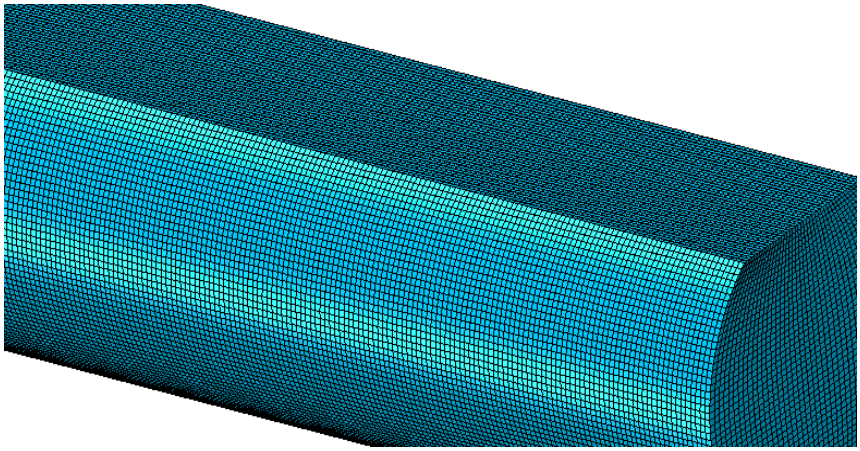

Figure D 10. Water Mesh

Table D 9. Properties of Water Mesh

	Pre-Test Model	Post-Test Model
Type of Part	Deformable, Solid	
Material(s)	WATER	
Number of Elements	C3D8: 130,772	C3D8: 433,693
Water Volume	3,789,530 in^3 (16,404.9 gallons)	3,761,040 in^3 (16,281.6 gallons)
Part Weight	137,983.4 lbf	136,940.2 lbf

Appendix E.
Modeling Techniques Common to Pre-Test and Post-Test Finite Element Models

This section describes the boundary conditions, initial conditions, constraints, and contact definitions within the FE model. In addition to the typical initial conditions, such as the initial speed of the impactor, using the SPH approach to modeling the gas phase requires additional considerations when defining contact interactions, boundary conditions, and other constraints within the FE model.

E.1 Part-Level Contact Definitions

At the part-level of the model, an additional surface must be defined to ensure the SPH particles are treated properly during contact interactions. In the DOT-112 FE model, the gas phase of the lading is initially meshed using C3D8R brick elements. The elements are converted to particles, with one particle replacing each brick element. While the Abaqus FE software has the capability of converting the elements into particles at time=0, this approach leads to the volume of particles being distributed among multiple domains (i.e., being solved by multiple processors). Because of the overall large size of the model, a multi-processor execution is necessary to achieve runtimes on the scale of days. Based on experience gained from this modeling process as well as anecdotal evidence found in the Abaqus Knowledge Base (a support forum), the FE model is more stable (i.e., more likely to execute without terminating) when all particles are solved within a single domain. In order to ensure that the solver places all particles within a single domain, the particles are converted from elements at a non-zero time. In this particular model, the elements are converted at $t=1x10^{-6}$ seconds. This early but non-zero time conversion ensures that all particles are solved within a single domain, and it ensures that particles are representing the air for essentially the entire duration of the simulation. Figure E 1 illustrates the distribution of the lading across multiple domains, with the air being contained within a single domain. Each domain is indicated by a single color in this image.

Figure E 1. Distribution of Lading into Domains in FE Model

One additional consequence of creating particles via conversion from a Lagrangian part involves the surface that is created in the general contact domain. By default, general contact in Abaqus/Explicit only considers the exterior surfaces of a solid, Lagrangian part. Therefore, only the exterior faces of the initial air part will be included in the contact domain. When the Lagrangian part is converted into particles, only those particles whose parent elements included an exterior face will be included in the general contact domain. This means that a particle that was initially located in the center of the air part (i.e., surrounded on all sides by air particles) will not be included in the contact domain. However, it is possible for that particle to move freely among the other particles, making its way out to the interior surface of the tank. Because this particle was not generated from an element on the outer surface of the tank, this particle will not be included in the contact domain between the air and the tank, and will simply pass through the tank's wall.

The solution to this problem is to create a part-level surface that includes both the interior and exterior elements in the Lagrangian parent mesh. If all of the elements in the parent mesh are included within the initial contact domain, the particles that are generated from these elements will also be included within the contact domain.

E.2 Interaction-Level Contact Definition

At the interaction-level, the contact definitions must also be specially defined in order to contain the SPH particles. General contact is applied to the model. Typically, general contact is defined between all exterior surfaces within the model. However, rather than choosing all exterior surfaces for the contact domain, individual contact pairs are defined. The first contact pair is defined between all surfaces in the model, and the surface that includes all of the particles. This pair ensures that the interior particles can be involved in contact, if applicable. A second contact pair is then defined between all other exterior surfaces in the model.

Contact exclusions are also defined within the model. The contact exclusions are all related to the presence of the symmetry wall at the symmetry plane of the model. Because the tank, jacket, water, rigid wall, impactor, and symmetry wall all occupy the same space on the symmetry plane, contact exclusions must be defined in order to prevent the model from giving a non-physical response (e.g., the impactor striking the symmetry wall). Exclusions are defined between the rigid backing wall, the rigid impactor, the deformable jacket, deformable tank (both solid and shell parts), skid, and the liquid phase of the lading. This approach ensures that contact will still be enforced between the air particles and the symmetry wall, but permits the other parts within the model to pass through the symmetry wall without being affected.

Contact properties are defined for several different surface pairs within the model. Generally, a low coefficient of friction (0.02) is applied throughout the post-test model. This is intended to represent a frictionless contact for most of the parts within the model. Experience with the modeling has indicated stability issues arise from using a true frictionless contact throughout the model, particularly between the water and the interior of the tank. Frictionless contact is used for the SPH part for contact with any other surface. Finally, a friction coefficient of 0.3 is used for contact between the tank head and all other surfaces. In the pre-test model, this coefficient of 0.3 was inadvertently applied to the entire interior surface of the tank, resulting in an overly stiff response from the fluid. Applying a higher coefficient to the water within the head is intended to provide stability for the water within the head, limiting the amount of mesh distortion that occurs. Experience with using this model has indicated that deformation of the water within the

tank head can dominate the stability of the model, owing to the double-curvature of the water within the head. Because the head is located at a large distance from the impact zone at the center of the tank, the inclusion of friction between the water in the head and the tank within the head is not believed to result in a significant effect on the global behavior of the model.

One further step taken to ensure containment of the particles and stability in the model is to define a pure master-slave relationship between the particles and all surfaces within the model. This is intended to prevent the particles from being able to penetrate any surfaces they encounter in contact. Because the particles represent an ideal gas, if even one particle is able to penetrate any of the surfaces containing the air mesh, the particle will be able to displace to an infinite distance (i.e., a gas expanding to fill an infinite vacuum), causing the model to terminate prematurely. Specifically, the particles should remain contained by the surfaces making up the interior of the tank, the water, and the symmetry plane.

E.3 Symmetry Conditions

During the impact test, the test plan called for the impactor to strike the DOT-112 tank car at its longitudinal center. To facilitate computational efficiency, this permitted a half-symmetric model to be used to simulate the test. A symmetry boundary condition was applied to the tank (solid and shell element portions), the jacket, and the water. Because boundary conditions are not directly applicable to particles, a symmetry wall was used to ensure that the air particles did not escape from the mesh.

E.4 Rigid Impactor Boundary Conditions

The rigid impactor was constrained against all motion except for longitudinal displacement. The impactor was given an initial velocity corresponding to the simulated impact speed. The pre-test model was run at 15 mph, and the post-test model at 14.7 mph.

E.5 Rigid Wall and Symmetry Wall Boundary Conditions

Both the rigid backing wall and the symmetry wall were restrained against motion in all DOF.

E.6 Jacket-to-Tank Tie

The jacket and tank were attached to one another using a tied constraint acting over the region of the bolster in the physical tank car. Standoffs between the tank and jacket were not included in this model, so this tied constraint represented the only connection between the tank and jacket. A “Tied Constraint” was defined between the arc representing the bolster on both the tank and the jacket parts. A position tolerance of 0.7 inch was used to account for the gap between the tank and jacket, where the thermal protection (not modeled) exists in the physical car.

E.7 Tank-to-Skid Coupling

The tank was connected to the rigid skid through a kinematic coupling. This coupling applied to all 6 degrees-of-freedom (DOF). The coupling was between the arc of nodes on the tank representing the bolster and the rigid body reference point of the skid, as shown in Figure E 2.

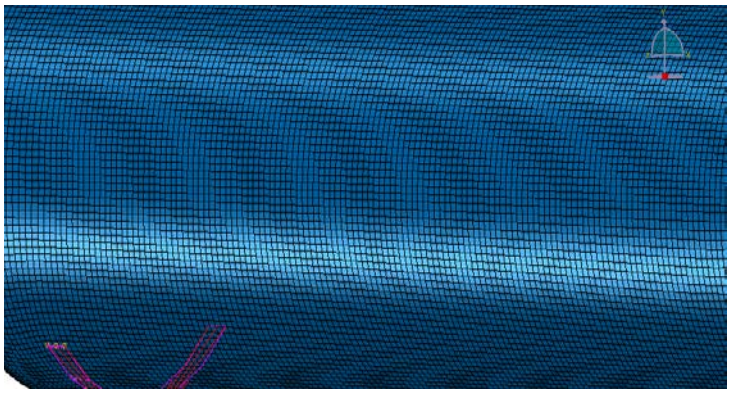

Figure E 2. Tank-to-Skid Coupling

Additionally, a "Cartesian" type of connector was used to constrain the motion of the skid. A nonlinear spring was defined between the skid and ground in the plane of the ground. This connector acted as a nonlinear spring, inhibiting the motion of the skid as an approximation of ground friction.

E.8 Shell-to-Solid Coupling

A shell-to-solid coupling was used to attach the patch of solid elements in the vicinity of the impact zone to the rest of the shell-meshed tank. This type of constraint is necessary to ensure a smooth transition from solid elements, which possess only translational displacement DOF, and shell elements, which possess translational and rotational DOF. As previously described in Section D.2.2, the meshes on the solid part and the shell part were controlled such that every element on the shell edges involved in the coupling spanned three solid elements. Since the shell part corresponded to the midplane thickness of the tank, the shell part was aligned with the midplane of the solid patch. The interface between the solid patch and the shell tank is shown in Figure E 3.

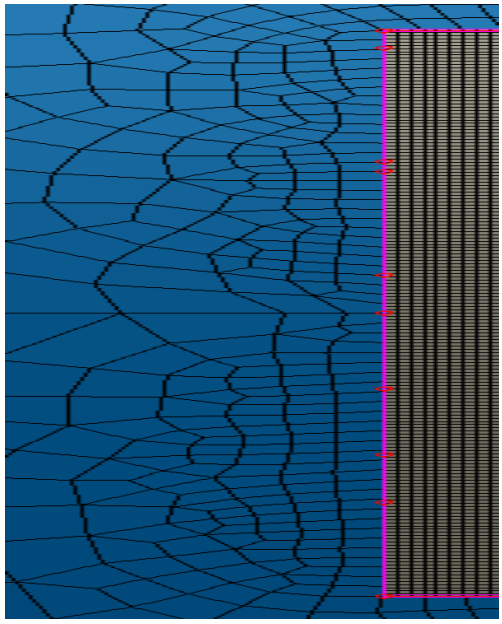

Figure E 3. Shell-to-Solid Coupling Region

E.9 Internal and External Pressures

The lading within the tank was given an initial pressure of 14.7 psi (1 atm). This was accomplished by defining an initial stress state of hydrostatic pressure (S11=S22=S33=-14.7) for the elements within the air and water parts. The pressure within the lading was free to change due to deformation of the tank as the analysis progressed.

Because the lading was given an initial pressure of 1 atmosphere, a load condition was defined on the outer surface of the tank part to maintain initial equilibrium. A pressure load with a magnitude of 14.7 psi was defined over the outer surface of the tank. This pressure load was applied instantaneously, so that the interior pressure (from the air and water) and the external pressure (from the "atmosphere") of the model were in equilibrium. This external pressure was maintained at 14.7 psi throughout the analysis, regardless of the change in pressure within the tank.

E.10 Springs

Soft springs ($k=1x\ 10^{-6}$ lbf/inch) were placed within the model at locations corresponding to the string potentiometers installed within the tested tank (see Section 2.3). The use of springs allowed a direct comparison between the change-in-length of a string potentiometer during the test and the change-in-length of the corresponding spring in the FE model.

Appendix F.
Material Behaviors in FE Models

F.1 A1011

Abaqus/Explicit requires metal plasticity to be defined in terms of plastic strain and true stress. The plastic behavior of A-1011 was input to the model according to Equation 1, based on the engineering quantities given in Table 6.

Equation 1. Stress-strain Relationships

$$\sigma_{true} = \sigma_{nom} \cdot (1 + \varepsilon_{nom})$$

$$\varepsilon_{ln}^{pl} = \ln(1 + \varepsilon_{nom}) - \frac{\sigma_{true}}{E}$$

σ_{true}	True Stress
σ_{nom}	Nominal (engineering) stress
ε_{nom}	Nominal (engineering) strain
ε_{ln}^{pl}	Plastic strain

The plastic stress-strain relationship, as input to the FE model, is shown in Figure F 1.

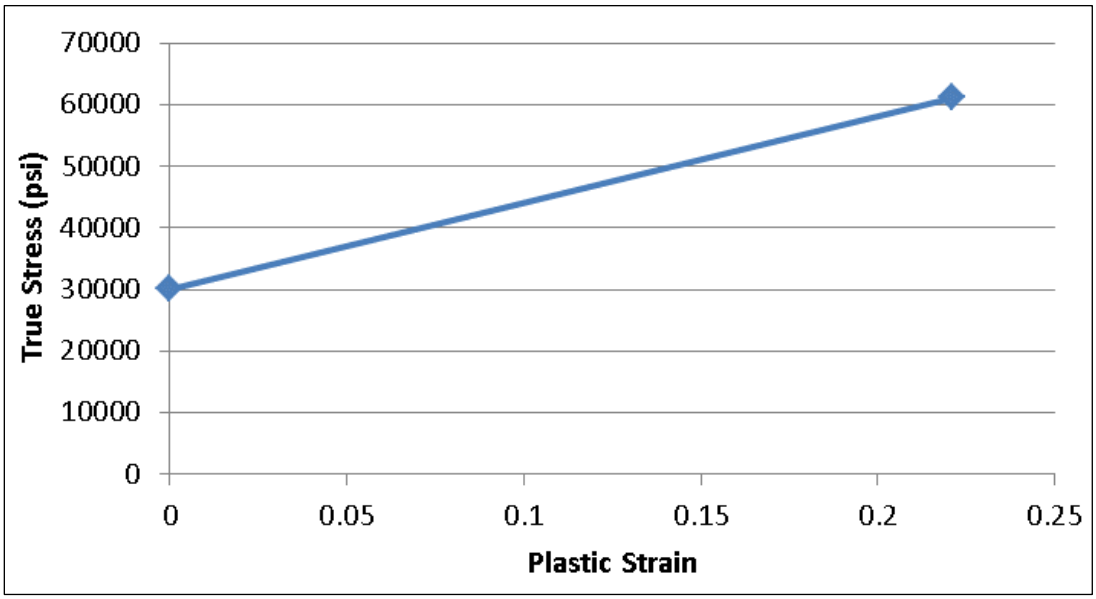

Figure F 1. True Stress-strain Relationship for A1011

Material failure was also included in the FE model for parts made of A1011. Because the jacket is a thin (11 gauge, or ~1/8-inch) sheet, a simplified failure behavior was implemented rather than developing a full B-W envelope for this material. In the simplified material failure model, a uniform plastic equivalent strain (PEEQ) was used as a failure initiation criterion. When PEEQ values exceeded the critical value at an element's integration point, that element begin to soften.

In the pre-test FE model, this critical PEEQ was 0.4. In the post-test FE model, based on the limited tearing of the jacket observed in the test, this value was increased to 0.5.

The final component of material failure used by the Abaqus program is the maximum damage progression. Once an integration point has exceeded the failure envelope, the element begins to soften until this maximum value is reached. At that point, the element has lost all load-carrying capacity at that section point, and is removed from the analysis. For A1011, a value of 0.25 was used in both pre-test and post-test models. This corresponds to the minimum elongation at failure for this material.

F.2 TC128

Abaqus/Explicit requires metal plasticity to be defined in terms of plastic strain and true stress. The formulae shown in Equation 1 were used to define the plastic behavior of the TC128B based on the engineering properties defined in Table 9.

The plastic stress-strain relationship, as input to the pre-test FE model, is shown in Figure F 2.

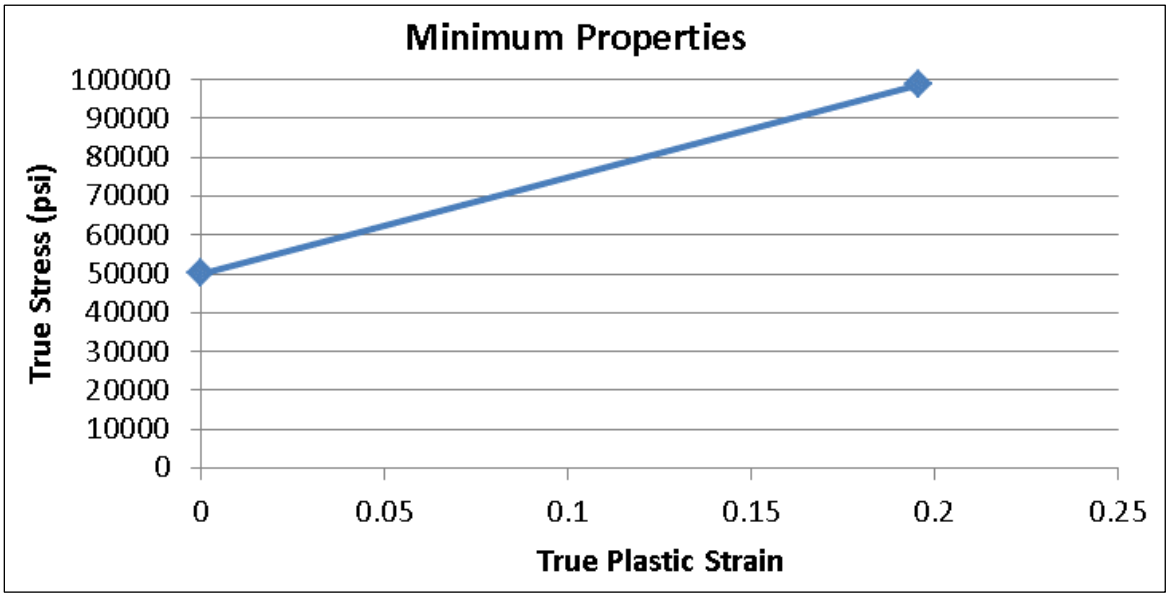

Figure F 2. True Stress-strain Relationship for TC128B in Pre-Test Model

Material failure was also included in the FE model for parts made of TC128B. The modified quick calibration approach to determining the B-W envelope parameters was used to derive the failure envelope [3]. The key input parameters to this model are the modulus of elasticity, ultimate tensile strength, yield strength, and percent reduction in area. Because reduction in area is not a specified property for TC128, another source of this information was sought. For this material model, the average percentage reduction in area measured during tensile testing of TC128B samples from cars retired from the tank car fleet was used [4]. The average reduction in area reported was 58 percent. The B-W envelope used for minimum-properties TC128B is shown in Figure F 3.

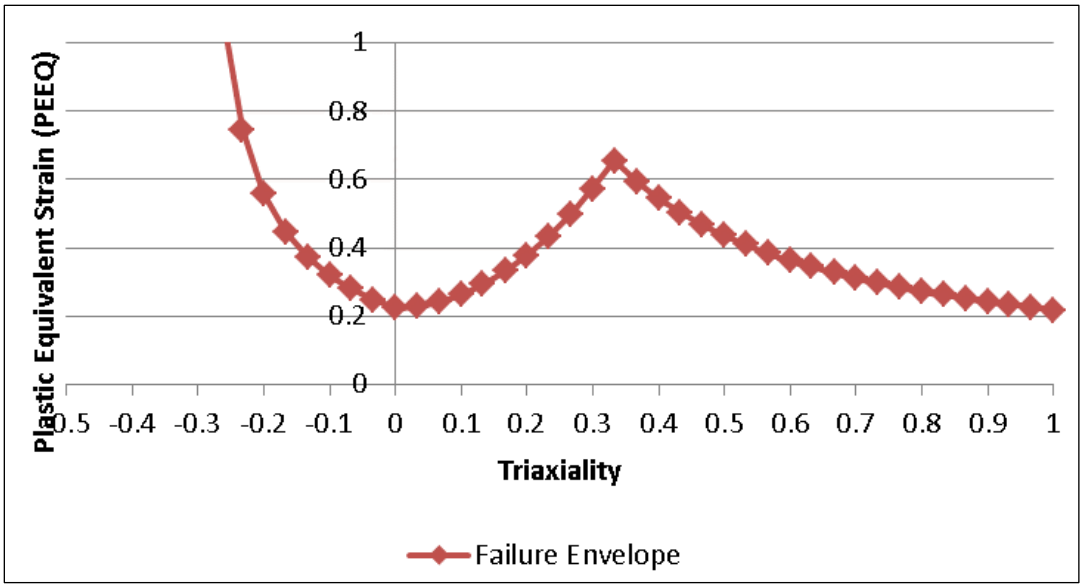

Figure F 3. B-W Envelope for TC128B (Minimum)

The final component of material failure used by the Abaqus program is the maximum damage progression. Once an integration point within an element has exceeded the failure envelope, the element begins to soften until this maximum value is reached. At that point, the element has lost all load-carrying capacity at that section point, and is removed from the analysis. For minimum TC128B, a value of 0.22 inches was used. This corresponds to the minimum elongation at failure for this material. This value is consistent with the damage progression modeling used in previous Volpe modeling of TC128 material fracture [5]. Previously, values of 0.27 and 0.275 inches had been used to describe the behaviors of actual material samples, based upon the elongation at failure for those materials.

Abbreviations and Acronyms

B-W	Bao-Wierzbicki
DOT	Department of Transportation
EOS	Equations-of-state
FE	Finite Element
FEA	Finite Element Analysis
FRA	Federal Railroad Administration
PEEQ	Plastic Equivalent
SPH	Smoothed Particle Hydrodynamics
TIH	toxic by inhalation
TTCI	Transportation Technology Center, Inc.